12-2006

# Linear and Nonlinear Chiroptical Effects

Watheq Ahmad Al-Basheer
*University of Tennessee - Knoxville*

To the Graduate Council:

I am submitting herewith a dissertation written by Watheq Ahmad Al-Basheer entitled "Linear and Nonlinear Chiroptical Effects." I have examined the final electronic copy of this dissertation for form and content and recommend that it be accepted in partial fulfillment of the requirements for the degree of Doctor of Philosophy, with a major in Physics.

Robert N. Compton, Major Professor

We have read this dissertation and recommend its acceptance:

Joseph H. Macek, Charles Fiegerle, Hanno Wietering, David J. Pegg

Accepted for the Council:
Carolyn R. Hodges

Vice Provost and Dean of the Graduate School

(Original signatures are on file with official student records.)

To the Graduate Council:

I am submitting herewith a dissertation written by Watheq Ahmad Al-Basheer entitled "Linear and Nonlinear Chiroptical Effects." I have examined the final electronic copy of this dissertation for form and content and recommend that it be accepted in partial fulfillment of the requirements for the degree of Doctor of Philosophy, with a major in Physics.

Robert N. Compton
Major Professor

We have read this dissertation
and recommend its acceptance:

Joseph H. Macek

Charles Feigerle

Hanno Weitering

David J. Pegg

Accepted for the Council:

Linda Painter
Interim Dean of Graduate Studies

(Original signatures are on file with official student records)

# Linear and Nonlinear Chiroptical Effects

A Dissertation

Presented for the

Doctor of Philosophy

Degree

The University of Tennessee, Knoxville

Watheq Ahmad Al-Basheer

December 2006

# DEDICATION

*This dissertation is dedicated to my parents, Moyasser and Ahmad Al-Basheer, for their endless unconditional love and caring, to my brothers and sisters, for setting a model of success, to the rest of my family, and to my friends for always believing in me, encouraging me, and supporting me during the course of this endeavor.*

# ACKNOWLEDGEMNTS

I would like to thank my advisor, Dr. Robert N. Compton, for allowing me to become a member of his group. His successful life time career in scientific research made all problems and questions doable through a creative and critical way of thinking, while enjoying the experience. From Dr. Compton I have learned that the answer of many scientific mysteries can lie in the most marginal experimental findings. His patience and dedication have positively influenced my character for a long time to come, both as a scientist and a person.

I would like to thank Dr. Feigerle for help and assistance in performing Raman related experiments, as well as for teaching me physical chemistry spectroscopy courses.

I would like to thank the other members of my committee; Dr. Joseph H. Macek for teaching me Atomic and Molecular physics, his explanations made the understanding of theoretical basis of my topic research easy; Dr. David J. Pegg; Dr. Hanno Weitering; for their willingness to serve and useful suggestions.

I would like to thank Dr. Richard M. Pagni for working with me, and for many useful conversations, insightful advices, and suggestion toward the advancement of my research.

I also gratefully acknowledge the travel funding support of the Chemical Physics Program at the University of Tennessee, especially the help of Dr. Janice Musfeldt and Dr. Robert N. Compton.

I would like to thank Dr. Prasad L. Polavarapu, and his graduate student Jiangtao He, of Vanderbilt University for making their FTIR machine available, and to their experimental assistance and useful comments.

Last, but certainly not the least, special thanks goes to all my friends and colleagues in Dr. Compton's group; Nathan Hammer, Rodney Sullivan, Wesley Robertson, Andy Fischer, Nasrin Mirsaleh-Kohan, Jeff Steill, Shaun Ard, Olga Ovchinnikova, and many others.

# ABSTRACT

Chiroptical effects of linear and nonlinear nature are investigated by employing a variety of spectroscopic methods, such as linear and nonlinear circular dichroism, optical rotation, vibrational Raman scattering, infrared absorption and Vibrational Circular Dichroism. (2+1) Resonance Enhanced Multiphoton Ionization Circular Dichroism (REMPICD) is a direct demonstration of the nonlinear chiroptical effects of a sample of *R*-(+)-3-methylcyclopentanone. Solvent effects on circular dichroism is studied for 35 common solvents, which is significantly attributed to the solute-solvent electrostatic and Van der waals interactions for CD and ORD of *R*3MCP. Hartree-Fock and Density Function Theoretical calculations of *R*3MCP CD and ORD in solvation are also employed to support the experimental findings.

Enantiomers (*R*, *S*) of chiral molecules are known to exhibit optical activity effects which are equal in magnitude and opposite in sign. For some carbonyl molecules (possessing the C=O) the equatorial and axial conformers also exhibit CD and ORD of opposite sign but not necessarily the same absolute magnitude. Studies of the temperature variation of the CD and Raman spectra are shown to be a useful technique to study the conformer's populations and energy difference. IR absorption and Vibrational Circular Dichroism (VCD) of carvone, and limonene, are also studied as an example of molecules having different conformers. IR and VCD Density Function theory (DFT) calculations of the vibrational levels are compared with experimental results in order to establish the dominate (lowest energy) conformer.

# TABLE OF CONTENTS

# LIST OF TABLES

# LIST OF FIGURES

# ABBREVIATIONS

| | |
|---|---|
| OPO | Optical Parametric Oscillator |
| CD | Circular Dichroism |
| ECD | Electronic Circular Dichroism |
| ORD | Optical Rotatory Dispersion |
| OR | Optical Rotation (Specific Rotation) |
| LCPL | Left -Circularly Polarized Light |
| RCPL | Right -Circularly Polarized Light |
| 3MCP | 3-Methylcyclopentanone |
| *R*3MCP | *R*-(+)-3-Methylcyclopentanone |
| *R* | Enantiomer notation for handedness |
| (+) | Clockwise rotation of plane of polarization |
| *S* | Enantiomer notation for handedness |
| (-) | Counterclockwise rotation of plane of polarization |
| IR | Infrared absorption |
| VCD | Vibrational Circular Dichroism |
| MPI | Multiphoton Ionization |
| REMPI | Resonantly Enhanced Multiphoton Ionization |
| REMPICD | Resonantly Enhanced Multiphoton Ionization Circular Dichroism |
| (2+1) | Two photons to reach intermediate state and one photon to ionize |
| (3+2) | Three Photons to excite and two photons to ionize |
| DFT | Density Function Theory |
| HF | Hartree-Fock |
| SOM | Single Oscillator Model |
| COM | Coupled Oscillator Model |
| UV/VIS | Ultra Violet/ Visible |
| CDAD | Circular Dichroism of Angular Distribution |
| TOFMS | Time of Flight Mass Spectrometer |
| NMR | Nuclear Magnetic Resonance |
| TDCD | Temperature Dependent Circular Dichroism |
| TDVCD | Temperature Dependent Vibrational Circular Dichroism |
| RUN | Raman under Liquid Nitrogen |
| PEM | Photo-elastic Modulator |
| FTIR | Fourier Transform Infrared |
| Eq (T) | Equatorial Trans |
| Ax (C) | Axial Cis |
| Eq (C) | Equatorial Cis |
| Ax (T) | Axial Trans |

# CHAPTER I
# INTRODUCTION

This dissertation presents a comprehensive investigation of chirality by employing different spectroscopic techniques on electronic and vibrational levels of chiral molecules. Linear chiroptical effects are investigated by applying low intensity laser light which correspond to a single photon excitation wavelength of a particular molecular transition under study. Nonlinear optical activity is demonstrated by using relatively-high intensity pulsed OPO lasers.

This dissertation can be divided into two main parts; the first part, covers Chapters II through V, in which Circular Dichroism (CD) and Optical Rotatory Dispersion (ORD) are extensively studied for *R*-(+)-3-methylcyclopenatnone ($C_6H_{10}O$) both in the gas and solution phases.

The second division represents a study of a number of chiral molecules using vibrational spectroscopic techniques such as, Raman, Infrared and Vibrational Circular Dichroism (VCD). Chapter II provides a theoretical basis for the optical activity of chiral molecules with two experimental applications: (1) CD of *R*-(+)-3-methylcyclopentanone (*R*3MCP) in the gas phase and (2) study of the CD for the *R*, and *S* enantiomers of carvone. Chapter III presents a description of a powerful new nonlinear chiroptical technique involving multiphoton ionization. Resonance-enhanced (2+1) multiphoton ionization circular dichroism (REMPICD) for nozzle-jet expanded molecular beams of the equatorial conformer of *R*-3MCP is presented. Monitoring mass-selected cations produced via (2+1) REMPI through the $n \rightarrow 3s$

Rydberg transition, in which two gas samples, racemic 3MCP and *R*3MCP are studied.

In Chapters IV and V, another aspect of the optical activity of *R*3MCP is examined by recording CD and ORD spectra in 35 common solvents of varying polarity and refractive index. Furthermore, temperature dependent CD spectra in these solvents are related to the equatorial and axial conformers population as well as their energy and entropy difference between these two molecular states (see figure 1.1). Calculations using the Gaussian03 software package is also employed to support experimental findings by using Density function and Hartree-Fock theory.

Raman vibrational spectra of *R*3MCP at liquid nitrogen and at varying temperatures are also presented in Chapter VI, with an emphasis on the C-H stretch region which is believed to be sensitive to the axial and equatorial *R*3MCP conformations. Chapter VII involves the experimental and predicated Infrared (IR) and Vibrational Circualr Dichroism (VCD) spectra for limonene ($C_{10}H_{16}$) and carvone ($C_{10}H_{14}O$) conformers, and the temperature dependent VCD signals of limonene and carvone enantiomers, these two samples were chosen to investigate multiple conformation populations. Another importance of studying the three mentioned molecules is their high optical activity and existence in many living organisms. The enantiomers of limonene and carvone are common natural products.

In the coming chapters a variety of chiroptical spectroscopic methods will be described to obtain new information on chiral molecules. Studies of chirality have significant applications in biochemistry and the pharmaceutical industry.

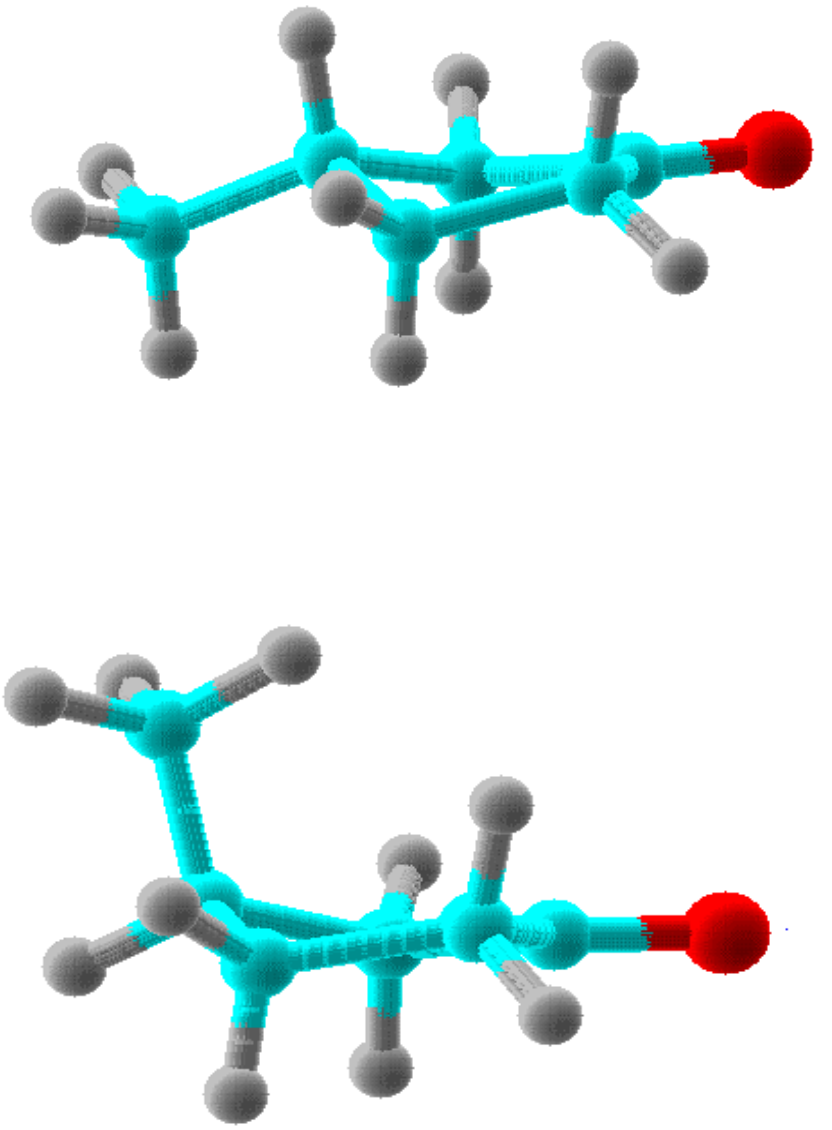

Figure 1.1 *R*-(+)-3-methylcyclopentanone dominant conformers; Equatorial methyl (above), and Axial methyl (bottom).

# CHAPTER II
# CHIRALITY PRINCIPLES AND OPTICAL ACTIVITY

## Introduction

The concept of chirality, or handedness, pervades many fields of physics, biology, and chemistry. Chirality is a common feature of many organic molecules and most biological systems and is exhibited by optical activity. Interestingly, optical activity for atoms is a result of the weak interactions within the nucleus. Optical activity is believed to be the most efficient tool to understand chirality due to the fact that atoms and molecules tend to interact with light as a result of its charge arrangement; all molecules can be classified as either chiral or achiral molecules. A molecule is achiral if it contains a plane of symmetry. The most common cause of chirality in most organic molecules is the presence of a carbon atom bonded to four different atoms or groups; such carbons are referred to as chirality centers. Mirror-Image molecules that are not super- imposable are chiral and called enantimors (Greek enantio, “opposite”). These two distinct forms are said to have opposite absolute configurations, which in turn produce optical activity of equal magnitude and opposite sense at a given wavelength.

The modern system for specifying the absolute configuration of most chiral molecules is based on the *R* (for rectus) and *S* (for sinister) system of Cahn, Ingold, and Prelog,[1] supplemented with the plus (+) and minus signs (-) for clockwise and counterclockwise rotation of light polarization, respectively. Optical activity describes two related phenomena; Optical Rotatory Dispersion (ORD) and Circular

Dichroism (CD). Both ORD and CD result from the interaction of the electromagnetic field (light) with chiral matter (molecules). ORD refers to the dependence of the rotation of the electric field component of a linearly polarized light beam on the frequency ($\omega$) or wavelength ($\lambda$). ORD was the first historically to be noticed due to the simplicity of creating and detecting linearly polarized light. CD describes the ellipticity of the outcomming wave, and is defined as the differential absorption between left-and right-circularly polarized light. CD is widely used to investigate the chirality of many chemical or biological substances.

ORD and CD of chiral molecules can be explained as a direct result of the interaction of light with the electric and magnetic dipole and quadruple moment of the molecule. Because a chiral molecule has no reflection plane, when interacting with polarized light, any rearrangement of its electrons will likewise not have one either. This explains why achiral molecules do not interact with Right Circularly Polarized Light (RCPL) and Left Circularly Polarized Light (LCPL) differently. Due to the fact that electric field vectors of circularly polarized light trace out helices, one concludes that that the interaction between chiral molecules and left-and right CPL will be different.

Many common helical physical objects are chiral. For example, screws, coils and springs exist in chiral forms. Perhaps the most important of these is the alpha (right- handed) helix of DNA.[2] Louis Pasteur was the first to experimentally observe chiral arrangement by studying the optical activity of organic molecules, Pasteur also identified chiral molecules as one of the characteristic of life.[3]

Relatively recent observations have provided evidence for the formation of optically active substances in nature[4,5] which appears to be independent of living matter. Approximately ninety-five percent of naturally occurring compounds are chiral. Optical activity is manifested by many natural products, such as proteins, nucleic acids, sugars, lipids, amino acids, hormones, and vitamins. In addition to the naturally occurring optical activity in chiral molecules, it was proven experimentally that chirality can be induced in most achiral samples. A significant induced optical activity was recorded when placing achiral molecule in chiral environment, the induction of optical activity can be explained as a result of the appropriate coupling between the electrical transition moments of the guest achiral molecule and of the chiral host.

Historical Perspective

The origins of chirality goes back to 250 B.C. when the famous Greek philosopher Archimedes of Syracuse designed his famous mechanism of irrigation called the water screw by studying the spiral structure.[6] The word chirality was coined by Lord Kelvin and derived from the Greek word χειρ (kheir) meaning hand. Almost two thousand years later in 1809 Malus discovered that the light reflected from certain transparent media, glass or water, gives two instead of one images when transmitted through a doubly refracting crystal such as calcite. The then-current Newtonian theory, at that time, accounted for the double refraction by assuming that light consists of a beam of asymmetric particles, which are normally randomly oriented but becomes ordered in a doubly- refracting crystal to give two rays. Malus

supposed that the light particles are dipolar, like a magnet, and that a reflecting surface oriented the dipoles to give what he termed "polarized light".[7] Another French scientist Dominque F.J. Arago in 1811 discovered the rotation of the plane of polarization of light in quartz crystals by modifying Malus experiment. He inserted a quartz plate, cut perpendicular to the optic axis, between the polarizer, composed of a pile of glass plates, and the calcite analyzer, he observed a spectrum of colored images as the polarizer or the analyzer was rotated, this simple experiment was the first manifestation of optical activity.

A year later Arago's colleague Biot showed that this phenomenon was not confined to crystalline substances. Solutions of certain natural products also possessed the property of rotating the plane of polarization of plane polarized light. For example, he noticed a significant optical rotation of polarized light in sugar solutions. Biot studied the physical laws describing this phenomenon in detail and showed, in particular, that the angle of rotation varies linearly with the thickness of the solution through which the beam of light passes, as well as the concentration of the optically active product.[8] Furthermore, in 1817 he established an approximate inverse square law between the angle of optical rotation, $\alpha$, and the wavelength of the light, $\lambda$,

$$\alpha = \frac{K}{\lambda^2} \tag{2.1}$$

where $K$ is a constant characteristic of the optically active substance, Biot concluded that the optical rotation is essentially a molecular property, characterized by what

he described as the "molecular rotatory power ". In 1835 he introduced the term specific rotation, [α],

$$[\alpha] = \frac{\alpha}{lc} \tag{2.2}$$

where α is the observed rotation in degrees, $l$ is the path length in decimeters, and c is the concentration of the optically active substance in g/cm$^3$.

In 1848 Louis Pastor stated that nature has a chiral asymmetry by studying tartaric acid ($C_4H_6O_6$) which occurs as three distinct isomers, the dextro-,levo- and -meso forms. It is well known today that the dextro- and levo- forms of tartaric acid are optically active since they are chiral while the meso- form is optically inactive because it is achiral (Figure 2.1). Pastor also deduced that that the rotatory power was connected with the existence of non-superimposable mirror image asymmetry in the molecule. Pastor observed the consumption of the dextrorotatory tartaric acid by a growing yeast when ammonium salt of racemic tartaric acid was added, he argued that the two chiral forms, forming racemic tartaric acid, are composed of identical atomic sequences, and have an overall helical structure forms that are nonsuperposable mirror images of each other.

Le Bel proposed the molecular dissymmetry concept attained a three-dimensional structural content with the tetrahedral model for the orientation of the carbon valencies. Forty years later Friedrich Reinitzer discovered the chiral phase of certain liquid crystals, coining of the term "liquid crystals". Pierre Curie showed a link between molecular chirality and the chirality of the macroscopic structure, he

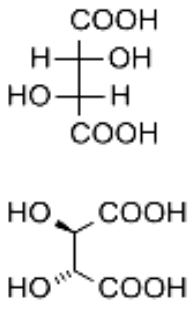


(a)

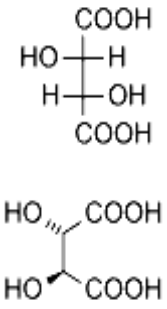


(b)

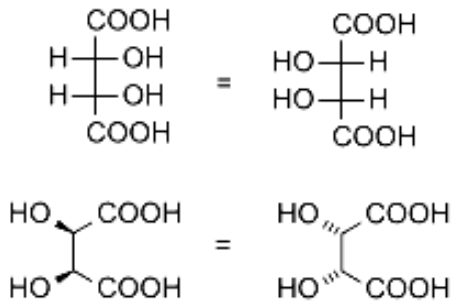


(c)

Figure 2.1 The tartaric acid isomers ($C_4H_6O_6$), (a) Dextrotartaric acid, (b) Levotartaric acid and (c) Mesotartaric acid.

pointed out that chiral properties of molecules can be transferred into the structures formed by groups of molecules.

In the early 20th century, Cotton was the first to study optical rotatory dispersion in detail and stated that each optically active material absorbs left -and right - circularly polarized light to a different extent. He introduced the term circular dichroism.[8] Thus a racemic mixture, which is a sample of equal percentage of two enantiomers, irradiated with circularly polarized light (left or right) of a certain wavelength, is expected to become enriched in the enantiomer with the smaller absorption coefficient for the particular hand of circularly polarized light employed. Without success Cotton searched for the anticipated effect, and the first photoresolutions of racemic mixtures by irradiation with circularly polarized light were attained some thirty years later.

In the1950s Pauling, Corey, Watson and Francis Crick discovered the alpha helix and the DNA double helix. A major input to this field was introduced in 1973 by Howard C. Berg and Robert A. Anderson[9,10] with their prediction and confirmation of rotary motion in bacterial flagella. Although ORD and CD have been known for more than 100 years, until the middle of the twentieth century most applications in chemistry utilized just optical rotation at some transparent wavelength, usually the sodium D line at 589 nm. More recent studies are focusing on other wavelengths.

Theoretical Background

In order to understand optical activity it is useful to write down the Hamiltonian for interaction of light with matter (molecule) classically,

$$H_{tot} = H_{rad} + H_{mol} + H_{Int} \tag{2.3}$$

Optical activity is described in the third part of the Hamiltonian $H_{\text{Int}}$, which results from the coupling of the molecule with the radiation fields;

$$H_{Int} = -\mu \cdot \mathrm{E} - m \cdot B - \frac{1}{2} Q \cdot \nabla \mathrm{E} + \text{Higher order terms} \tag{2.4}$$

where E and $B$ are the electric and magnetic fields. μ and $m$ are the electric and magnetic moments, respectively, and determined by summing over the electronic density distributions of the molecule

$$\mu = e \sum_{i} (r_i) \tag{2.5}$$

$$m = \frac{e}{2M} \sum_{i} \{ r_i x p_i \} \tag{2.6}$$

where $e$ is the negative electron unit charge, $r_{\text{i}}$ denotes the position vector of the $i$th electron, $p_{\text{i}}$ is the momentum vector of the $i$th electron, and $M$ is the mass of an electron .

Fresnel described the phenomological model of optical activity, by assuming a difference in the indices of refraction for left $n_L$ and right $n_R$ circularly polarized light. According to his model both ORD ($\phi$) and CD or ellipticity ($\theta$) are related by the complex rotatory power $\Phi$[11,12]

$$\Phi = \phi - i\theta = \left( \frac{\pi \mathrm{l}}{\lambda} \right) \left[ (n_L - n_R) - i(\kappa_L - \kappa_R) \right] \tag{2.7}$$

Where λ is the vaccum wavelength of the radiation, l is the path length, and $\kappa_L$ and $\kappa_R$ are the respective absorption indices for left- and right -circularly polarized light. The real and the imaginary parts of the equation above are related by Kronig-Kramers theorem[13-16] quantitatively as follows

$$\theta(\lambda_o) = \frac{-2}{\pi\lambda_o}\int_0^\infty \phi(\lambda)\frac{\lambda^2}{(\lambda_o^2-\lambda^2)}d\lambda$$
$$\phi(\lambda_o) = \frac{1}{2\pi}\int_0^\infty \theta(\lambda)\frac{\lambda}{(\lambda_o^2-\lambda^2)}d\lambda \qquad (2.8)$$

In practice, the most employed form of these equations is the so-called molar rotation [$\phi$] and molar ellipticity [$\theta$], defined as

$$[\phi] = \phi\frac{18}{\pi}\frac{M}{C\mathrm{l}} \qquad (2.9)$$

$$[\theta] = \theta\frac{18}{\pi}\frac{M}{C\mathrm{l}} \qquad (2.10)$$

Ellipticity, an old measure of CD, is obtained from the ratio of the minor and major axes of the ellipse traced out by the electric field vector of the elliptically polarized light when circularly polarized light emerges from the circular dichroic sample

$$\tan\theta = \tanh\left[\frac{\pi\mathrm{l}}{\lambda}(n_L - n_R)\right] \qquad (2.11)$$

For small ellipticities

$$\theta(radians) \approx \frac{\pi\mathrm{l}}{\lambda}(n_L - n_R) \qquad (2.12)$$

This can be expressed in terms of the difference in extinction coefficients $\varepsilon_L$ and $\varepsilon_R$ for the absorption of left- and right- circularly polarized light, respectively.

$$\theta(rad) = \frac{2.303\mathrm{l}\,C}{4}(\varepsilon_L - \varepsilon_R) \tag{2.13}$$

This can be expressed in degrees as

$$\theta(\deg rees) = 32.98C\mathrm{l}\,(\varepsilon_L - \varepsilon_R) \tag{2.14}$$

$$= 32.98(A_L - A_R) \tag{2.15}$$

where $A_L$ and $A_R$ are in terms of the absorbance units defined as

$$\left(A_L - A_R\right) = C\mathrm{l}\,(\varepsilon_L - \varepsilon_R) \tag{2.16}$$

Condon[20] classically concluded that in an optically active medium, the electric displacement D is not only linear, as in the case of isotropic, optically inactive medium, but it is also linear in the time derivative of magnetic field intensity *H*

$$D = \varepsilon E - g\frac{\partial H}{\partial t} \tag{2.17}$$

where ε is the dielectric constant and g is a constant. The magnetic induction *B* must be linear both in *H* and the time derivative of the electric field intensity as

$$B = \mu H - g\frac{\partial E}{\partial t} \tag{2.18}$$

Employing Maxwell's equations yields the indices of refraction:

$$n_R = \sqrt{\varepsilon\mu} - 2\pi\nu g \tag{2.19}$$

$$n_L = \sqrt{\varepsilon\mu} + 2\pi\nu g \tag{2.20}$$

Rosenfeld[21]derived an expression for the induced electric $\mu$ and magnetic *m* dipole moments of an individual molecule as a result of interaction with radiation as

$$\mu = \alpha E' - \frac{\beta}{c}\frac{\partial H'}{\partial t} + \gamma H' \tag{2.21}$$

$$m = \delta H' + \frac{\beta}{c}\frac{\partial E'}{\partial t} + \gamma E' \qquad (2.22)$$

One will note that these equations resemble eqs. (2.17) and (2.18). α, β, γ, and δ are constants, and *c* is the velocity of light in a vacuum. The primes are added to distinguish the molecular induced local fields from the applied external fields. The Dutch scientist, Drude, proposed a model for optical activity in which a single electron was constrained to move in a helix which was elastically bound to equilibrium positions on a curve. Until 1933 this single oscillator model was the basis of most theoretical work used to explain optical activity. More accurate experimental data available to Drude (1902) enabled him to replace Biot's inverse squares law by

$$\alpha = \sum_j \frac{A_j}{\lambda^2 - \lambda_j^2} \qquad (2.23)$$

where $A_j$ is a constant suitable to the UV/VIS absorption wavelengths $\lambda_j$. Kuhn[17]pointed out a major error in Drude's treatment. He applied the Single Oscillator Model (SOM) correctly and showed that SOM has no rotatory power. Kuhn results were crucial since it provided a case in which the rotatory power vanished in spite of the proper kind of dissymmetry being present. From this he concluded that the Coupled Oscillators Model (COM) would be essential to explain optical activity.

Later Condon[18] built a SOM in the dissymmetric field that exhibited a rotatory power. He introduced a relation connecting the oscillator strength $f_{ba}$, transition frequency $\nu_{ba}$ and rotatory strength, $R_{ba}$, as

$$f_{\mathrm{ba}} = \frac{8\pi^2 M}{3e^2 h} \nu_{ba} S_{ba} \tag{2.24}$$

Where $e$ and $M$ denote the electron charge and mass, and $S_{\mathrm{ba}}$ is the transition frequency strength. Kuhn[19] introduced another relationship to indicate optical activity at certain transitions and called it the dissymmetric factor $g_{\mathrm{ba}}$

$$g_{ba} = \frac{R_{ba}}{S_{ba}} \tag{2.25}$$

which is related to the difference in the molar extinction coefficients ε due to the absorption of LCPL and RCPL as

$$g = \frac{\varepsilon^L - \varepsilon^R}{\varepsilon} = \frac{2\left(\varepsilon^L - \varepsilon^R\right)}{\varepsilon^L + \varepsilon^R} \tag{2.26}$$

such that

$$\varepsilon = \frac{1}{c\mathrm{l}} \log \frac{I_{\mathrm{o}}}{I_{\mathrm{1}}} \tag{2.27}$$

Equation 2.27 is another form of the Beer-Lambert law for light absorption, i.e. $A = \varepsilon c\mathrm{l}$ , where $I$ is the intensity of light wave and c is the concentration of absorbing molecules in moles per liter. ε is in the units of $\mathrm{dm}^3/(\mathrm{mol}^4.\mathrm{cm}^4)$. It is widely observed that all organic molecules absorb light in the UV/VIS region of the electromagnetic spectrum which extends from the far UV (< 200 nm) to the near infrared (800-1000 nm).

Later in another landmark publication, Condon[20] introduced a standard measure of circular dichroism based on the fact that chiral molecules absorb circular polarized light differently. He related the difference in the Einstein coefficient ($B$) for left-and right-CPL in terms of the Optical Rotatory Tensor $R$ as

$$B^L - B^R = \left(\frac{8\pi}{3\mathrm{h}^2}\right) R_{ij}^{2\leftarrow 1} \tag{2.28}$$

$R_{ij}^{2\leftarrow 1}$ is commonly called the rotational strength in single-photon absorption and is also related to the transitions in electric and magnetic dipole moments by Rosenfeld quantum-mechanical equation[21] which was derived using time-dependent perturbation theory

$$R_{ij}^{2\leftarrow 1} = \mathrm{Im}\left\{\left\langle \Psi_1 / \mu_i / \Psi_2 \right\rangle \cdot \left\langle \Psi_2 / m_j / \Psi_1 \right\rangle\right\} \tag{2.29}$$

where $\mu_i^{12}$ and $m_j^{21}$ are the transition electric and magnetic dipole moments between the excited and the ground states. As a result of molecular radiation absorption by chiral molecules an electronic transition occurs because either the electric field or the magnetic field (or both) pushes the electrons to a new stationary state, the effect of the radiation electric field is to cause a linear rearrangement of electrons, and the net linear displacement of charge during a transition is called the transitional electric dipole moment $\mu^{12}$.

In contrast to the linear effect of electric field, the radiation magnetic field induces a circular rearrangement of electron density, whereas, the net circulation of charge is the transitional magnetic dipole moment $m^{12}$. In achiral molecules the effect of radiation absorption is a net planar rearrangement of electrons[22]; therefore for a CD effect to occur both $\mu^{12}$ and $m^{12}$ must be unequal to zero. Although it is given for achiral molecule to have zero rotatory strength even when the oscillator strength is nonzero, it is also known that chiral molecules may have vanishing rotatory strength if either transitional electric or magnetic dipoles is forbidden by

spectroscopic selection rules. ORD and CD are closely related and are considered as the real and the imaginary parts of the complex rotatory power Φ. This close connection is not surprising since linear polarized light can be considered as a superposition of left -and right- circularly polarized light of equal amplitude and phase (Figure 2.2).

The rotational strength is proportional to the area of the CD band. Therefore, the CD spectrum may be obtained directly from the rotational strengths by multiplying them with normalized bandshape functions (Gaussians type functions) which are summed to give the final CD curve as

$$\Delta\varepsilon(\lambda) = \frac{16\pi^2 N_A}{3\mathrm{h}c\cdot 10^3 \ln 10}\frac{1}{\Gamma_a\sqrt{\pi}}\sum_a R_{12}\exp\left[-\left(\frac{\lambda-\lambda_a}{\Gamma_a}\right)^2\right] \qquad (2.30)$$

Where $N_A$ is Avogadro's number, λ is radiation wavelength and Γa the half-width of the Gaussian at $1/e$ of its maximum.

Chromophores Circular Dichroism

Moscowitz et. al.[23, 24] first introduced the chromophore principle and defined it as the light absorbing unit in the chiral molecule that is only slightly perturbed by the rest of the system. The Cotton effect can be thought of as the rapid descending in the ORD and CD spectra around the UV/VIS region. Moffitt et. al.[25] classified chromophores into inherently chiral (dissymmetric), where optical activity has its origin within the dissymmetry of the chromophore itself, and inherently achiral (symmetric) which in turn can not exhibit optical activity without inducing chirality due to perturbation effect.

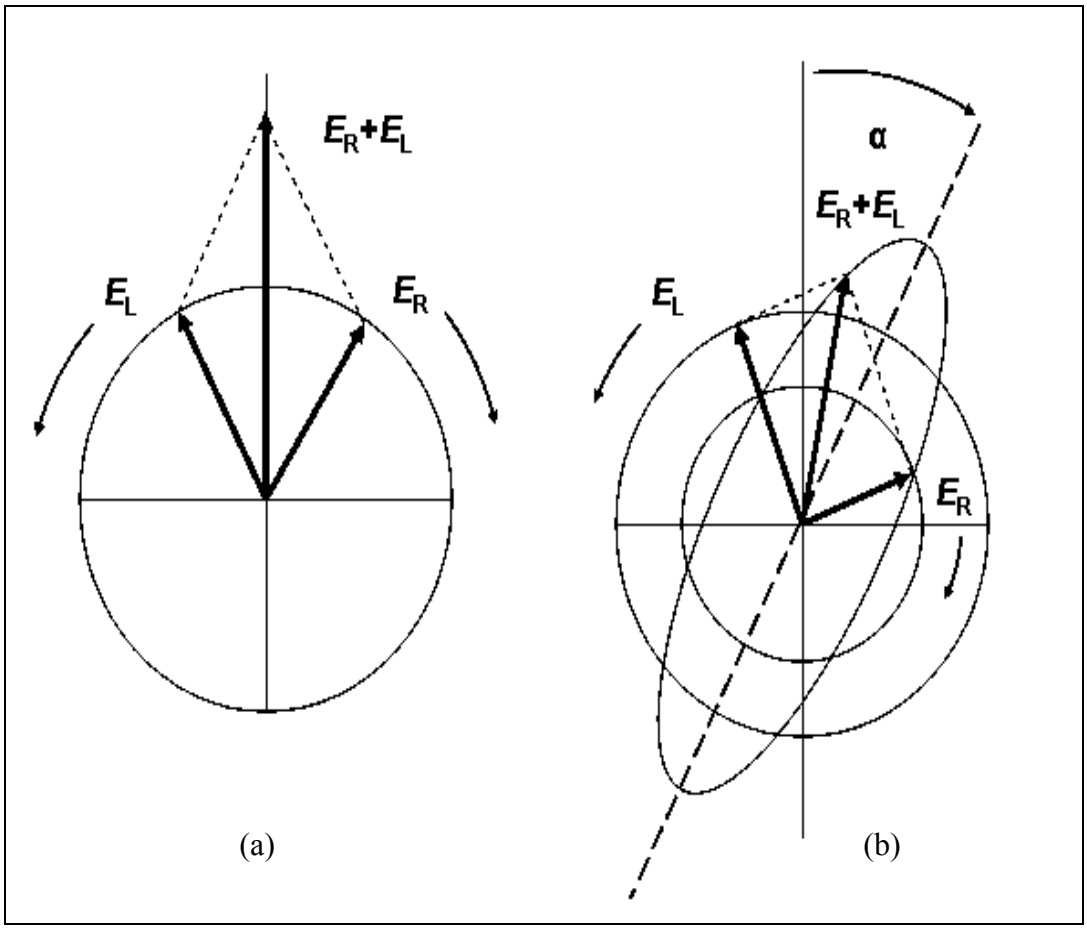


Figure 2.2 Electric field components of Circular polarized light, (a) linear polarized light can be viewed as a superposition of opposite circular polarized light of equal amplitude and same phase. (b) Different absorption of the left- and right hand polarized component leads to ellipticity (CD) and optical rotation (ORD).

Of particular interest is the carbonyl chromophore, which is commonly refered to as molecules that have a carbon oxygen double bond (C=O) and classified as carbonyl functional group molecules. Carbonyls are of significant importance due to their existence in most living substances and in many biological systems. Since optical activity of carbonyl chromophores originates from chiral perturbers within the molecule but lying distant from the chromophore, it can be a very sensitive chiroptical probe for detecting extrachromophoric stereochemistry.

Moscowitz and Djerassi et. al.[23] introduced the octant rule which is a useful method to determine the absolute configuration of a saturated ketone when its conformation is known or to determine the conformation when its absolute configuration is known. In the octant rule, all space surrounding the carbonyl chromophore is divided up into eight octants and the octant occupied by a particular perturber determines the sign of its contribution to the rotatory strength of $n \rightarrow \pi^*$ transition. These octants under discussion are derived, in part, from the local symmetry ($C_{2\upsilon}$) of the carbonyl group and from a consideration of the relevant orbitals of the $n \rightarrow \pi^*$ transition. All ketones have an $n \rightarrow \pi^*$ UV/VIS absorption near 300 nm which involves the promotion of an electron from an oxygen nonbonding ($n$) orbital ($P_y$) to a $\pi^*$ antibonding orbital comprising a linear combination of oxygen and carbon $P_x$ orbitals. Although such a circular movement of charge leads to a large induced magnetic dipole ($m$=1 Bohr Magneton) along the C=O bond, it does not induce an electric dipole moment in the same direction($\mu = 0$). Thus on the basis of local symmetry, the $n \rightarrow \pi^*$ transition is an electric dipole forbidden but magnetic

dipole-allowed ($m \neq 0$) transition. This explains the typically observed weak UV/VIS absorbance for ketones near 300 nm ($\varepsilon \sim$ 10-100).[26] However the electric dipole intensity is greatly increased by vibronic coupling with electric dipole-allowed transitions of higher energy, i.e. $\pi \rightarrow \pi^*$ or $\sigma \rightarrow \sigma^*$.

In the remains of the chapter, two applications of the CD of carbonyl functional group molecules will be presented. The first application is to describe the CD in the gas phase for R-(+)-3-methylcyclopentanone, while the second application will give an insight into the relation between the CD signals of carvone enantiomers both in the gas phase and solution phase.

In the CD spectrometer[27] (figure 2.3) a wide range of wavelengths of light are emitted from a Xenon lamp (Xe). The wavelength of the light was then selectively filtered by passing through a monochrometer consisting of a diffracting prism. This monochromatic light was then made linearly polarized by a $MgF_2$ polarizer and passed through a modulator plate driven by 50KHz oscillator to produce a strain-induced birefringence oriented 45° to the axis of the impinging linearly polarized light. The amplitude of the modulation is adjusted to give +90° and -90°retardation along one birefringence axis thus producing alternately left -and right -circularly polarized light. After passing through the sample, the light intensity is detected by a photomultiplier tube (PMT). By varying the dynode voltage, this photo-current is maintained at a constant value. The magnitude of this voltage will have a small alternating current (AC). This small AC signal compared to the average magnitude of the transmitted light is a measure of the circular dichroism.

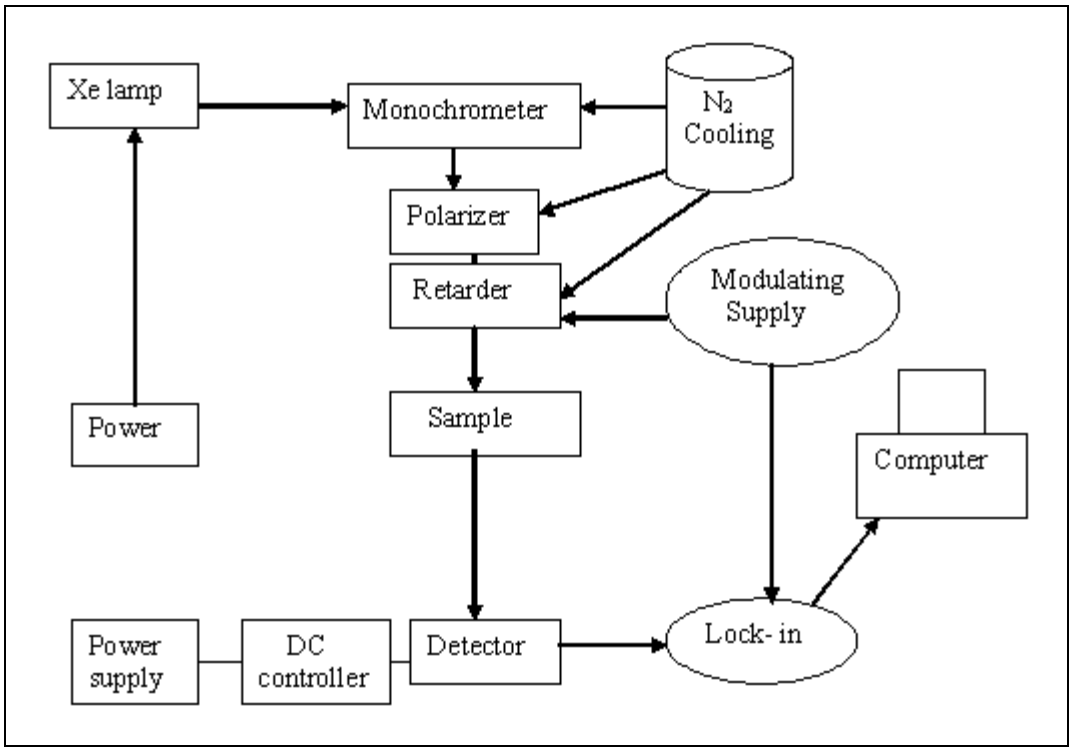


Figure 2.3 Simple sketch shows the main components of the CD spectrometer.

Application I: CD of *R*-(+)-3-methylcyclopentanone

*R*3MCP has the chemical formula $C_6H_{10}O$ and is a carbonyl chromophore chiral molecule possessing a relatively high optical rotation (148°in methanol at the sodium D-lamp wavelength). *R*3MCP has two optically active conformations; the axial form in which the methyl group is perpendicular to the cyclopentanone plane and an equatorial form in which methyl group is radial to the plane. By understanding the optical activity of this molecule we hope to gain a better understanding of the behavior of many living substances since carbonyl groups exist in steroids and other biological substances.

CD spectra of *R*3MCP was recorded with an Aviv model 202 series circular dichroism spectrometer by recording the differential absorption between LCPL and RCPL. Vapor phase CD was recorded by placing a small drop of *R*3MCP in a quartz cuvette and allowing it to vaporize at room temperature to reach an equilibrium vapor pressure of ~ 3 Torr.

Like most molecules that have a carbonyl chromophore, *R*3MCP was expected to absorb somewhere between 185-345 nm. Two main optically active regions were seen, the first one extends over the wavelength region (185-205 nm) corresponding to the Rydberg transition $n\rightarrow\sigma^*$ ($n\rightarrow$3s) which represents the promotion of an electron to the antibonding $\sigma^*$ orbital. The negative CD signal in this region indicates that the absorption of the RCPL was higher than that of the LCPL. The other noticeable peak (260-330 nm) which corresponds to the $n\rightarrow\pi^*$ Rydberg

transition, represents the promotion of an electron from a lone pair on the oxygen atom to the π* antibonding molecular orbital (figure 2.4).

The significant fine structure observed is due to the difference in absorption between left- and right- CPL due to excitations from different vibrational levels in the electronic ground state (*n*) to the to vibrational levels of the excited states (σ*,π*). One notices the small sub-bands between the major band indicating the sensitivity and resolution of this technique.

Application II: CD of carvone enantiomers

As an application for the relation between CD spectra of carbonyl functional group molecule enantiomers we choose the carvone molecule. Carvone ($C_{10}H_{14}O$) is found naturally in many essential oils. *S*-carvone is the principal constituent (50-70%) of caraway seeds oil, whereas, *R*-carvone is present in high levels in spearmint oil. CD spectra for both enantiomers were recorded in the vapor phase (figure 2.5) and the solution phase (figure 2.6) when dissolved in highly purified isopropyl alcohol at $5 \times 10^{-3}$ M concentration.

The CD spectra exhibit an expected equal magnitude and opposite sign, the vapor phase spectra exhibits two main peaks that maximize at 265 nm and ~324 nm corresponding to π→π* and *n*→π* transitions, respectively. The *n*→π* band is seen to have a sign inversion for the same enantiomer over the vibrational band. This represents an interesting case in which the CD changes sign over the vibrational progression. UV/VIS absorption spectrum of carvone shows a general correspondence with the CD peaks. With one interesting difference, the first peak

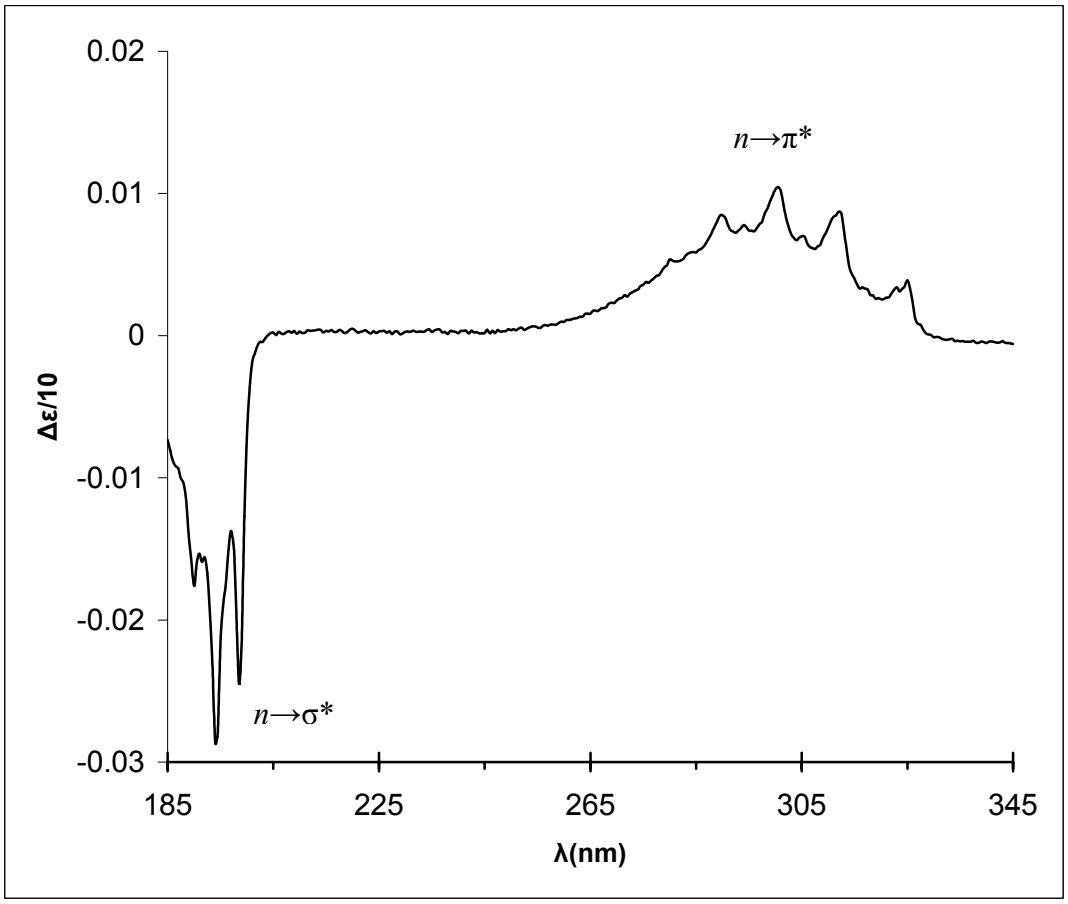


Figure 2.4 Circular Dichroism spectrum of *R*-(+)-3-methylcyclopentanone in the vapor phase at room temperature.

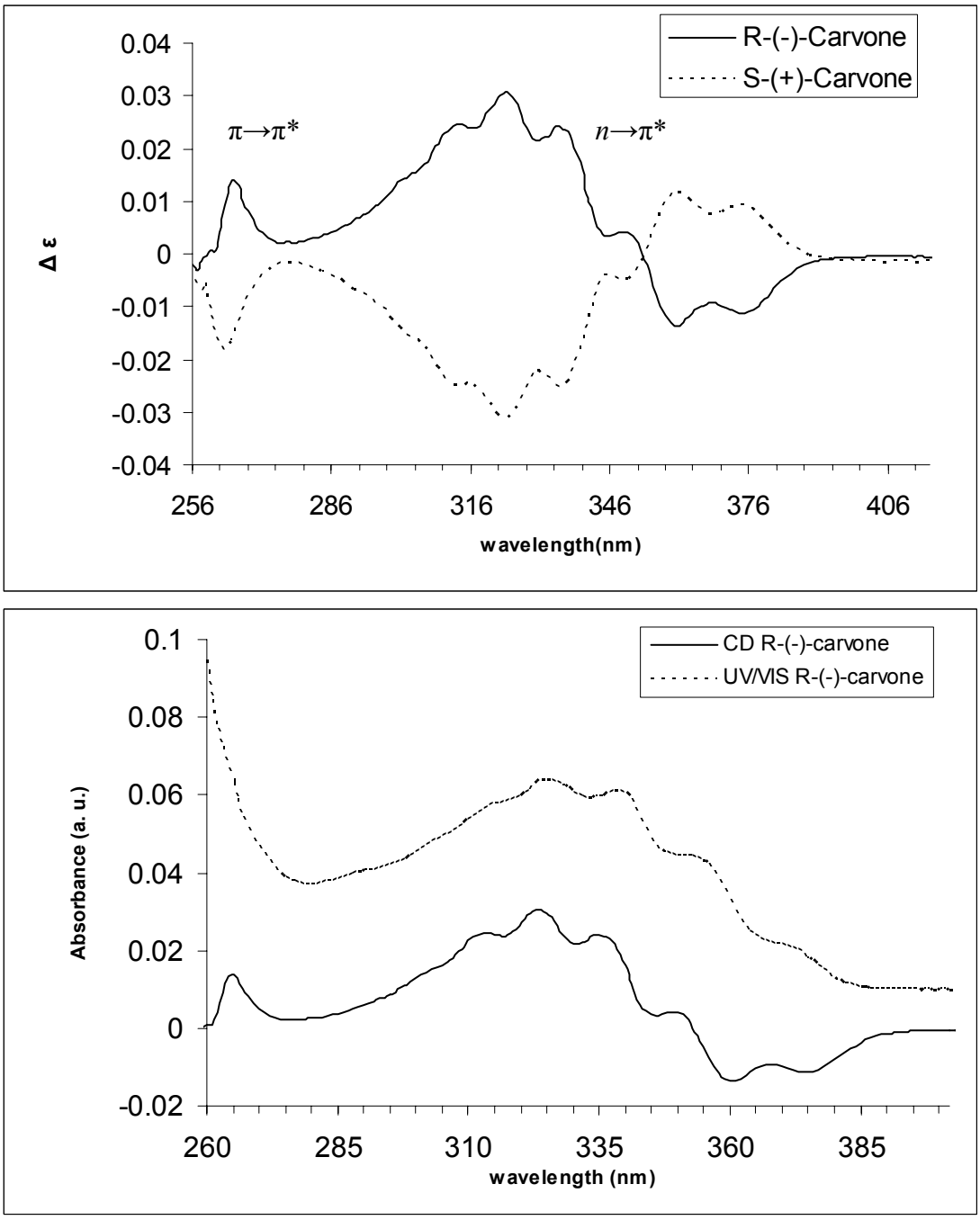


Figure 2.5 CD and UV/VIS spectra of carvone enantiomers. The top graph shows the circular dichroism of carvone enantiomers in vapor phase while the bottom graph contains the UV/VIS spectrum of *R*-(-)-carvone in cyclohexane combined with the CD spectrum.

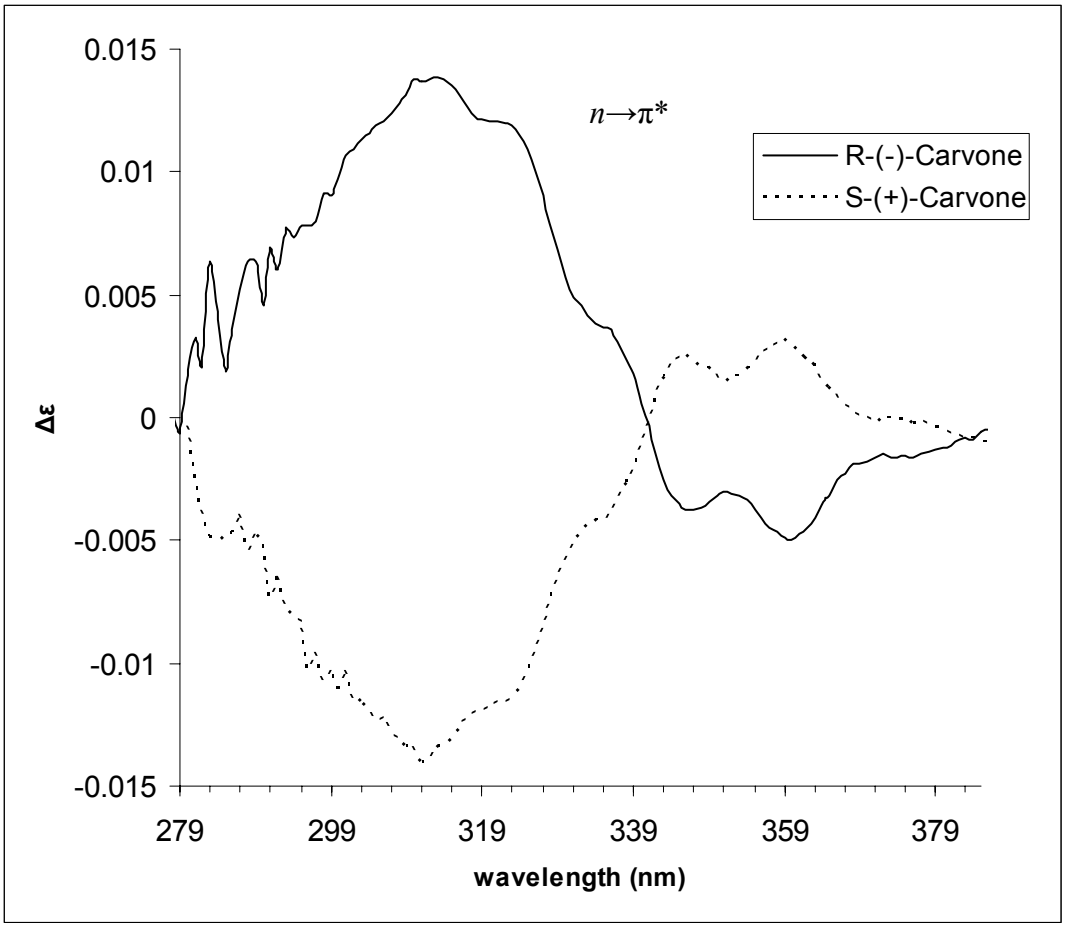


Figure 2.6 CD spectra of carvone enantiomers in Isopropyl alcohol solution.

(Presumably a vibrational transition) in the UV/VIS spectrum consists of two peaks in the CD spectrum. This interesting observation is not yet explained.

A similar relation between carvone enantiomers CD was observed in solution phase with slight spectra smearing due to solvent effects. The $\pi \rightarrow \pi^*$ transition was not recorded due to overlapping noise from the solvent with the CD signal. The $n \rightarrow \pi^*$ transition CD was slightly shifted to the shorter wavelength, with a maximum at 309 nm. This blue shift is attributed to the isopropyl alcohol polarity that effects the energy difference between the ground state ($n$) and the excited state ($\pi^*$) differently.

# CHAPTER III
# RESONANTLY ENHANCED MULTI-PHOTON IONIZATION CIRCULAR DICROISM (REMPICD)

## Introduction

As a direct result of the development of the pulsed dye laser in the early 1960s, a new field of spectroscopy has emerged, Multi-photon ionization spectroscopy (MPI). As the name indicates, the ionization process for atoms and molecules takes place in a manner involving many photons. The photons involved can promote the atoms or molecules to an intermediate excitation level before reaching the ionization threshold such promotion is useful to gain extra information about atomic and molecular structure. MPI can be classified as non-resonant or resonantly enhanced (REMPI). The theory underlying MPI was first introduced by Bebb et al.[28] and Stehle[29] while some of the first REMPI experiments were carried out by Dalby et al.[30] on $I_2$ molecule and Compton et al. on Xenon[31] and Nitric oxide.[32]

CD effects have also been observed for achiral molecules or even atoms when the experimental geometry is configured to be chiral. For example, CDs of the angular distribution (CDAD) of photoelectrons ejected from aligned or oriented molecules have been reported for gaseous NO[33] or oriented CO molecules on a surface[34]. In these experiments, the chiral geometry was created by the different handed coordinated systems given by the directions of light propagation, photoelectron ejection and the alignment of the molecules. Cuellar et. al. studied the CDAD for Cs gas phase atoms that were first aligned with a pump laser and then ionized with RCPL and LCPL from a second laser.[35]

In another study, a significant CD effect was observed in the second harmonic generation for anisotropic achiral surfaces which was attributed to an electric-dipole-allowed surface nonlinearity.[36,37] *R*3MCP involves the Rydberg transitions $n \rightarrow 3s$, $n \rightarrow 3p$ and $n \rightarrow 3d$ corresponding to 199 nm, 177 nm and 165 nm, respectively. This molecule has well-known electronic transitions because of extensive previous research[38] due to its availability as a saturated ketone in most steroids and living substances and its highly observed optical activity.

Compton's research group have introduced a powerful new technique to investigate chirality by manipulating resonantly enhanced multiphoton ionization (REMPI). By observing ionization signals of left-and right-CPL, it is possible to record REMPICD spectrum. REMPI has been used previously to discriminate between enantiomers of chiral molecules such as 2-butanol.[39,40,41] *R*3MCP was an excellent candidate for this investigative tool (REMPICD) not just for the reasons stated above, but also for its relatively high vapor pressure (~ 3 Torr).

As described in the previous chapter, CD is a powerful method to investigate chirality, which is commonly expressed in terms of the dissymmetric factor or the g factor. The relatively small value of the g factor ($10^{-3}$-$10^{-5}$) makes its determination more challenging. The REMPICD technique is being presented as a sensitive and useful technique to investigate chirality of *R*3MCP. Since racemic mixtures of enantiomers are not expected to show optical activity, the racemic mixture of 3MCP is also studied and employed as background effect.

REMPICD Theory

Meath and Power[42,43] used a combination of quantum electrodynamics and a semiclassical approach to describe the theory of multi-photon ionization CD. The handedness of the radiation beam is characterized by complex polarization vectors ($e^L(k)$ and $e^R(k)$) perpendicular to the direction of propagation vector *k* and of unit length. These LCPL and RCPL are represented by,

$$\begin{aligned} e^L(k) &= (e_x + ie_y)/\sqrt{2} \\ e^R(k) &= (e_x - ie_y)/\sqrt{2} \end{aligned} \tag{3.1}$$

and related by

$$(e^L)^* = e^R \tag{3.2}$$

where $e_x$ and $e_y$ are real unit vectors perpendicular to the propagation direction (z). The electric, *E,* and magnetic fields , *B,* are related by

$$B = e_z \times E \tag{3.3}$$

The time and spatial dependence of *E* for LCPL and RCPL are given by

$$E_{\substack{L \\ R}} = \frac{E_0}{\sqrt{2}}\left[e_x \cos(\omega t - k\cdot r + \delta) \pm e_y \sin(\omega t - k\cdot r + \delta)\ \right] \tag{3.4}$$

Inserting (3.4) into the interaction Hamiltonian (2.4) yields

$$\begin{aligned} E_{\substack{L \\ R}} = &-\mu\cdot(\frac{E_0}{\sqrt{2}})\left[e_x \cos(\omega t + \delta) \pm e_y \sin(\omega t + \delta)\ \right] \\ &-m\cdot(\frac{E_0}{\sqrt{2}})\left[e_y \cos(\omega t + \delta) \mathrm{m} e_x \sin(\omega t + \delta)\ \right] \\ &-\frac{1}{2}Q\cdot(\frac{E_0}{\sqrt{2}})k\left[e_x \sin(\omega t + \delta) \mathrm{m} e_y \cos(\omega t + \delta)\ \right] \end{aligned} \tag{3.5}$$

where $E_o$, ω and δ are the amplitude, angular frequency and the phase of the field, respectively. In (3.5) the origin of the field coordinate, *r*, was chosen as the molecular center from which the multipoles are defined. The electric dipole terms usually dominate for the case of CD, and since the effect of electric dipole term vanishes, the other two terms contribution become important. Writing the interaction Hamiltonians separately for each handedness, gives

$$(H_{Int})_L = -\frac{1}{2}E_o\left[(D(L)\cdot e^L)^+ e^{i(\omega t+\delta)} + D(L)\cdot e^L e^{-i(\omega t+\delta)}\right] \tag{3.6}$$

$$(H_{Int})_R = -\frac{1}{2}E_o\left[(D(R)\cdot e^R)^+ e^{i(\omega t+\delta)} + D(R)\cdot e^R e^{-i(\omega t+\delta)}\right] \tag{3.7}$$

where

$$\begin{aligned} D(L) &= \mu + \frac{1}{2}iQ\cdot k - im \\ D(R) &= \mu + \frac{1}{2}iQ\cdot k + im \end{aligned} \tag{3.8}$$

For unspecified handedness

$$H_{Int} = -\frac{1}{2}E_o\cdot D\cdot e^L e^{-i(\omega t+\delta)} \tag{3.9}$$

By standard semi-classical time-dependent perturbation theory, the time dependent wave function for the molecule interacting with light is

$$\psi = \sum_{l=1}^{\infty} b_l(t)\psi_l \exp\left(\frac{-iE_1 t}{\mathrm{h}}\right) \tag{3.10}$$

where $\psi_l$ and $E_1$ are the wavefunction and energy for the 1 $^{th}$ state of the molecule in the absence of the field. The amplitudes can be expanded perturbatively:

$$b_l(t) = \sum_{n=0}^{\infty} b_l^{(n)}(t) \qquad (3.11)$$

and the time derivative, yields

$$\frac{d}{dt} b_l^{(n)} = \frac{i}{\hbar} \frac{E_o}{2} \sum_{p=1}^{\infty} \left[ (D^{lp}(\xi) \cdot e^{\xi})^{+} e^{i\delta} e^{(\frac{i}{\hbar}(E_{lp}+\hbar\omega)t)} + D^{lp}(\xi) \cdot e^{\xi} e^{-i\delta} e^{(\frac{i}{\hbar})(E_{lp}-\hbar\omega)t} \right] \qquad (3.12)$$

where

$$E_{lp} = E_l - E_p \quad \text{, and } D^{lp}(\xi) = \langle l / D(\xi) / p \rangle \text{ , } \quad \xi = L, R$$

for left -and right- CPL. If a transition occurs from ground state /1> to a discrete excited state /2>, induced by the absorption of light having circular frequency

$$\omega \cong E_{21} / \hbar s \quad , \quad s = 1, 2, 3, \ldots$$

the semi-classical rates of absorption can be obtained by solving eq.(3.12). However, the process becomes more complicated as n and s become large. Equation (3.12) can be solved readily for the dominant resonant term in $b_2^{(n)}$

$$b_2^{(n)} = (-1)^{(n)} e^{-in\delta} \left(\frac{E_o}{2}\right)^n \mu^{(n)} \frac{\left\{ \exp\left[ -(i/\hbar)(n\hbar\omega - E_{21})t \right] - 1 \right\}}{(n\hbar\omega - E_{21})} \qquad (3.13)$$

where

$$\mu^{(n)} = \sum_{p_1} \sum_{p_2} \cdots \sum_{p_{n-1}=1}^{\infty} \frac{D^{2p_{n-1}} \cdot e^L D^{p_{n-1}p_{n-2}} \cdot e^L \cdots D^{p_2 p_1} \cdot e^L D^{p_1 1} \cdot e^L}{(\hbar\omega - E_{p_1 1})(2\hbar\omega - E_{p_2 1}) \cdots [(n-1)\hbar\omega - E_{p_{n-1}}]} \qquad (3.14)$$

Thus the absolute value of $b_2^{(n)}$ squared becomes

$$\left| b_2(n) \right|^2 = 4 \left(\frac{E_o}{2}\right)^{2n} \left| \mu^{(n)} \right|^2 \frac{\sin[\frac{1}{2}\hbar^{-1}(n\hbar\omega - E_{21})t]}{(n\hbar\omega - E_{21})^2} \qquad (3.15)$$

Taking the time derivative of the amplitude square of n-photon absorption gives

$$\Gamma^{(n)} = \frac{d}{dt}\left|b_2^{(n)}\right|^2 \tag{3.16}$$

$$\Gamma^{(n)} = \frac{2}{\mathrm{h}}\left(\frac{E_o}{2}\right)^{2n}\left|\mu^{(n)}\right|^2 \frac{\sin\left[\mathrm{h}^{-1}\left(n\mathrm{h}\omega - E_{21}\right)t\right]}{\left(n\mathrm{h}\omega - E_{21}\right)} \tag{3.17}$$

$\Gamma^{(n)}$ is the absorption rate which is related to the Einstein $B$ coefficient of absorption and the radiant energy per unit area per unit time $I^{(n)}$ and the radiation density $\wp$ (energy per unit volume per unit frequency ) by

$$\Gamma^{(n)} = \wp I^{n-1} B^{(n)} \tag{3.18}$$

This yields the well known multi-photon Einstein absorption equation

$$B^{(n)} = \frac{(2\pi)^n}{\mathrm{h}^2 c^{n-1}}\left|\mu^{(n)}\right|^2 \tag{3.19}$$

Using quantum electrodynamics theory to describe the effect of handedness where the fields of radiation $E(r)$ and $B(r)$ for the electric and magnetic fields are represented by creation and annihilation operators for photons of mode λ with frequency $\omega_\lambda$, and for simplifying the equations, modes are denoted by wave vector $k$

$$E(r) = i\sum_k \left(\frac{2\pi \mathrm{h} c k}{V}\right)^{1/2}\left[(a^L(k)e^L(k) + a^R(k)e^R(k))e^{ik\cdot r} - (a^{L+}(k)e^{-L}(k) + a^{R+}(k)e^{-R}(k))e^{-ik\cdot r}\right]$$

$$B(r) = i\sum_k \left(\frac{2\pi \mathrm{h} c k}{V}\right)^{1/2}\left[(a^L(k)e^L(k) - a^R(k)e^R(k))e^{ik\cdot r} - (a^{L+}(k)e^{-L}(k) - a^{R+}(k)e^{-R}(k))e^{-ik\cdot r}\right]$$

Such that

$$e^R = e^{-L}$$

The Hamiltonian for the absorption of a circularly polarized photon with wave vector $k$ and handedness $\zeta$ is

$$H = -iD(\zeta).e^{\zeta}a^{\zeta}(k)\left(\frac{2\pi\hbar\omega}{V}\right)^{\frac{1}{2}} \tag{3.20}$$

$$\begin{aligned} D(L) &= \mu + \frac{1}{2}iQ\cdot k - im \\ D(R) &= \mu + \frac{1}{2}iQ\cdot k - im \end{aligned} \tag{3.21}$$

Meath[42] generalized the absorption rate coefficient of linearly polarized light for n-photons

$$B^{(n)} = \frac{(2\pi)^{(n)}}{\hbar^2 c^{n-1}}\left|\mu^{(n)}\right|^2 \tag{3.22}$$

where

$$\mu^{(n)} = \sum_{l_1}\sum_{l_2}\cdots\sum_{l_{n-1}=1}^{\infty}\frac{\mu_{2l_1}\mu_{l_1l_2}\cdots\mu_{l_{n-1}1}}{[(n-1)\hbar\omega - E_{l_1 1}][(n-2)\hbar\omega - E_{l_2 1}]\cdots[\hbar\omega - E_{l_{n-1}1}]} \tag{3.23}$$

$$\mu_{l_1 l_2} = \langle l_1 / \mu / l_2 \rangle \tag{3.24}$$

Later Meath and Power[43] extended the n-photon absorption rates for chiral molecules

$$B^{(n)} = \frac{(2\pi)^{(n)}}{\hbar^2 c^{n-1}}\left|\mu^{(n)}\right|^2 \tag{3.25}$$

where $\mu^{(n)}$ is given by

$$\mu^{(n)} = \sum_{p_1}\sum_{p_2}\cdots\sum_{p_{n-1}=1}^{\infty}\frac{D^{2p_{n-1}}.e^L D^{P_{n-1}p_{n-2}}.e^L\cdots D^{p_2 p_1}.e^L D^{p_1 1}.e^L}{(\hbar\omega - E_{p_1 1})(2\hbar\omega - E_{p_2 1})\cdots[(n-1)\hbar\omega - E_{p_{n-1}1}]} \tag{3.26}$$

We can see clearly that semi-classical theory eq(3.19) and QED eq(3.25) arrive at a similar relationship for the n-photon absorption coefficient $B$.

The differential absorption between left- and right- circularly polarized light was also derived for multiphoton excitations by Power and Thirunamachchandran[44] and showed that the quadrupole moment does not contribute to CD for chiral molecules.

For two photon excitations ($n$ = 2), which was first tackled by Tinoco[45] and Power[46] the difference of Einstein coefficients becomes

$$B^{(2)L} - B^{(2)R} = \frac{4\pi^2}{\mathrm{h}^2 c(\mathrm{h}\omega)^2}(\mu^{21} \cdot \mathrm{Im}\, m^{21} - \mu_z^{21}(\mathrm{Im}\, m^{21})_z)[(\mu^{22} - \mu^{11})^2 - (\mu^{22} - \mu^{11})_z^2] \quad (3.27)$$

where $\mu^{22}$ and $\mu^{11}$ are the permanent electric dipole moments in the two states. It can be seen that the permanent electric dipole moment plays an important rule in the case of two photon CD. In fact, multiphoton CD is non-existent for non-polar molecules.

For $n$=3,Unlike the case for two photon CD, the three-photon dichroism for a two-level system exists without the necessity of a permanent electric dipole moment. Furthermore, Andrews and Thirunamachandran[47] studied the response of chiral molecules by matrix treatment and rotationally averaging in 3-dimensional space.

$$B^{(3)L} - B^{(3)R} = \frac{4\pi^3}{105\mathrm{h}^2 c^2(\mathrm{h}\omega)^4}[(\mu^{21} \cdot \mathrm{Im}\, m^{21})(3\left|\mu^{21}\right|^4 - 16(\mu^{21} \cdot (\mu^{22} - \mu^{11}))^2$$

$$+6\left|\mu^{21}\right|^2\left|(\mu^{22} - \mu^{11})\right|^2 + 8\left|(\mu^{22} - \mu^{11})\right|^4 \quad (3.28)$$

$$+2((\mu^{22} - \mu^{11}) \cdot \mathrm{Im}\, m^{21})(\mu^{21} \cdot (\mu^{22} - \mu^{11}))(-\left|\mu^{21}\right|^2 + 2\left|(\mu^{22} - \mu^{11})\right|^2)]$$

The three-photon CD in the absence of a permanent electric dipole moment, $(\mu^{22} - \mu^{11}) = 0$, reduces to

$$B^{(3)L} - B^{(3)R} = \frac{4\pi^3}{35\mathrm{h}^2 c^2 (\mathrm{h}\omega)^4}[(\mu^{21} \cdot \mathrm{Im}\, m^{21})\left|\mu^{21}\right|^4] \tag{3.29}$$

It worth mentioning here that Meath and Power[43] managed to generalize all previous results and deduced the circular dichroism of the n-photon absorption of chiral molecules.

Resonantly enhanced multiphoton ionization circular dichroism (REMPICD) is experimentally determined by recording the ionization intensities due to left and right circularly polarized light that can be explicitly expressed in the averaged parameter (dissymmetric g factor) as

$$g = \frac{I_L - I_R}{(I_L + I_R)/2} \tag{3.30}$$

where $I_L$ and $I_R$ are the ionization intensities due to left –and right- circularly polarized light, respectively.

Note that, as defined, the dissymmetric g factor is twice that of the Kuhn anisotropy factor that is mathematically defined as

$$g = \frac{Y^{LCP} - Y^{RCL}}{Y} \tag{3.31}$$

where $Y$ is the sum of the ionization yields for left circularly ($Y^{LCP}$) and right circularly ($Y^{RCP}$) polarized light.

Experimental Setup

To obtain the first REMPI spectrum, the third Harmonic output (λ=355 nm) of a seeded Q-switch Nd:YAG (Continum, Powerlite 9000) operating at 10 Hz was used to pump a dye laser (Quanta-Ray DCR-1) using Exalite 398 dye solution in *p*-dioxane at 2 x $10^{-4}$ M concentration for both oscillator and amplifier parts, this dye selection was based on the wavelength range (393 – 403 nm) of OPO laser light produced when pumped by the 355 nm output pump laser. Both pulsed lasers used are widely tunable, with high peak power, and narrow line width. The 6 ns pulsed laser width with pulse-to-pulse stability of less than 3% when operated in the seeded mode, was used to ionize *R*3MCP gaseous sample. *R*3MCP was purchased from Sigma Aldrich with 99% purity and used without any further purification.

The estimated 3 Torr sample vapor pressure was seeded with 450 Torr helium, and the gas mixture was injected into the vacuum chamber via an ultrasonic expansion through a pulsed nozzle valve (RM Jordan Company Inc.). The pulsed valve has a nominal gas pulse duration of 60 microseconds and maximum repetition rate of 10 Hz with standard nozzle diameter of 0.5 mm (see figure 3.1). Employing a supersonic pulsed valve is important to molecular spectroscopy due to the dramatic cooling of the translational ($T_{tra}$≈ 1 °K), rotational ($T_{rot}$≈ 3 °K), and vibrational ($T_{vib}$≈ 30 °K) temperatures[48,49] of the molecules entrapped in the expanding gas jet. As a result, molecular spectra of molecules under observation are simplified significantly and high resolution spectroscopic measurements can be made while maintaining improved signal to noise ratio.

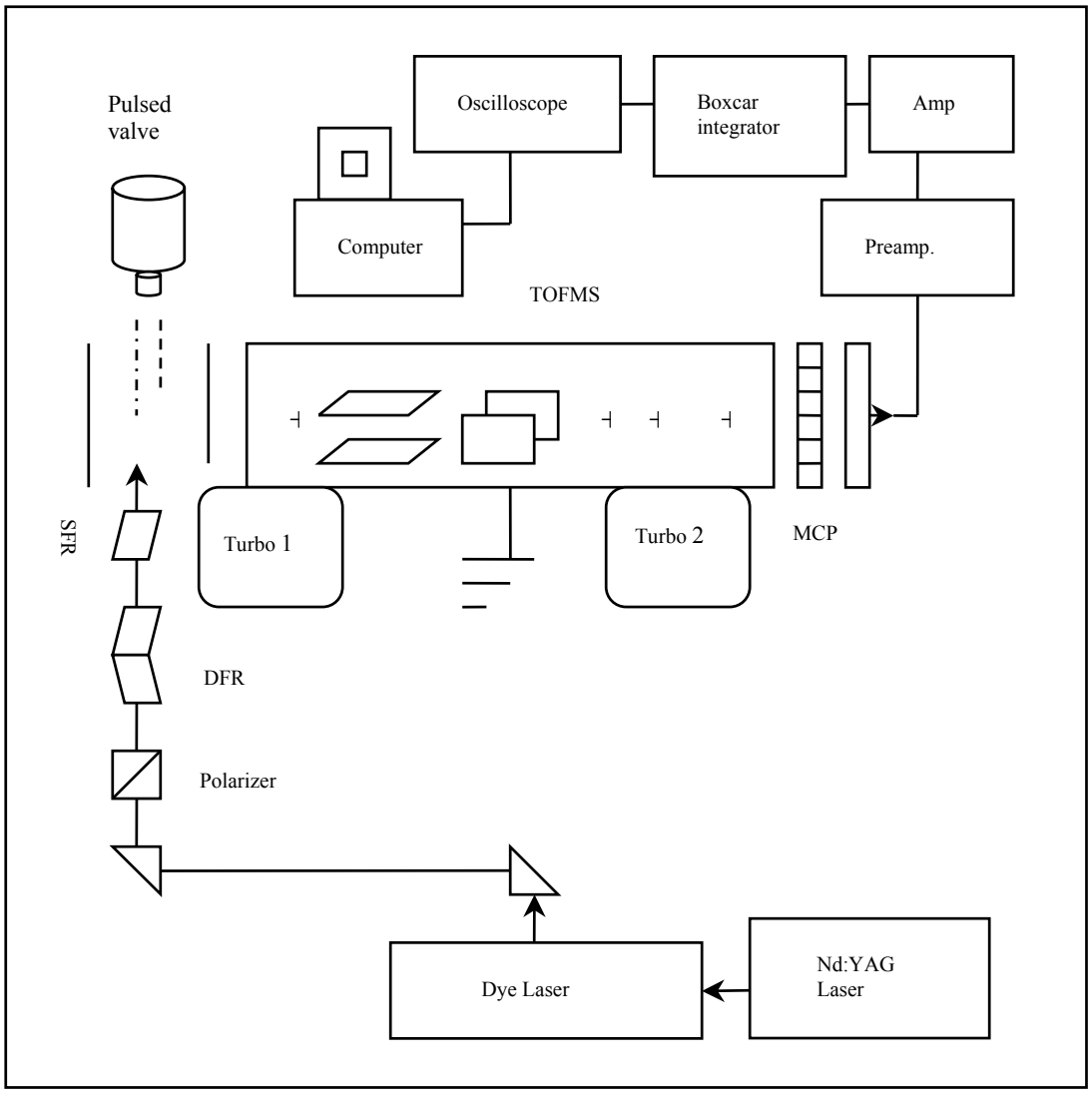


Figure 3.1 Simple sketch of the Resonantly Enhanced Multi-Photon Ionization Circular Dichroism (REMPICD) Experimental setup.

A two meter Time- of- Flight (TOF) mass spectrometer was employed to identify and record the positive ions produced in REMPI. The time of flight (*T)* of positive ions is related to its mass (*m*) through the simple classical mechanics relation ($T = \sqrt{(m/2E)}$l ), where *E* is the ion produced kinetic energy and l is the path length of the ions. Three roughing mechanical pumps were used to reduce the pressure inside the chamber to 10 mTorr, consequently, followed by a 200 L/s Turbo molecular pump was used to evacuate the main flight tube while a 500 L/s Turbo Molecular pump was directly below the pulsed nozzle in the interaction region, in order pump the main part of the molecular beam.

The pressure in the main chamber during operation was ~5 x $10^{-7}$ Torr. Positive ions produced via (2+1) REMPI[50] through the 3s Rydberg intermediate state were extracted by a high voltage and detected by dual microchannel plate detector. These two channel plates were set in back- to-back position at an angle so that there is a reduction in backward reflection of ions.[51]The direct signal intensity was first fed into an Ortec 474 Timing Filter Amplifier to increase signal intensity and also integrate the signal for a period of time (~ 25 ns), and then the output signal was integrated and processed with (SRS 250) boxcar integrator (Stanford Research System, SRS 250) so that only the voltage corresponding to the positive *R*3MCP ions was recorded and averaged over a certain number of voltage shots. The output voltage signal was also monitored with a digital oscilloscope, and the gated voltage reading was introduced to a computer acquisition card and processed by data acquisition software created by labview experimental data collection software.

Results and Data Analysis

The biggest peak in the MPI spectrum corresponds to the (2+1) REMPI[50] ion fragments of the equatorial conformer (see figure 3.2). All three photons involved have the same wavelength (λ=397.5 nm), thus the first two photons excited the molecule to the 3s state while the third one resulted in ionization. The mass spectrum shown in figure 3.3, show very little of the parent ion ($C_6H_{10}O^+$). This indicates that the ionization was followed by rapid dissociation by absorption of a fourth photon. The experimental apparatus was then modified to record the REMPICD. The output laser was passed through a combination of Glan-Taylor polarizer to first obtain highly purified linearly- polarized light. A rotatable double Fresnel rhomb was used to rotate the linearly polarized light + 45° or - 45° relative to the optical axis to produce right- and left- circularly polarized light, respectively. A Single Frensel rhomb was then used to generate circularly polarized light. Before recording any data, the purity of CPL was checked by using a sample of Xe gas and since that the electronic levels are well known for Xe the (3+2) REMPI[52] signal disappears if light was totally circularly polarized. The 6s intermediate state is forbidden in three photon absorption using CPL.

In order to enhance the signal to noise ratio in the measurements and to delineate the very small signal difference using alternately right- and left-circularly polarized light, the integrated signal intensity (peak area) of one mass-selected positive ion signal or electron signal was recorded and averaged for 1000 shots using

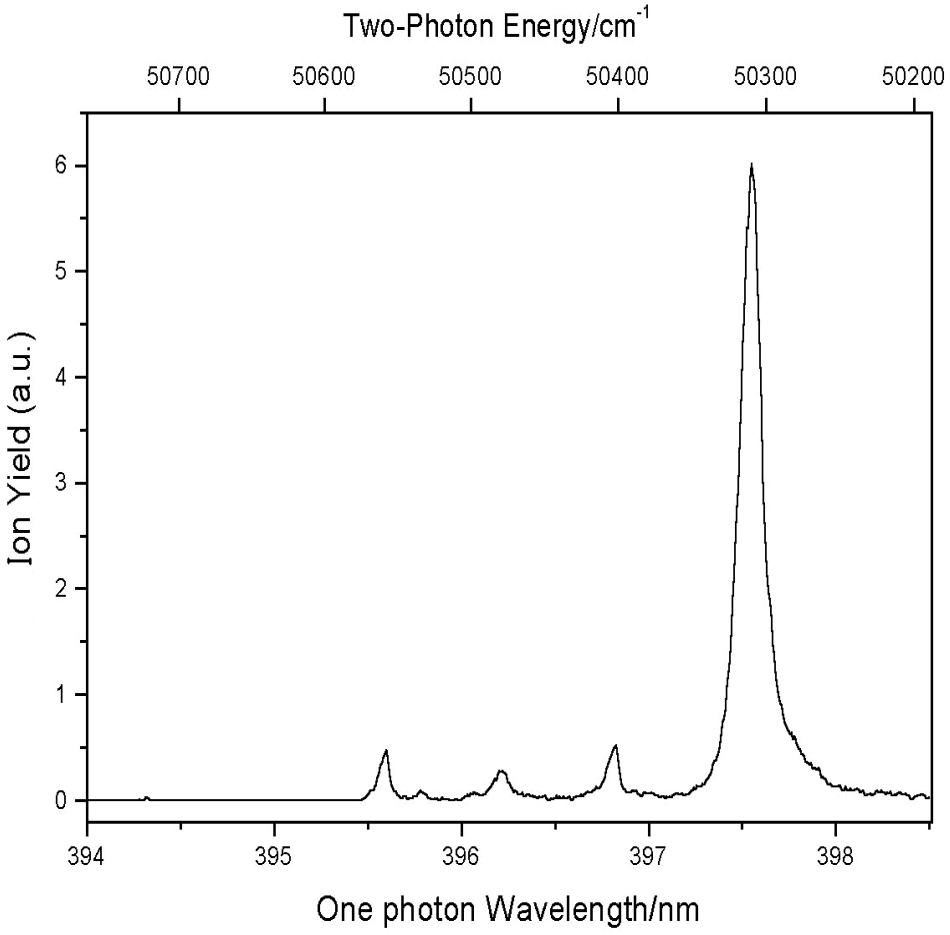


Figure 3.2 (2+1) REMPI spectrum of R3MCP for nozzled-jet expanded molecular beams of the $n \rightarrow$ 3s transition, the strong peak to the right corresponds to 0-0 vibronic band origin of the equatorial form.

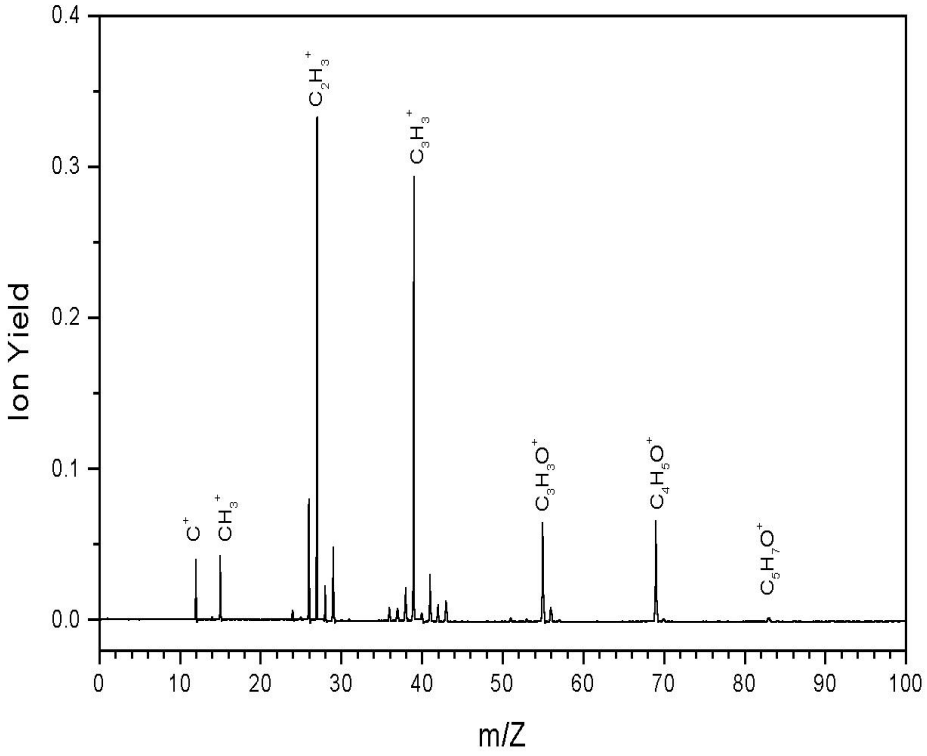


Figure 3.3 (2+1) REMPI time of flight mass spectrum of *R*3MCP via two-photon Excitation of 3s Rydberg state at 397.5 nm.

an Agilent Infiniium 500 MHz oscilloscope. The mean value was used as the final signal intensity. The same measurement was repeated 30 times with one sample and then changed to another sample immediately without the change of any other experimental conditions. Setting the laser wavelength at the two-photon resonance with the most intense n→3s 0-0 transition, the REMPI signal corresponding to the mass 39 cation intensity was recorded using LCPL and RCPL. Figure 3.4 shows the signal intensity after being normalized by the average signal $(I_L+I_R)/2$, where $I_L$ and $I_R$ are the original intensity using LCPL and RCPL excitation, respectively.

From this figure, one can see that signals using LCPL are always larger than those using RCPL for *R*-(+)-3-methylcyclopentanone. The average g factor for 30 runs for 3MCP is 1.62%. Figure 3.5 exhibits the distribution of 30 runs of both LCPL and RCPL for *R*3MCP versus normalized intensities, which shows two Gaussian distributions (solid lines). Identical experiments were carried out using a racemic mixture of 3-methylcyclopentanone. Figures 3.6 and 3.7 show normalized signals using LCPL and RCPL excitation for racemic 3-methylcyclopentanone[53] and the distribution of combined ionization intensities of left -and right- CPL, respectively. The data show that there is a statistical variation of $I_L$-$I_R$ about zero, i.e., sometimes $I_L>I_R$ and sometimes $I_L<I_R$, which is definitely different from the case for the resolved enantiomer($I_L>I_R$). The averaged g factor for 30 runs is +0.12 ±0.2 %. If this is considered as background introduced by a systematic error, then the 2+1 REMPI CD[53] for *R*-(+)-3-methylcyclopentanone can be taken to be 1.5 ± 0.5%(Binomial distribution).

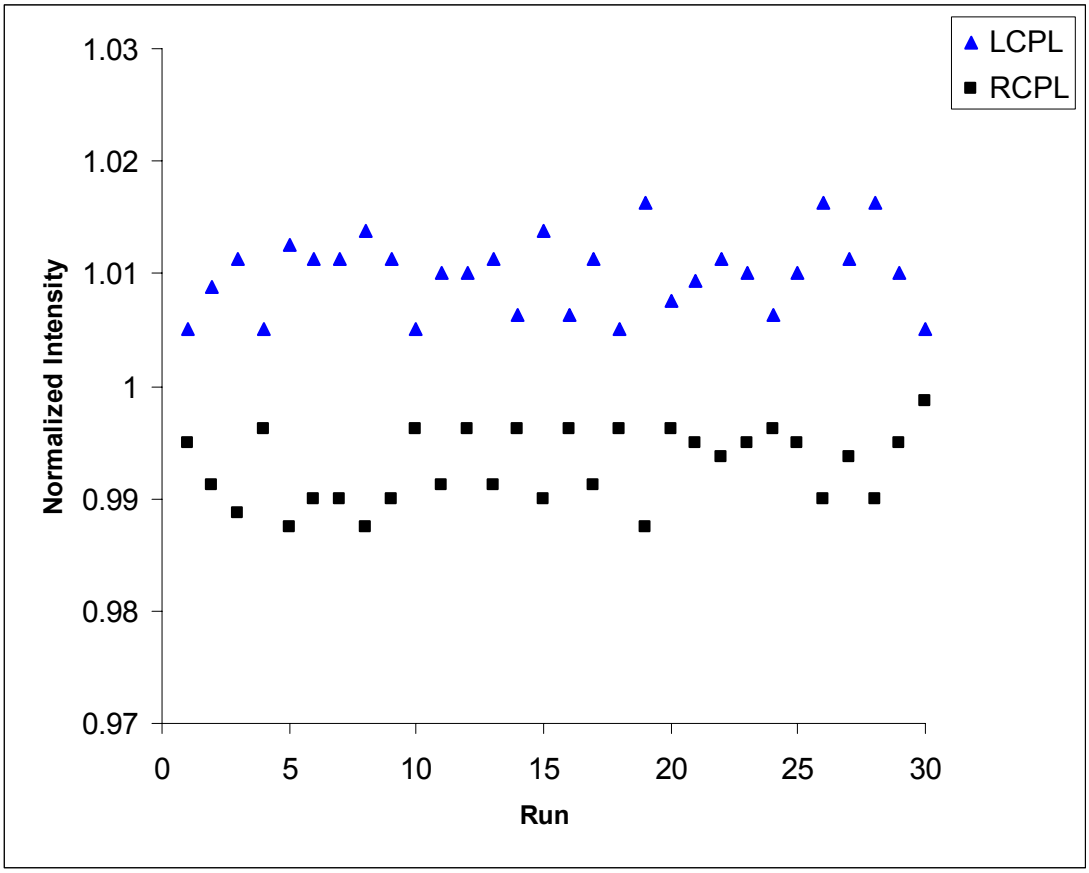


Figure 3.4 Signal intensities of (2+1) REMPICD for *R*-(+)-3-methylcyclopentanone using left and right CPL at 397.5 nm, signal intensity was normalized with $(I_L+I_R)/2$, $C_3H_3^+$ was recorded in experiment. LCPL, left-hand circularly polarized light; RCPL, right-hand circularly polarized light.

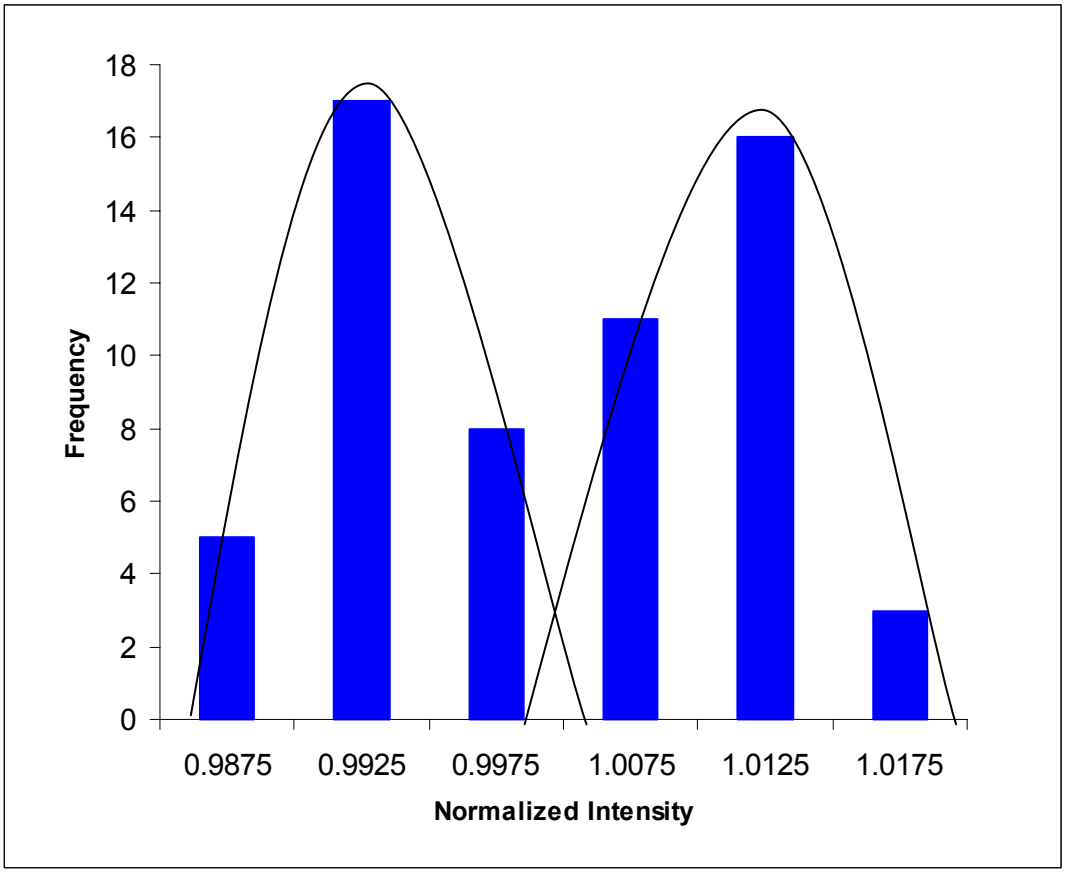


Figure 3.5 Frequency of occurrence of number of runs due to combined left and right circularly polarized light ionization versus normalized intensity of 0.005 interval for *R*3MCP enantiomer sample using REMPICD method, the trendline curve follows Gaussian normal distribution.

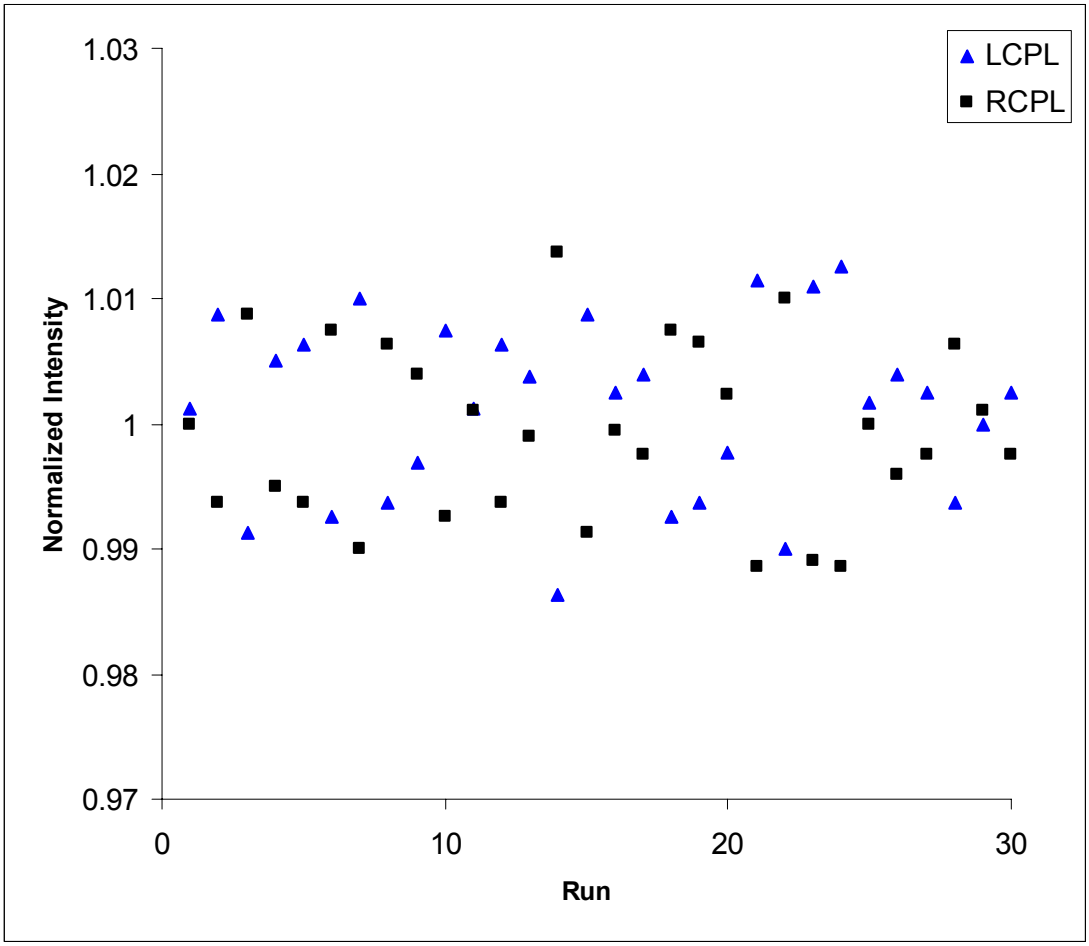


Figure 3.6 Normalized intensities of REMPI for racemic 3-methylcyclopentanone using different circularly polarized light excited at 397.5 nm, $C_3H_3^+$ was recorded in experiment.

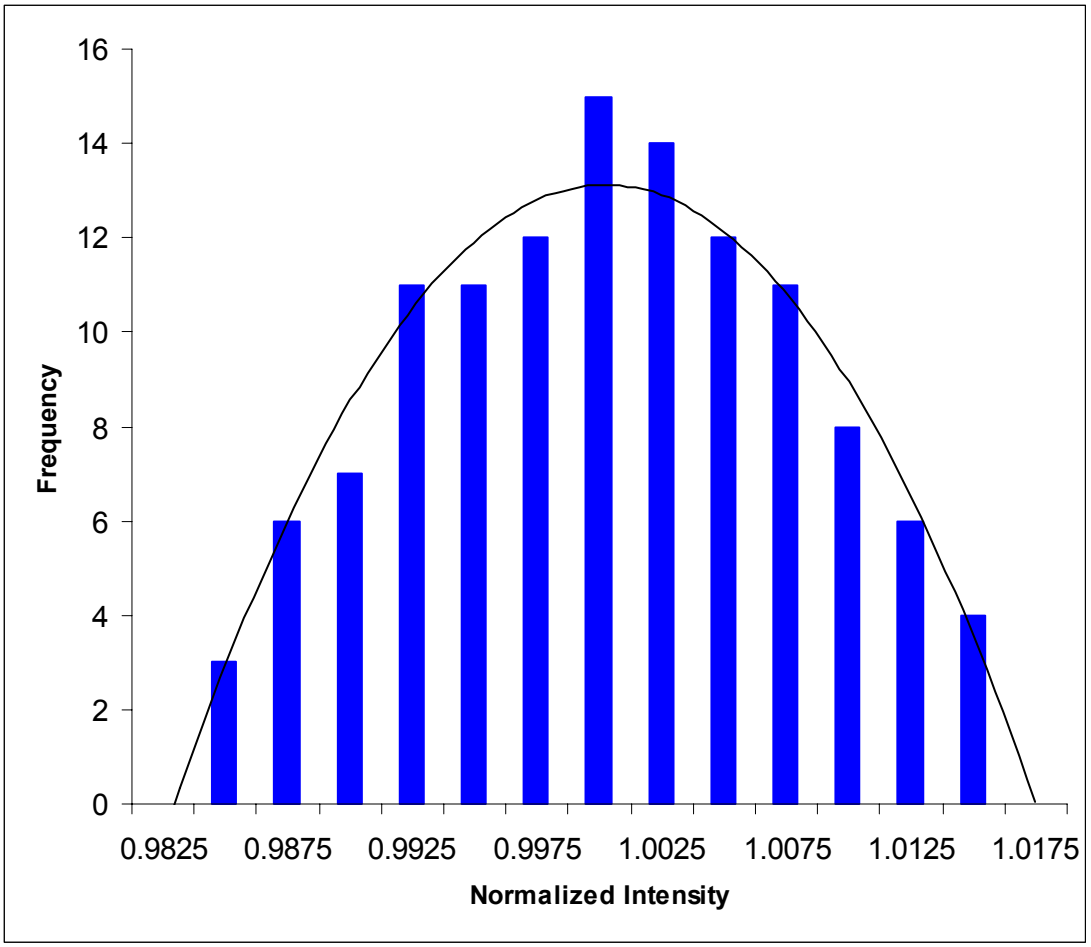


Figure 3.7 Frequency of occurrence of number of runs due to combined left and right circularly polarized light ionization versus normalized intensity of 0.005 interval for Racemic 3MCP sample using REMPICD method, the trendline curve follows Binomial normal distribution.

Summary and Conclusion

In summary, Circular Dichroism of (2+1) resonantly enhanced multi-photon ionization of nozzled-jet expanded molecular beams of *R*3MCP enantiomer and racemic mixture of 3-methylcyclopenatnone was studied; the (2+1) multi-photon ionization spectrum of *R*3MCP for of the $n \rightarrow 3s$ transition was first recorded corresponding to 0-0 vibronic band origin of the equatorial conformer. Other CD studies of conformations *R*3MCP conformation will be an extensively reported in the next chapter.

The REMPI mass spectrum was obtained using a linear time- of- flight mass spectrometer. It was found that the intense laser power produced significant fragmentation of parent ions immediately following the initial ionization process. The REMPI signal corresponding to the mass 39 cation intensity was recorded using LCPL and RCPL excitation, respectively. To determine the g factor the signal intensities were normalized to $(I_L+I_R)/2$. The (2+1) REMPICD signal for *R*3MCP enantiomer was found to be opposite in sign to that of the resonance intermediate one- photon step but is of the sign as that corresponding to the one photon step and that of the one- photon step into the continuum (ionization) transition,[53] this suggests that the REMPICD is primarily determined by both the initial step and the continuum. The observed CD is significant (g ~ 1.5 %) and approximately three times larger than that corresponding at the $n \rightarrow 3s$ one photon CD. The Kuhn anisotropy factor is + 0.75% due to signal fluctuations between left and right CPL as

a direct consequence to laser power fluctuation. Analysis of data for over 30 runs was necessary to obtain an accurate g factor value.

Measuremnts of the CD for the racemic (the ratio of *R*3MCP: *S*3MCP is 50:50) mixture (2+1) REMPICD was significantly small and considered as background effect, as expected for optically active medium that contain equal numbers of opposite enantiomers. The statistical distribution for 30 runs frequency of occurrence as a function of normalized intensity with 0.005 interval of REMPICD data of racemic 3MCP and *R*3MCP shows a Gaussian distribution. A bell-shaped symmetry for the distribution of signals for R-and L- CPL was seen for racemic 3MCP. The distribution of data about ~ 1 was somewhat larger than these observed for the attributed resolved *R*3MCP. This effect is attributed to the signal fluctuations due to the small number of ions produced in each laser pulse. We estimate that ~ 10-50 ions are produced in each laser volume. Under these assumptions this variation of ions (standard deviation) is expected to be in the order of $\sqrt{10}$ to $\sqrt{50}$.

Throughout this study, only one enantiomer (*R*3MCP) was studied, due to its availability. Unfortunately, the other enantiomer, *S*-(-)-3-methylcyclopentanone was not commercially available. We collaborated with Dr. Buchwald's group at Massachusetts Institute of Technology (MIT) to make this enantiomer, but all attempts to produce a sufficiently pure sample failed. It is expected that *S*3MCP will show equal in magnitude but opposite in sign g factor with signal intensities due to right CPL higher than that for left CPL ($I_{RCPL} > I_{LCPL}$). In this regard, future studies should include molecules in which both enantiomers could be studied.

# CHAPTER IV
# SOLVENT AND TEMPERATURE EFFECT ON DISTRIBUTION OF *R*3MCP CONFORMERS

## Introduction

Conformers are defined as different structures of the same enantiomer. The conformer population for a given enantiomer is of particular interest due to its wide applications in the biochemistry and pharmaceutical industry. Previously, conformational analysis of five member ring ketones has been investigated by employing different spectroscopic techniques such as Nuclear Magnetic Resonance NMR[54], Infrared absorption[55,56], electron diffraction[57], the Vibrational Circular Dichroism.[56] However, Electronic Circular Dichroism CD, which is defined as the differential absorption between left -and right- circularly polarized light, furthermore, is widely considered as one of the most efficient investigative tools to probe chirality for molecules that lack a plane of symmetry.

Djerassi et al.[58- 65] performed the first temperature dependent circular dichroism measurements for various dissymmetric chromophres. Saturated ketones are of particular interest to scholars due to their significant optical activity. CD effects are of the order of $10^{-2}$-$10^{-4}$ of the total absorption signal are observed near the ultraviolet $n\rightarrow\pi^*$ transition band. Ketones are known to exist in most living substances as well as many natural products such as steroids and alkaloids. Solvents are well-known to influence the chiral characteristics as well as their chemical and biological interactions. Optical activity studies in solutions are important since most biologically important processes occur in the solution phase. Optical activities of

solutes of permanent electric dipole moment in different solvents are sensitive to the polarity and nature of the solvent in three aspects.

Firstly, there is a significant effect on the CD signal in rigid chiral molecules for the carbonyl $n \rightarrow \pi^*$ transition when measured in different achiral solvents[66,67], which is due to the alteration of the net dissymmetry as a direct result of the association of solvent to the solute by hydrogen bonding and electrostatic forces. Unlike rigid chiral molecules, the saturated ketones like *R*-(+)-3-methylcyclopentaone are found to change conformer population ratio between two dominantly equatorial-methyl and axial-methyl out of possible five[68] by varying the temperature of the sample solution.

Kim and Baer[69] used the MPI technique in order to determine the conformer energy difference between equatorial and axial conformational isomers of 3MCP in the gas phase to be $\Delta H° = 4.97 \pm 0.59$ kJ/mol. The temperatures in these experiments were not well characterized. Later He[56] et. al. used a temperature dependent infrared absorption method to determine conformer population and energy difference in which they concluded $\Delta H° = 4.84 \pm 0.08$ kJ/mol. Secondly, a wavelength shift for the $n \rightarrow \pi^*$ transition band can be either hypsochromic (producing blue shift) with increasing solvent polarity. This is mainly caused by electrostatic interactions such as, hydrogen bonding, dipole-dipole and dipole-induced dipole interactions. The mechanism of such blue shift can be explained as an adaptation in the solvent shell orientation to the electrostatic interactions in the ground state. However, since the reorientation process is slower than the excitation process, the excited state solute is surrounded by the solvent shell and was modified accordingly with the ground state

interactions. Consequently, the cross section of the interaction of the solvent shell with the ground state (*n*) is higher than that for the excited state, π*, which causes an increase in the excitation energy.[70]

In other solvents the shift may be Bathochromic (or red) as a result of the dispersion forces such as Van Der Waals such that the excited state (π*) is less dipolar but more polarizable than the ground state. During the excitation process one *n*-electron is promoted from a nonbonding orbital on the oxygen atom to an antibonding π* orbital, consequently this electron will be delocalized over the carbonyl group.[71] One further observed solvent effect is the gradual smearing out of the CD spectra. Ketones are known to show a well-defined vibrational band structure which is clearly seen in the gas phase CD spectrum. However, as the solvent polarity increases the occurrence of such fine structure decreases.[66]

Temperature dependent circular dichroism measurements have been employed to determine the conformer population and energy difference for different ketones by observing the significant changes on the CD signal for the $n \rightarrow \pi^*$ transition. Solvents can affect conformational equilibria for ketones, i.e R3MCP, since the Gibbs free energy difference between conformational isomers are relatively small(ca. 0-13 kJ/mol),[72] as a comparative example to the challenge of determining conformers energy difference in isomers, it is well-known that hydrogen bonding strength in water is ~ 492 kJ/mol.

Solute-Solvent Interactions Theory

In general, solutions are homogeneous liquid phases of matter consisting of more than one substance in variable ratios. By convention, the component which is in excess is called the solvent and the minor component is termed the solute. Due to the fact that solute – solvent interactions are too strong to be treated by the laws of the kinetic theory of gases, yet too weak to be treated by the laws of solid state physics, the solvent is neither an indifferent medium in which the dissolved material diffuses in order to distribute itself evenly and randomly, nor does it posses an ordered structure resembling a crystal lattice.[71]

Solute-solvent interactions are classified as intermolecular forces which are defined as those forces which can occur between closed shell molecules. These are also called Van der Waals forces, due to the similarity in its non – ideal behavior to the real gases. In addition to the hydrogen bonding, intermolecular forces are usually classified into different categories; directional, induction, and dispersion forces. In order to study the R3MCP-solvent interaction, it is more comprehensive to understand all types of solute – solvent interactions

Solute-Solvent Interaction type I: Dipole-Dipole Forces

When two dipole molecules are optimally oriented with respect to one another at a distance *r,* then the force of attraction is proportional to $1/r^3$. A possible rearrangement is the anti-parallel arrangement of dipoles. Unless the dipole molecules are significantly voluminous, the second arrangement is the more stable. These two situations exist only when the attractive energy is larger than their thermal

energies. Consequently, the thermal energy will prevent the dipoles from optimal orientation. If all possible orientations are equally probable, in other words the dipoles correspond to a freely rotating molecule, then attraction and repulsion compensate each other.[71] In summary, the dipole orientations cause a strongly dependent interaction energy as

$$U_{dipole-dipole} = \frac{-1}{\left(4\pi\varepsilon_{\mathrm{O}}\right)^2} \cdot \frac{2\mu_1^2 \cdot \mu_2^2}{3k_B \cdot T \cdot r^6} \tag{4.1}$$

where $\mu_1$ and $\mu_2$ are the electric dipole moments, and $k_{\mathrm{B}}$ is the Boltzmann constant. As the temperature increases, the dipole-dipole interaction energy becomes less negative until at a very high temperature all dipole orientations are equally populated and the potential energy is essentially zero.[71]

Solute-Solvent Interaction type II: Dipole-Induced Dipole Forces

The electric dipole of a molecule possessing a permanent dipole moment $\mu$ can induce a dipole moment in a neighboring molecule. This induced moment always lies in the direction of the inducing dipole. Thus, attraction always exists between the two partners and is temperature independent. The induced dipole moment is

$$\mu_{Ind} = 4\pi \cdot \varepsilon_{\mathrm{o}} \cdot \alpha \cdot E \tag{4.2}$$

where $\varepsilon_{\mathrm{o}}$ is the permittivity of vacuum, α electric polarizability of the molecule and $E$ is the electric field strength. The induced dipole moment is proportional to the polarizability of the apolar molecule experiencing the induction of the permanent dipole. The net dipole-induced dipole energy of interaction for two different

molecules, each possessing a permanent dipole moment $\mu_1$ and $\mu_2$ and polarizabilities $\alpha_1$ and $\alpha_2$, is given by

$$U_{dipole-indueddipole} = -\frac{1}{(4\pi\varepsilon_o)^2} \cdot \frac{[\alpha_1 \cdot \mu_2^2 + \alpha_2 \cdot \mu_1^2]}{r^6} \tag{4.3}$$

Similarly, a charged particle such as an ion introduced into the neighborhood of an uncharged, apolar molecule will distort the electron cloud of this molecule in the same way.[71] The polarization of the neutral molecule will depend upon its inherent polarizability *α,* and on the polarizing field afforded by the ion with charge *ze*. The energy of such an interaction is given by

$$U_{ion-induced-dipole} = -\frac{1}{(4\pi\varepsilon_o)^2} \cdot \frac{(ze)^2 \cdot \alpha}{2r^4} \tag{4.4}$$

Solute-Solvent Interaction type III: Instantaneous Dipole-Induced Dipole Forces

In non-polar molecules and even in atoms, the continuous electronic movement and rearrangements result in a small dipole moment, which can fluctuatingly polarize the electronic system of the neighboring atoms or molecules. This coupling cause the electronic movements to be synchronized[71]in such a way that a mutual attraction results. The energy of such so-called dispersion or London interaction can be expressed as

$$U_{dispersion} = -\frac{1}{(4\pi\varepsilon_o)^2} \cdot \frac{(3\alpha_1 \cdot \alpha_2)}{2r^6} \cdot \left[\frac{I_1 \cdot I_2}{I_1 + I_2}\right] \tag{4.5}$$

where $\alpha_1$ and $\alpha_2$ are the polarizabilities and $I_1$ and $I_2$ are the ionization potentials of the solute and solvent molecules. Equation (4.5) can also be applied to only one substance (neat solute) resulting in

$$U_{dispersion} = -\frac{1}{\left(4\pi\varepsilon_0\right)^2} \cdot \frac{3\alpha^2 \cdot I}{4r^6} \tag{4.6}$$

It should be mentioned here that dispersion forces are significantly short ranged and depend on the inverse sixth power of the distance between interacting molecules ($1/r^6$). Dispersion forces are universal for all atoms and molecules; they are alone responsible for the aggregation of molecules which possess neither free charges nor permanent dipole moments.[71]

Solute-Solvent Interaction type IV: Hydrogen Bonding

Liquids possessing hydroxyl groups or other groups with a hydrogen atom bound to an electronegative atom are strongly associated and have abnormal boiling points. This observation has led to the assumption that a strong intermolecular force must apply. A general definition of the hydrogen bond is when a covalently bound hydrogen atom forms a second bond to another atom. This second bond is referred to as a hydrogen bond. The most important hydrogen bond acceptors (electron pair donors), are the oxygen atoms in alcohols, ethers, and carbonyl compounds (i.e. *R*-(+)-3-methylcyclopenatnone). Since hydrogen bonding occurs only when the hydrogen is bound to an electronegative atom[71] the first assumption concerning the nature of the hydrogen bonding was that it can be described as a dipole-dipole or resonance interaction.

*R*3MCP Conformers Energy Difference Theory

The observed CD signal of R3MCP is believed to result both from the equatorial-methyl and axial-methyl conformers (out of possible five) with different population rates expressed as

$$\Delta\varepsilon_{Obs} = f_E \Delta\varepsilon_E + f_A \Delta\varepsilon_A \tag{4.7}$$

where $f_E$ and $f_A$ are the mole fractions of the equatorial and axial conformers, respectively. Their ratio, equilibrium constant *k*, is related to the Gibbs free energy , G, by

$$\Delta G = -RT \ln k = -RT \ln(f_A / f_E) \tag{4.8}$$

Assuming that the other 3 conformers of R3MCP have infinitesimal contribution to the CD signal we can make the statement

$$f_E = 1 - f_A = 1 - f_E e^{-\Delta G/RT} \tag{4.9}$$

where the mole fractions of the equatorial and axial conformers are given by

$$f_E = \frac{1}{1 + e^{-\Delta G/RT}} \tag{4.10}$$

$$f_A = \frac{e^{-\Delta G/RT}}{1 + e^{-\Delta G/RT}} \tag{4.11}$$

Plugging (4.10) and (4.11) into (4.7) yields

$$\Delta\varepsilon_{Obs}(T) = \frac{\Delta\varepsilon_E}{1 + e^{-\Delta G/RT}} + \frac{\Delta\varepsilon_A e^{-\Delta G/RT}}{1 + e^{-\Delta G/RT}} \tag{4.12}$$

Theoretical extrapolation of above equation for the two asymptotic cases T= 0, ∞ °K is useful to predict the contribution to total CD signal from each conformer.

For T = 0 °K, equation 4.12 gives

$$\Delta\varepsilon_{Obs}(T=0)=\Delta\varepsilon_{E} \tag{4.13}$$

whereas, for T = ∞ °K equation 4.12 yields

$$\Delta\varepsilon_{Obs}(T=\infty)=\frac{\Delta\varepsilon_{E}}{2}+\frac{\Delta\varepsilon_{A}}{2} \tag{4.14}$$

Substituting for (4.13) and (4.14) in (4.12) gives

$$\Delta\varepsilon_{A}=2\Delta\varepsilon(\infty)-\Delta\varepsilon(0) \tag{4.15}$$

Inserting(4.15) into (4.12) to substitute for axial conformer CD signal contribution gives an expression for observed CD signal ( $\Delta\varepsilon_{Obs}$ )

$$\Delta\varepsilon_{Obs}=\frac{\Delta\varepsilon(0)}{1+e^{-\Delta G/RT}}+\frac{(2\Delta\varepsilon(\infty)-\Delta\varepsilon(0))e^{-\Delta G/RT}}{1+e^{-\Delta G/RT}} \tag{4.16}$$

Equation 4.16 cab be arranged as

$$\Delta\varepsilon_{Obs}=\Delta\varepsilon(0)e^{-\Delta G/2RT}\frac{(e^{\Delta G/2RT}-e^{-\Delta G/2RT})}{(e^{\Delta G/2RT}+e^{-\Delta G/2RT})}+\frac{2\Delta\varepsilon(\infty)e^{-\Delta G/2RT}}{(e^{\Delta G/2RT}+e^{-\Delta G/2RT})} \tag{4.17}$$

Equation (4.17) above can also be expressed in more compact form as

$$\Delta\varepsilon(T)=2\Delta\varepsilon(0)\tanh(\frac{\Delta G}{2RT})+\frac{2\Delta\varepsilon(\infty)e^{-\Delta G/2RT}}{(e^{\Delta G/2RT}+e^{-\Delta G/2RT})} \tag{4.18}$$

This equation is essentially identical to that derived by Ballard, Mason and Vane[73] to calculate conformer energy difference for saturated ketones

$$\Delta\varepsilon_{T}=\Delta\varepsilon_{\infty}+(\Delta\varepsilon_{0}-\Delta\varepsilon_{\infty})\tanh(\frac{\Delta H}{2RT}) \tag{4.19}$$

Where $\Delta\varepsilon_{\infty}$ and $\Delta\varepsilon_{0}$ are, respectively, the limiting high-and low-temperature values of the Circular dichroism.

$$\Delta\varepsilon_{T}=\Delta\varepsilon_{\infty}+(\Delta\varepsilon_{0}-\Delta\varepsilon_{\infty})\left[\frac{e^{\Delta H/2RT}-e^{-\Delta H/2RT}}{e^{\Delta H/2RT}+e^{-\Delta H/2RT}}\right] \tag{4.20}$$

Employing basic Algebra

$$\Delta\varepsilon_T = \frac{\Delta\varepsilon_\infty e^{-\Delta H/2RT} + \Delta\varepsilon_0 e^{\Delta H/2RT} - \Delta\varepsilon_0 e^{-\Delta H/2RT} + \Delta\varepsilon_\infty e^{-\Delta H/2RT}}{e^{\Delta H/2RT} + e^{-\Delta H/2RT}} \qquad (4.21)$$

rearranging equation (4.21) above, yields

$$\Delta\varepsilon_T = \frac{2\Delta\varepsilon_\infty e^{-\Delta H/2RT}}{e^{\Delta H/2RT} + e^{-\Delta H/2RT}} + \Delta\varepsilon_0 \tanh\left(\frac{\Delta H}{2RT}\right) \qquad (4.22)$$

Thus equation (4.18) is a more accurate version of that given by Ballard's et. al. (4.22). Also equation (4.18) has the advantage of calculating entropy difference between conformers. All thermodynamic constants mentioned above are related by

$$\Delta G = \Delta H - T\Delta S \qquad (4.23)$$

The Van't Hoff Equation relates the Gibbs free energy ($\Delta G$) to the mole fraction ratio of axial to the equatorial conformers as

$$ln\left(\frac{f_A}{f_E}\right) = -\frac{\Delta H}{RT} + \frac{\Delta S}{R} \qquad (4.24)$$

These Van't Hoff plots will be used later to derive enthalpies and entropies of *R*3MCP in different common solvents with varying polarity.

The slope of Van't Hoff plot will be used to determine a difference in enthalpy or energy between equatorial and axial conformers of *R*3MCP, whereas, the y-intercept represents the ratio of entropy change between the two conformers states to the gas constant.

Temperature Dependent Circular Dichroism of *R*3MCP

*R*3MCP sample was purchased from Sigma Aldrich chemical company and dissolved without further purification in different common solvents with a 2.6 x $10^{-3}$ M concentration. The temperature was controlled and varied depending on the boiling and melting points of each solvent to avoid unrelated effects due to phase changes. A thermocouple inserted into the solution was used to obtain accurate temperature readings. The CD spectrum of *R*3MCP in water (figure 4.1) provides an initial insight into the polar solvent effects on CD transitions. Total "smearing" of the CD spectrum (i.e., no vibrational structure) was observed due to the high polarity of water that will affect and minimize rovibrational degrees of freedom of *R*3MCP. In addition, a solvent shift in molecular electronic transitions such as $n \rightarrow \sigma^*$ ($n \rightarrow 3s$) was observed at the wavelength maximum 193 nm. Whereas the $n \rightarrow \pi^*$ transition occurred at 287 nm exhibited a significant blue shift (-12 nm) and is attributed to water solvent polarity and explained by Franck -Condon effect.[74-79]

Density Functional theory calculations of B3LYP type were used to calculate rotatory and oscillator strengths of *R*-(+)-3-methylcyclopentanone for equatorial and axial conformers separately. The optimized calculations show an approximately equal and opposite Circular Dichroism effect. Of particular interest are the two molecular transitions $n \rightarrow \sigma^*$ corresponding to 163.72 nm and 166.59 nm for equatorial and axial conformers, respectively, and $n \rightarrow \pi^*$ transition corresponding to 299.16 nm and 299.21 nm for equatorial and axial conformers, respectively (see figure 4.2).

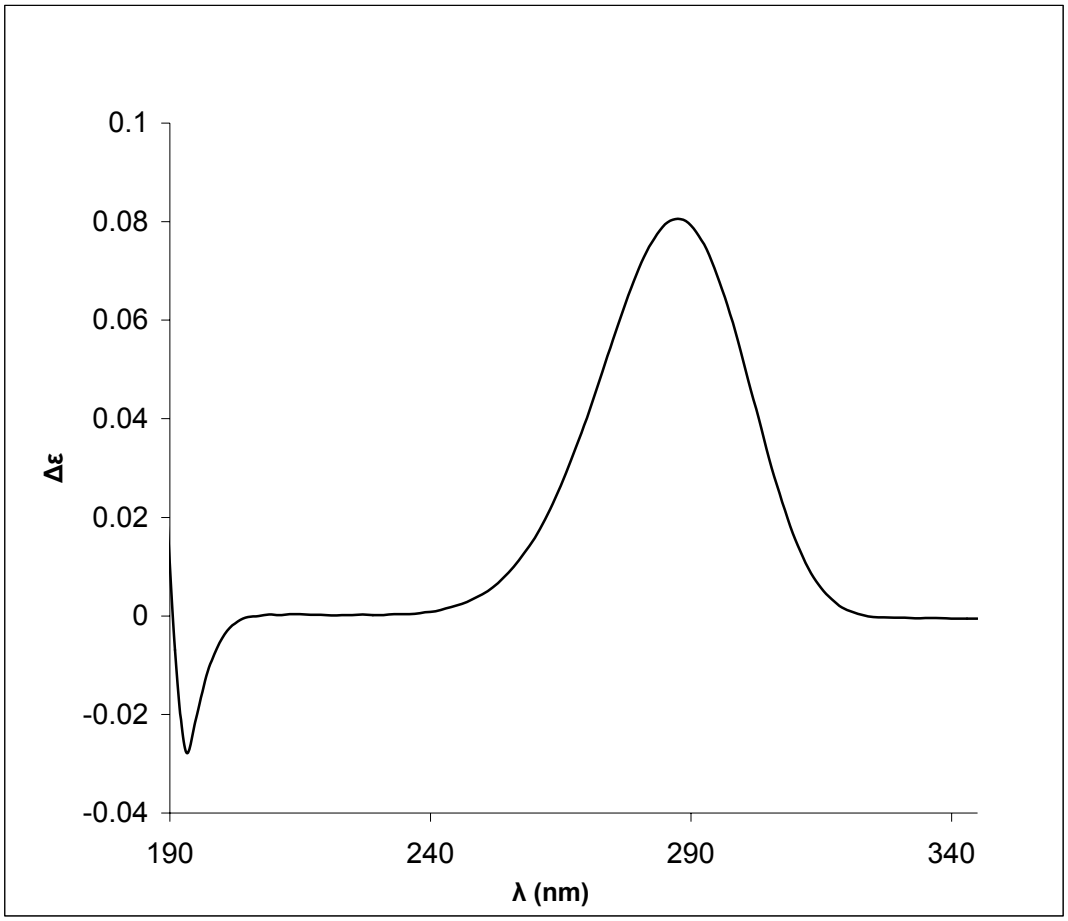


Figure 4.1 CD spectrum of *R*-(+)-3-methylcyclopentanone solution in water at T=25 °C.

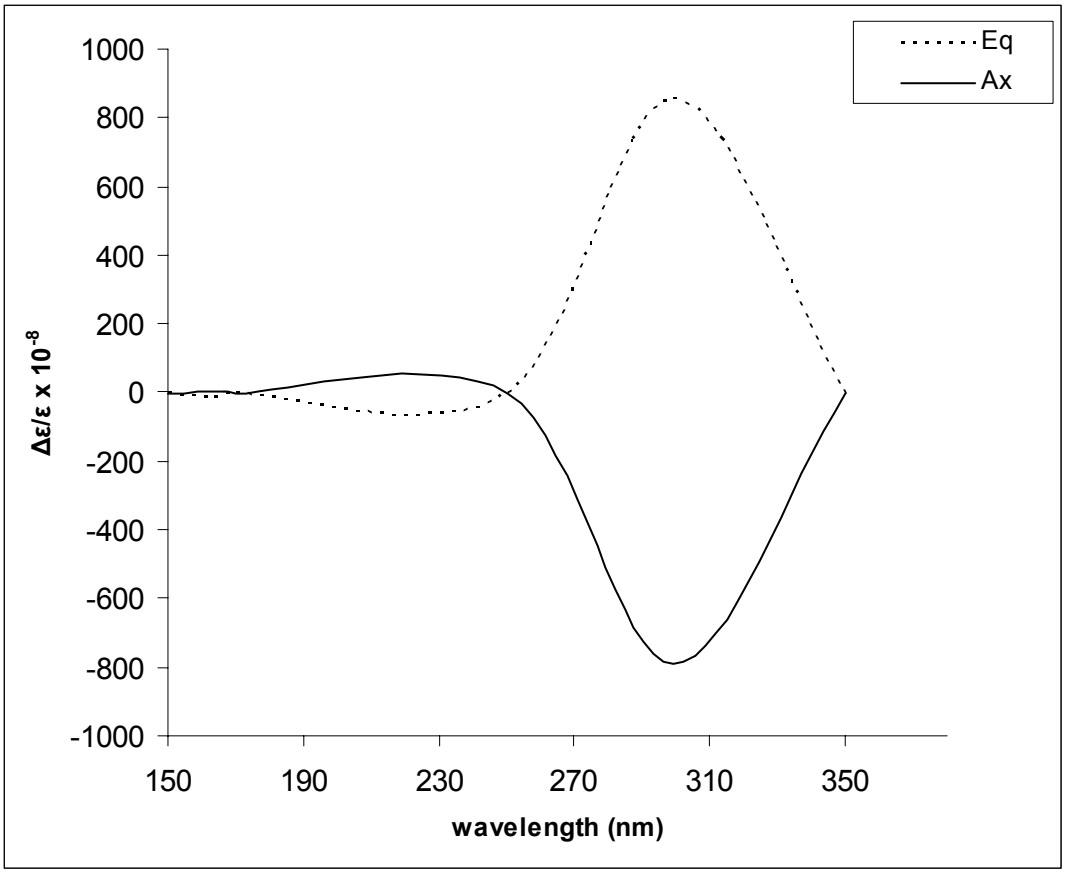


Figure 4.2 Circular Dichroism Calculations of *R*3MCP equatorial and axial methyl conformers using Gaussian03 and employing B3LYP type density functional Calculations with basis set 6-31G*.

Unlike the high energy transition $n \rightarrow \sigma^*$ the low energy transition band $n \rightarrow \pi^*$ was observed to show significant solvent and temperature dependence. Figure 4.3 shows the room temperature CD spectra for *R*3MCP in a few common solvents that exhibit blue and red shifts depending on solvent polarity.

The $E_T(30)$ parameter is a common measure of solvent polarity and was initially proposed by Dimroth and Reichardt[71]. $E_T(30)$ is defined as the transition energy of the dissolved betaine dye in units of (kcal .mol$^{-1}$), the blue shift of the CD spectra corresponding to the $n \rightarrow \pi^*$ transition band for trifluoroacetic acid($\Delta\lambda$= -22 nm), formic acid ($\Delta\lambda$= -14 nm), water($\Delta\lambda$= -10 nm), chloroform($\Delta\lambda$= -4 nm), acetonitrile ($\Delta\lambda$= -3 nm) and methanol ($\Delta\lambda$= -2 nm) solvents. These results can be explained as a result of the hydrogen bonding. Whereas, the red shift of *R*3MCP solution in dimethyl sulfite ($\Delta\lambda$= +20 nm) is due to the solute-solvent Van del waals force. Table 4.1 shows the wavelength maxima positions due to the solvent effects of 34 common solvents including the solvents mentioned above. These data show that molecules of the same molecular group share almost the same wavelength maxima position, i.e. all alcohols except 2-octanol are all in the range (297-300 nm). Solvents of infinitesimal polarity such as, cyclohexane, hexafluorobenzene, benzene and carbontetrachloride have a wavelength maxima between (297-300 nm). However, toluene, benzyl ether and anisole were seen to induce a blue shift of the $n \rightarrow \pi^*$ transition of ~ ($\Delta\lambda$= -10 nm), whereas, solvents that have a dipole- dipole interaction with *R*3MCP like nitriles have a smaller blue shift of ~ ($\Delta\lambda$= -3 nm ). Figures 4.4 – 4.7 show temperature dependence of $n \rightarrow \pi^*$ CD spectra in solvation.

Table 4.1 Observed wavelength absorption maxima for the $n \rightarrow \pi^*$ transition of *R*3MCP in 34 common solvents, and polarity parameters α, β, and π*.[80-82](a) C. Reichardt, Solvents and solvent Effects in Organic Chemistry, 3rd edition, 2003.(b) Y. Marcus, the Properties of Solvents,[83](1998).

| Solvent | $E_T(30)^{a,b}$ (kcal/mol) | Taft Parameters[a,b] | | | $\lambda_{max}$ (nm) |
|---|---|---|---|---|---|
| | | α | β | π* | |
| cyclohexane | 30.9 | | | | 300 |
| benzene | 34.3 | 0.00 | 0.10 | 0.55 | 299 |
| toluene | 33.9 | 0.00 | 0.11 | 0.49 | 310 |
| chlorobenzene | 36.8 | 0.00 | 0.07 | 0.68 | 298 |
| hexafluorobenzene | 34.2 | 0.00 | 0.02 | 0.27 | 297 |
| chloroform | 39.1 | 0.20 | 0.10 | 0.58 | 295 |
| carbon tetrachloride | 32.4 | 0.00 | 0.10 | 0.21 | 300 |
| tetrahydropyran | 37.4 | 0.00 | 0.55 | 0.55 | 299 |
| anisole | 37.1 | 0.00 | 0.32 | 0.70 | 309 |
| benzyl ether | 36.3 | 0.00 | 0.41 | 0.80 | 309 |
| acetonitrile | 45.6 | 0.19 | 0.40 | 0.66 | 296 |
| propionitrile | 43.6 | 0.00 | 0.37 | 0.64 | 297 |
| butyronitrile | 42.5 | 0.00 | 0.45 | 0.63 | 297 |
| valeronitrile | 42.4 | 0.00 | | 0.63 | 297 |
| adiponitrile | | | | | 296 |
| crotononitrile | | | | | 297 |
| glutaronitrile | | | | | 296 |
| trimethylacetonitrile | | | | | 298 |
| dimethyl sulfoxide | 45.1 | 0.00 | 0.76 | 1.00 | 297 |
| dimethyl sulfite | 41.5 | 0.00 | 0.45 | 0.7 | 319 |
| formic Acid | 57.7 | 1.23 | 0.38 | 0.65 | 285 |
| acetic acid | 55.2 | 1.12 | 0.45 | 0.64 | 290 |
| trifluoroacetic acid | | 2.38 | | 0.50 | 277 |
| methanol | 55.4 | 0.98 | 0.66 | 0.60 | 297 |
| ethanol | 51.9 | 0.86 | 0.75 | 0.54 | 298 |
| 2-propanol | 48.4 | 0.76 | 0.84 | 0.40 | 300 |
| isobutyl alcohol | 48.6 | 0.79 | 0.84 | 0.40 | 299 |
| 2-butanol | 47.1 | 0.69 | 0.80 | 0.40 | 300 |
| t-butanol | 43.0 | 0.42 | 0.93 | 0.41 | 299 |
| n-amyl alcohol | 49.1 | 0.84 | 0.86 | 0.40 | 299 |
| 2-Octanol | | | | | 310 |
| cyclopentanol | 42.0 | | | | 300 |
| phenethyl alcohol | 46.7 | | | | 298 |
| water | 63.1 | 1.17 | 0.47 | 1.09 | 287 |

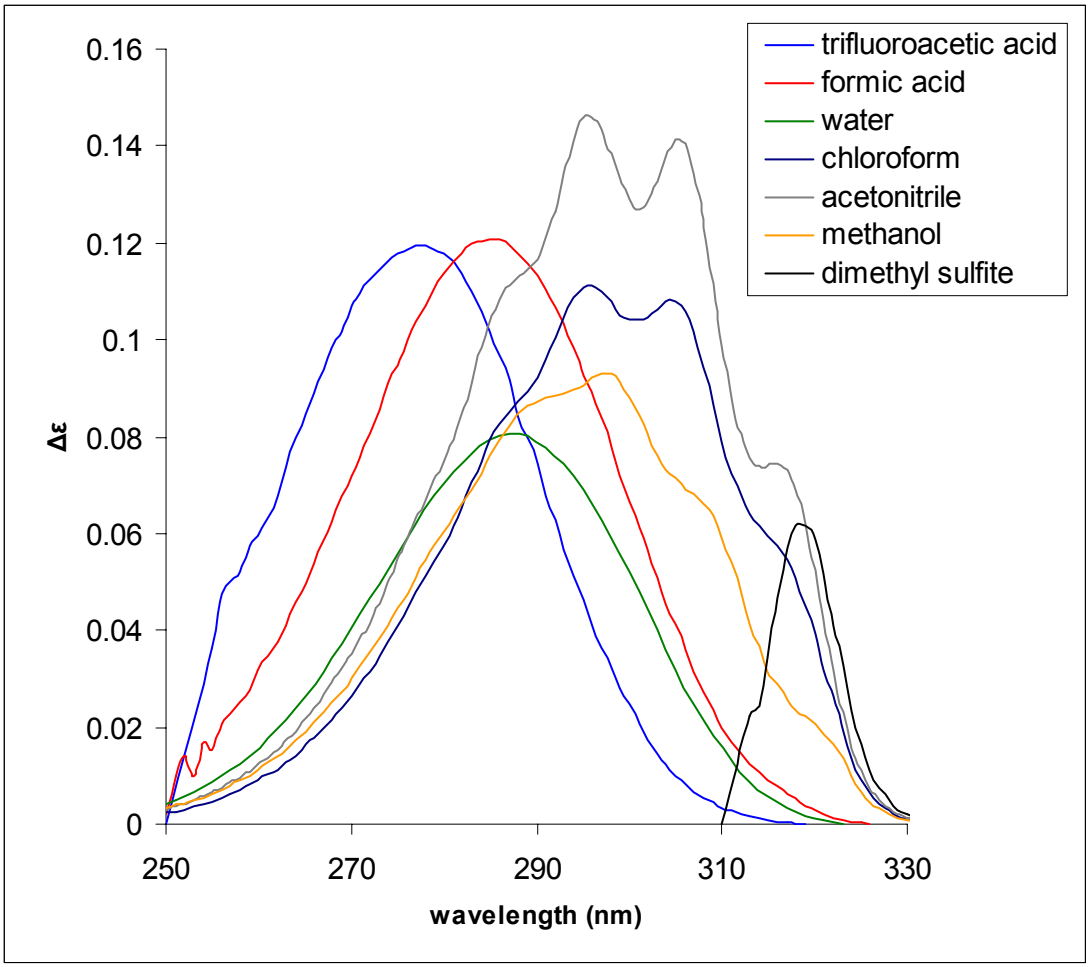


Figure 4.3 Room Temperature CD spectra for *R*3MCP $n \rightarrow \pi^*$ transition band at max. wavelength peak in solvation; trifluoroacetic acid ($CF_3COOH$) at 277 nm, formic acid ($HCOOH$) at 285 nm, water ($H_2O$) at 287 nm, chloroform ($CHCl_3$) at 295 nm, acetonitrile($C_4H_3N$) at 296 nm, methanol($CH_3OH$) at 297 nm and dimethyl sulfite($C_2H_6O_3S$) at 319 nm.

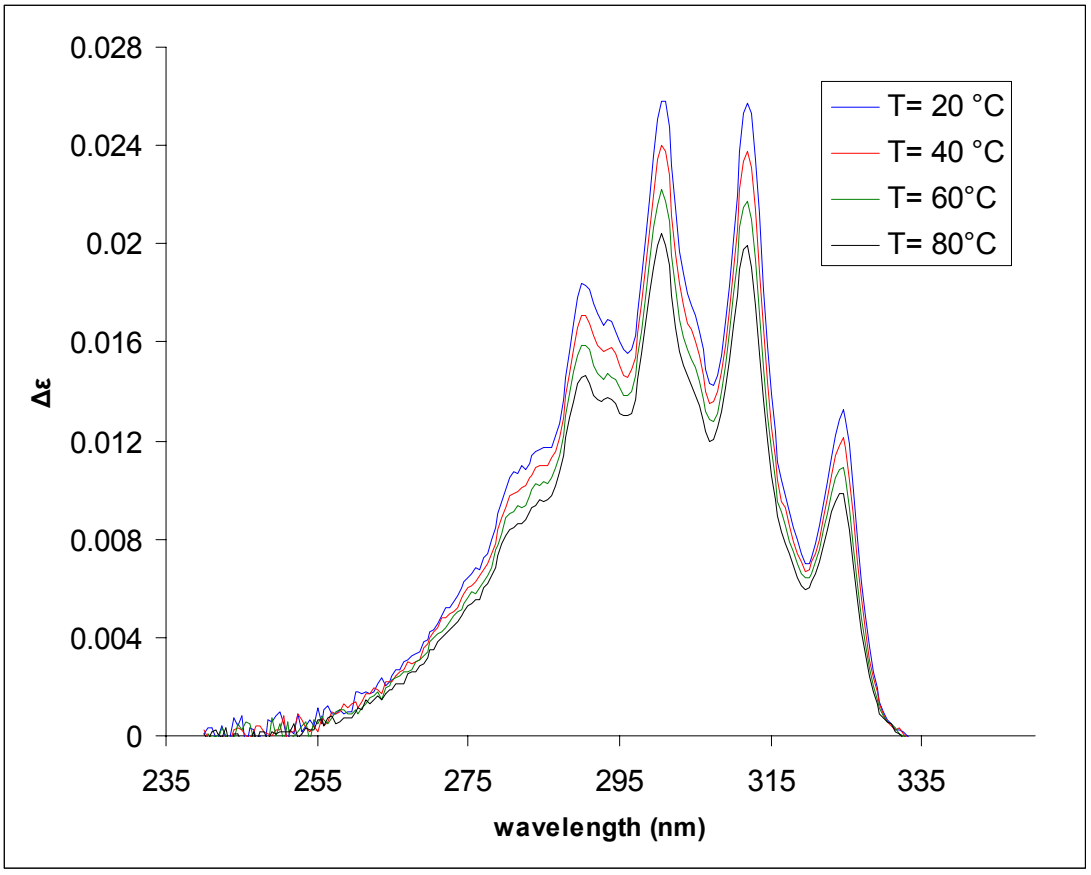


Figure 4.4 Temperature dependent Circular Dichroism spectra for $n \rightarrow \pi^*$ transition of *R*3MCP solution in cyclohexane.

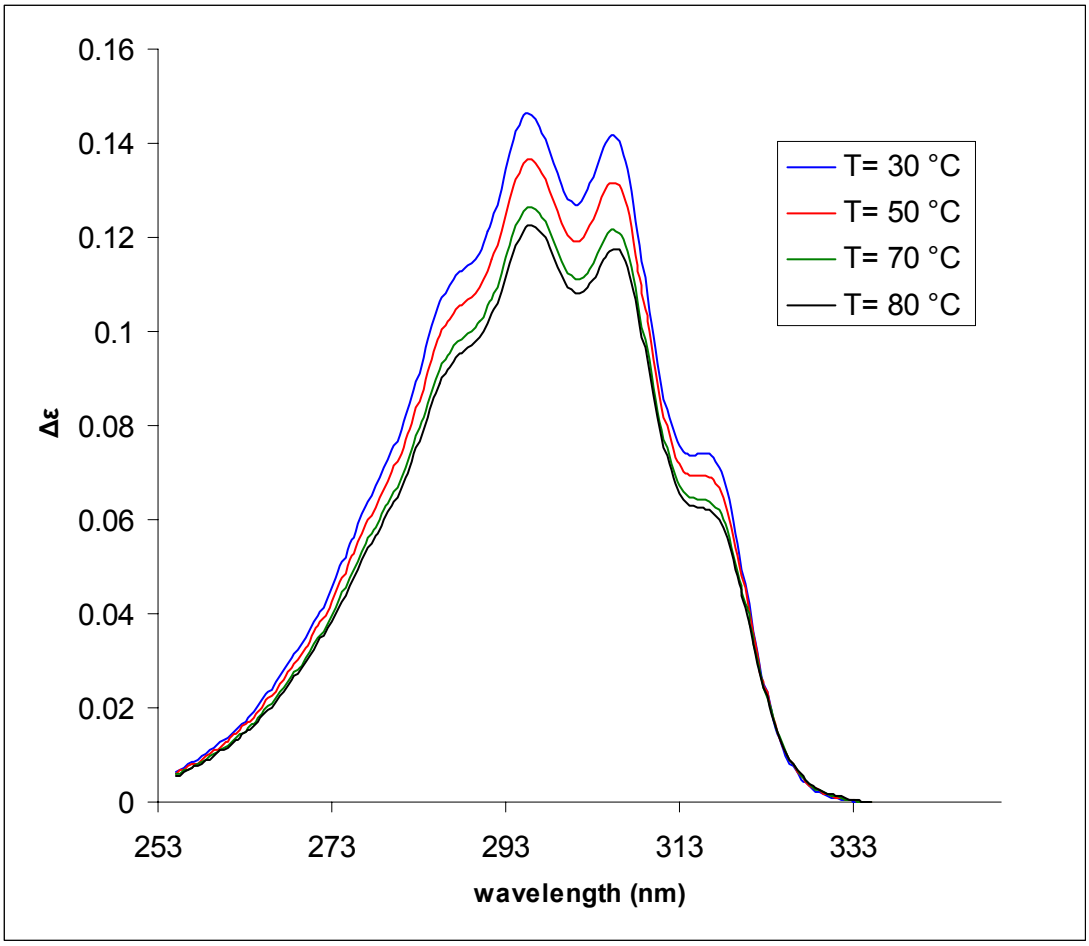


Figure 4.5 Temperature dependent Circular Dichroism spectra for $n \rightarrow \pi^*$ transition of *R*3MCP solution in acetonitrile.

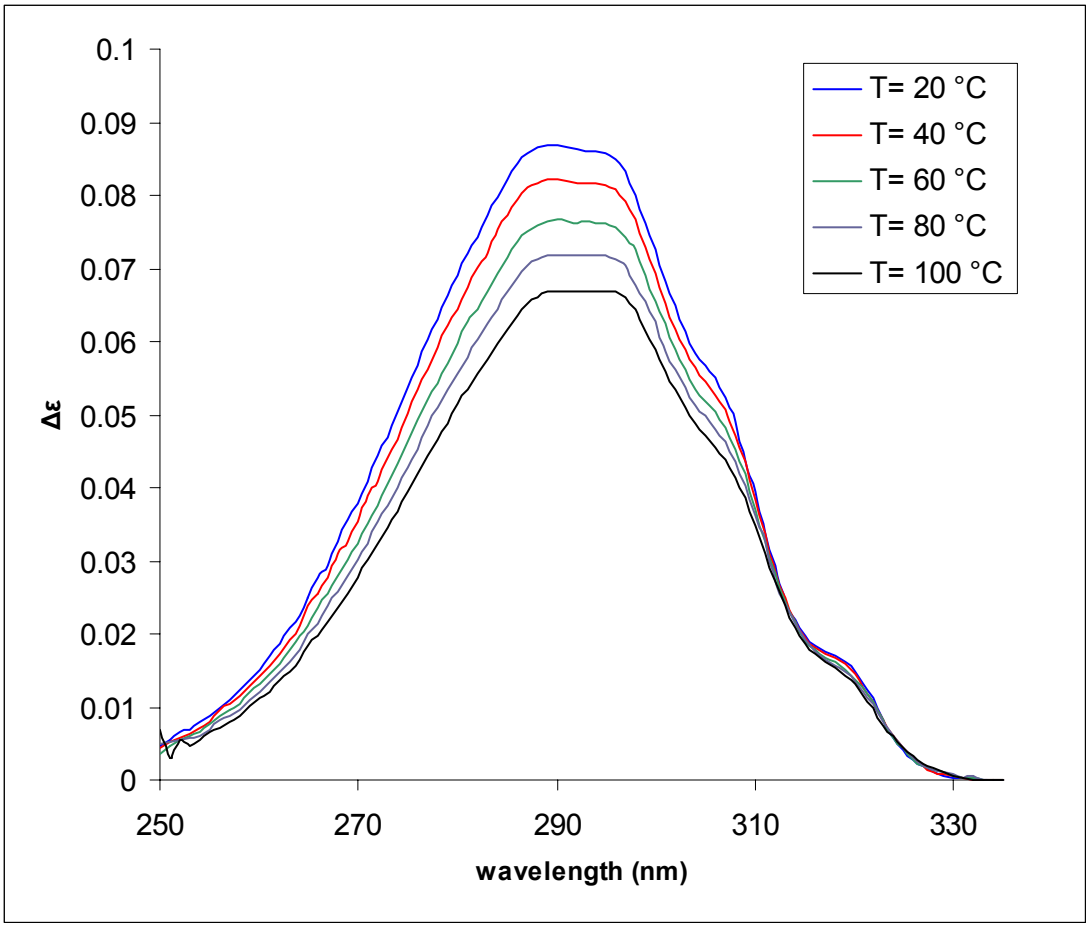


Figure 4.6 Temperature dependent Circular Dichroism spectra for $n \rightarrow \pi^*$ transition of *R*3MCP solution in acetic acid.

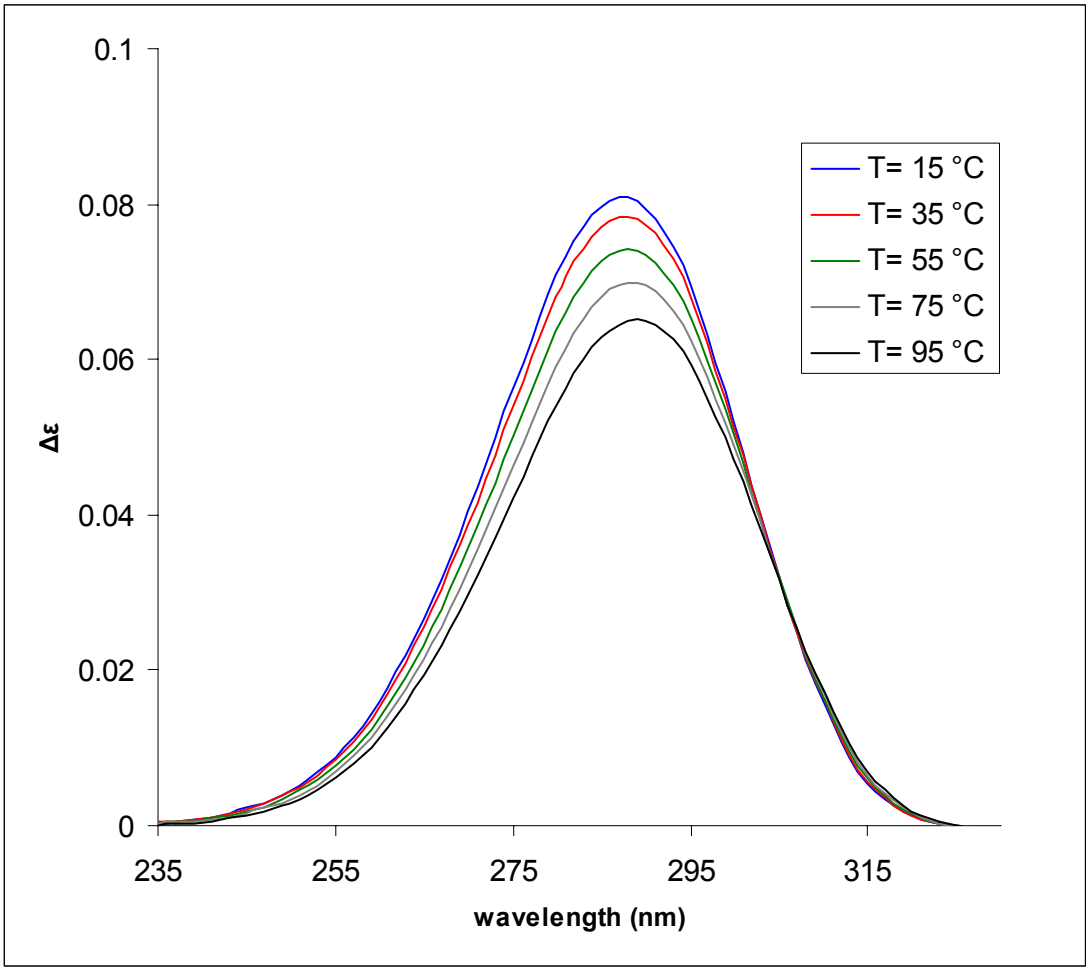


Figure 4.7 Temperature dependent Circular Dichroism spectra for $n \rightarrow \pi^*$ transition of *R*3MCP solution in water.

A gradual smearing of the CD spectrum was observed as the $E_T(30)$ value increases for the solvents studied. Figure 4.4 shows a CD spectrum for *R*3MCP solution in cyclohexane ($C_6H_{12}$), $E_T(30)$ = 30.9 kcal/mol, which exhibits a significant vibrational structure. The CD spectrum of R3MCP solution in water (figure 4.7), $E_T(30)$ = 63.1 kcal/mol, does not show vibrational resolution which provides a proof of hydrogen bonding effects on limiting the vibrational transitions of *R*3MCP. Temperature dependent CD spectra of R3MCP have been recorded for the $n\rightarrow\pi^*$ transition in 34 solvents. In all cases the magnitude of the CD signal peak decreases as sample temperature increases.

A plot of CD peak heights values versus temperature (T) was generated for each solvent. As an example of this method for *R*3MCP CD solution in acetonitrile, see figure 4.8. The extrapolation of the $\Delta\varepsilon$ versus temperature to $T\rightarrow 0$ °K gives the CD signal due to the equatorial conformer at T= 0 °K ($\Delta\varepsilon_{eq}$ = 0.2922) whereas, the extrapolation of $\Delta\varepsilon$ versus 1/T gives the equal contribution of both conformers at T= $\infty$ °K ( $\Delta\varepsilon$ = -0.0235). As seen in figure 4.9, plugging these values into equation 4.14, gives a CD signal of the axial conformer $\Delta\varepsilon_{ax}$ = -0.3392. Using this method it was possible to determine both conformers mole fractions. Van't Hoff plot was employed to determine conformers energy difference (see figure 4.10).

Table 4.2 shows the population of *R*3MCP conformers in acetonitrile solution for different sample temperatures, the mole fraction population of the equatorial conformer decreases from $f_{Eq}$ = 0.769 at T = 303.15 °K to $f_{Eq}$ = 0.732 at T = 353.05 °K, on the contrary, the mole fraction population of the axial conformer is seen to

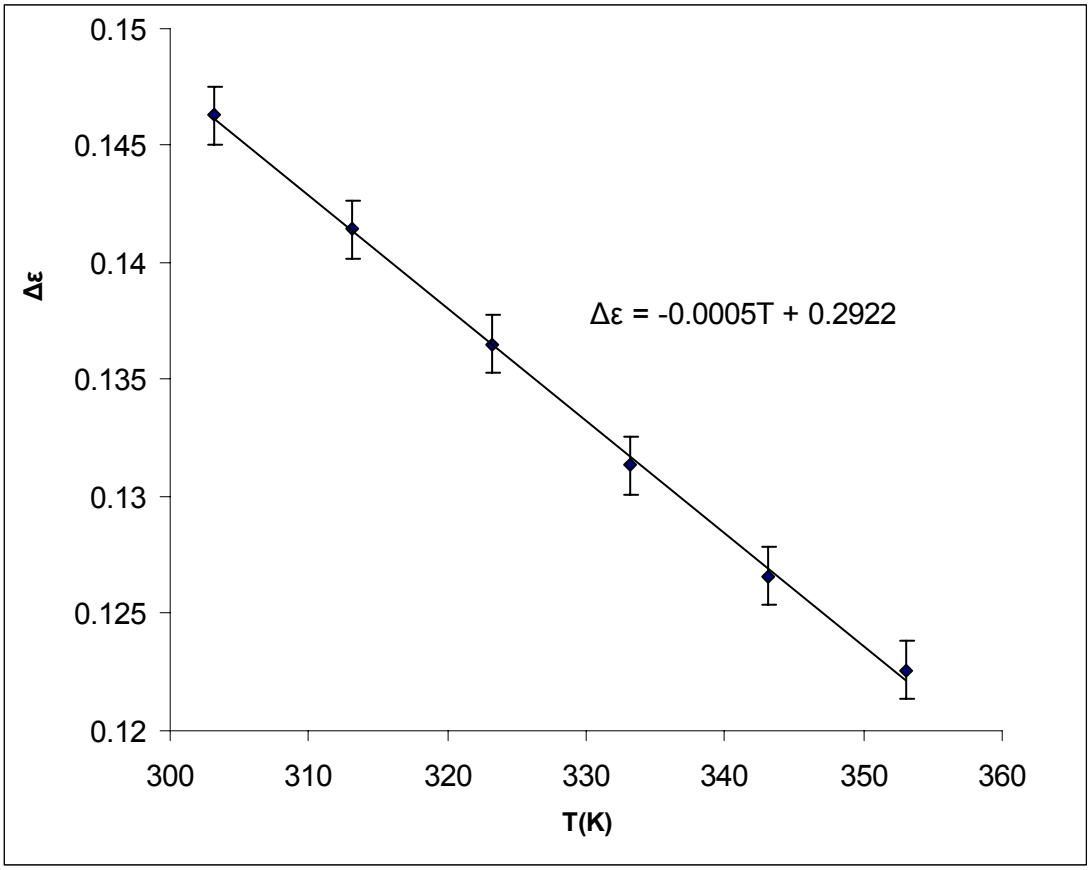


Figure 4.8 CD peak values for *R*3MCP in aceonitrile solution versus sample temperature T, the y-intercept gives the CD signal due to the equatorial conformer at T= 0 °K.

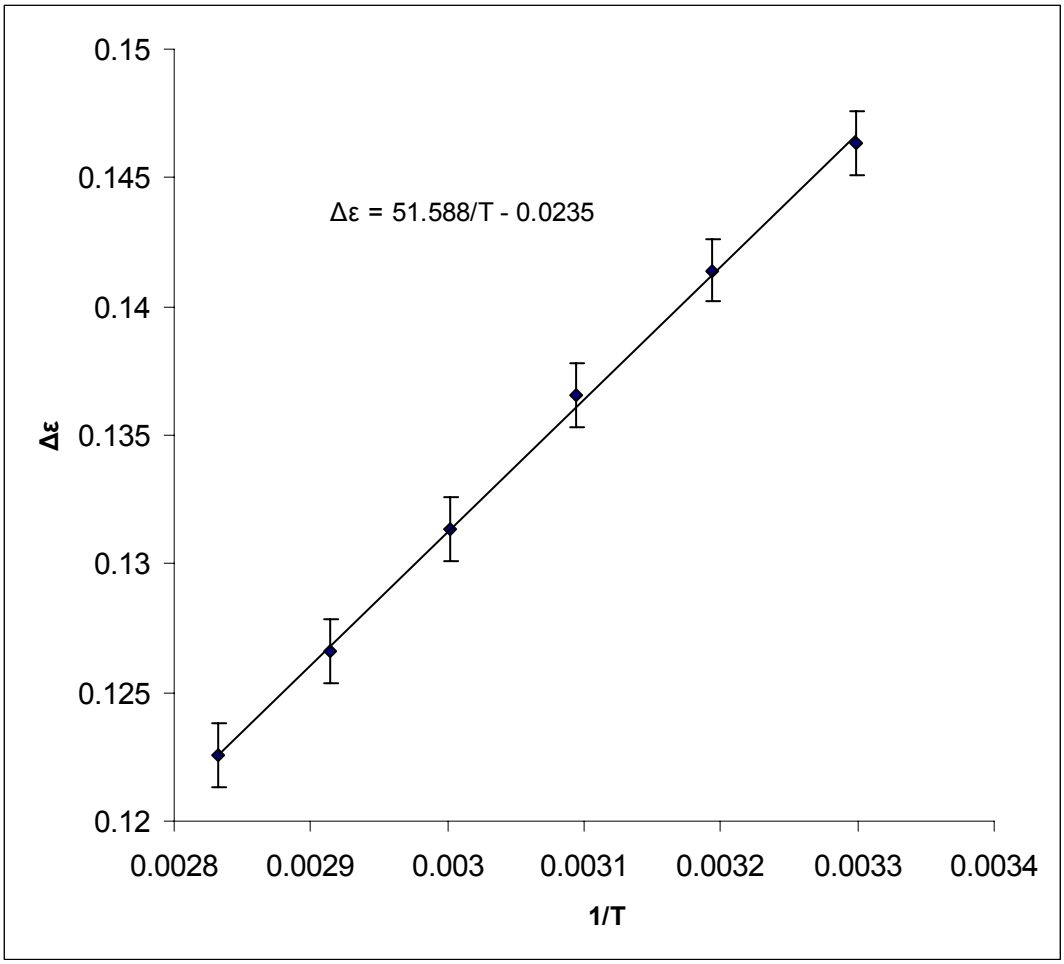


Figure 4.9 CD peak values for *R*3MCP in aceonitrile solution versus reciprocal of sample temperature 1/T, the y-intercept gives the CD signal due to the equal contribution of both equatorial and axial conformer at T= ∞ °K.

Table 4.2 Mole fraction population of axial and equatorial conformers of *R*3MCP solution in acetonitrile as a function of sample temperature.

| T(k) | 1/T | Δε | $f_{Ax}$ | $f_{Eq}$ | $k = f_{Ax}/f_{Eq}$ | ln $k$ |
|---|---|---|---|---|---|---|
| 303.15 | 0.0033 | 0.1463 | 0.231 | 0.769 | 0.3004 | -1.2024 |
| 313.15 | 0.00319 | 0.1414 | 0.238 | 0.762 | 0.3137 | -1.1591 |
| 323.15 | 0.00309 | 0.1365 | 0.246 | 0.754 | 0.3272 | -1.1170 |
| 333.15 | 0.003 | 0.13133 | 0.254 | 0.746 | 0.3418 | -1.0733 |
| 343.15 | 0.00291 | 0.1265 | 0.262 | 0.738 | 0.3555 | -1.0341 |
| 353.05 | 0.00283 | 0.1225 | 0.268 | 0.732 | 0.3673 | -1.0014 |

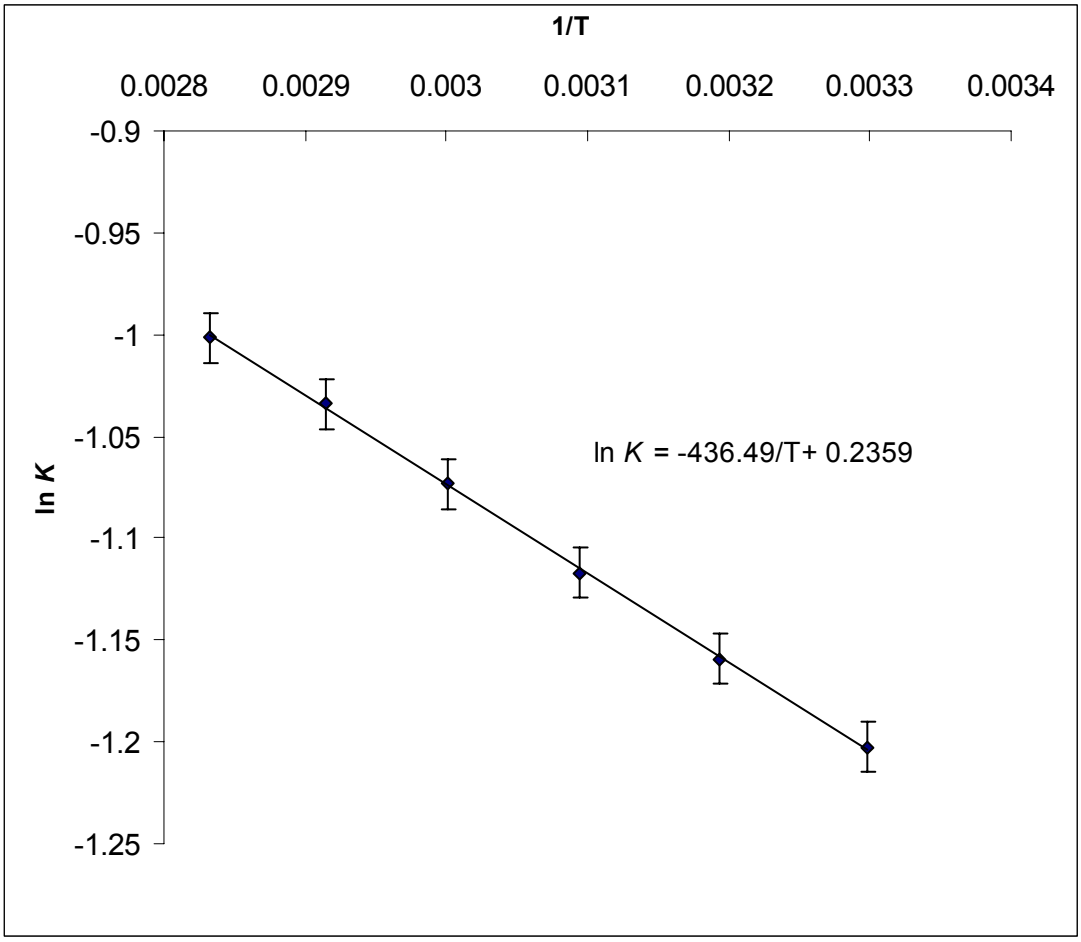


Figure 4.10 Van't Hoff plot of *R*3MCP in acetonitrile solution, the slope represents $\Delta H° = 3.63 \pm 0.05$ KJ/mol , the y-intercept is $\Delta S° = 1.96 \pm 0.10$ J/mol.K

increase as a function of temperature increase from $f_{Ax} = 0.231$ to $f_{Ax} = 0.268$. These results can be interpreted as a tendency for the equatorial molecules to transform to higher energy state (axial) as the temperature increases.

The same method was applied to *R*3MCP in 34 common solvents of different polarity and physical properties[84,85] (see Table 4.3). The thermodynamic constants ΔH° and ΔS° were determined directly from the Van't Hoff plot. ΔH° values range from 3.21± 0.05 KJ/mol in ethanol to 3.71 ± 0.05 KJ/mol in dimethyl sulfoxide , whereas, ΔS° range from 1.81 ± 0.1 J/mol.K in ethanol to 2.17 ± 0.1 J/mol.K in 2-propanol. ΔG° values were determined by equating the contribution of the enthalpy and entropy terms with experimental standard deviation ± 0.11.

We have also applied density function theory calculations of B3LYP type with basis set aug-cc-pvDz using Gaussian03 software package for the thermodynamic constants of *R*3MCP in few solvents. A PCM model was used to define the solute solvent interaction in terms of the solvent dielectric constant, see table 4.4. These optimized geometry calculations of the two conformers, equatorial and axial, were performed separately and then calculating the thermodynamic constants differences. The results show good agreement with experimental results within acceptable experimental error. Dipole moment calculations for both conformers in solvents using same DFT and basis set, yield a direct relationship between polarity parameter $E_T(30)$ of solvents and dipole moments of both conformers.

Table 4.3 *R*3MCP Thermodynamic constants in 34 common solutions.

| Solvent | ΔH° (KJ/mol) | ΔS° (J/mol.k) | ΔG°(K J/mol) |
|---|---|---|---|
| water | 3.55 | 1.88 | 2.99 |
| methanol | 3.37 | 2.11 | 2.74 |
| ethanol | 3.21 | 1.81 | 2.67 |
| t-butanol | 3.55 | 1.92 | 2.98 |
| n-amyl alcohol | 3.43 | 1.94 | 2.85 |
| cyclopentanol | 3.44 | 1.97 | 2.85 |
| 2-propanol | 3.48 | 2.17 | 2.83 |
| isobutyl alcohol | 3.43 | 1.94 | 2.85 |
| phenethyl alcohol | 3.43 | 1.94 | 2.85 |
| 2-butanol | 3.32 | 1.89 | 2.76 |
| 2-Octanol | 3.41 | 1.90 | 2.84 |
| hexafluorobenzene | 3.35 | 1.90 | 2.78 |
| cyclohexane | 3.50 | 1.94 | 2.92 |
| benzene | 3.45 | 1.94 | 2.87 |
| carbon tetrachloride | 3.30 | 1.94 | 2.72 |
| chlorobenzene | 3.67 | 1.95 | 3.09 |
| chloroform | 3.26 | 1.97 | 2.67 |
| tetrahydropyran | 3.70 | 1.96 | 3.16 |
| toluene | 3.62 | 1.95 | 3.04 |
| benzyl ether | 3.69 | 2.01 | 3.09 |
| anisole | 3.44 | 1.96 | 2.86 |
| glutaronitrile | 3.67 | 1.93 | 3.09 |
| adiponitrile | 3.56 | 1.94 | 2.98 |
| crotononitrile | 3.56 | 1.96 | 2.98 |
| valeronitrile | 3.59 | 1.99 | 2.99 |
| butyronitrile | 3.39 | 1.93 | 2.81 |
| acetonitrile | 3.63 | 1.96 | 3.04 |
| propionitrile | 3.34 | 1.94 | 2.76 |
| trimethylacetonitrile | 3.61 | 1.95 | 3.03 |
| formic Acid | 3.52 | 1.94 | 2.94 |
| acetic acid | 3.66 | 1.94 | 3.08 |
| trifluoroacetic acid | 3.33 | 1.96 | 2.75 |
| dimethyl sulfoxide | 3.71 | 1.95 | 3.13 |
| dimethyl sulfite | 3.43 | 1.94 | 2.85 |

Table 4.4 DFT calculations of B3LYP with basis set aug-cc-pvDz of thermodynamic constants of *R*3MCP in common solvents. (a) C. Reichardt, Solvents and solvent Effects In Organic Chemistry, 3rd edition, 2003 (b) Y. Marcus,[83] The Properties of Solvents, (1998).

| solvent | $E_T(30)^{a,b}$ (kcal/mol) | $\mu_{eq\ (D)}$ | $\mu_{ax\ (D)}$ | $\Delta H°_{cal.}$ (kJ/mol) | $\Delta S°_{cal.}$ (J/mol.K°) |
|---|---|---|---|---|---|
| gas phase | - | 3.275 | 3.297 | 5.09 | 0.20 |
| cyclohexane | 30.9 | 3.663 | 3.704 | 4.34 | 0.54 |
| toluene | 33.9 | 3.738 | 3.783 | 4.42 | 0.57 |
| benzene | 34.3 | 3.713 | 3.756 | 4.39 | 0.68 |
| chlorobenzene | 36.8 | 4.033 | 4.101 | 4.76 | 1.00 |
| chloroform | 39.1 | 3.998 | 4.063 | 4.72 | 1.13 |
| dimethyl sulfoxide | 45.1 | 4.283 | 4.375 | 5.08 | 1.23 |
| acetonitrile | 45.6 | 4.275 | 4.364 | 5.04 | 1.31 |
| ethanol | 51.9 | 4.251 | 4.338 | 5.00 | 1.18 |
| methanol | 55.4 | 4.270 | 4.358 | 5.03 | 1.26 |
| water | 63.1 | 4.305 | 4.393 | 4.92 | 1.21 |

Conclusion

This study reports solvent effects on the $n \rightarrow \pi^*$ transition circular dichroism spectra due to solvent polarity and its ability to form dispersion forces with *R*3MCP molecules. A blue shift in this transition band was observed in polar molecules that is related to solute-solvent interaction such as dipole-dipole , dipole-induced dipole, and hydrogen bonding, whereas, a red shift was observed in solvents that form a van der Waals force with solute *R*3MCP. The $n \rightarrow \pi^*$ transition was ideal for this study due to its significant CD signal that corresponds to a weakly absorbing-symmetry-forbidden molecular electronic transition, as well as being sensitive to equatorial-methyl and axial-methyl conformers population.

It was concluded experimentally and supported by theoretical density function calculations that *R*3MCP exhibit equal and opposite sign CD effect. Observing sample temperature variation CD measurements for the above mentioned transition, mole fractions of each conformer were determined at different sample temperatures. The average population ratio between equatorial and axial conformers at room temperature was 78:22 which is reasonably consistent with results using other techniques such as MPI[69] and Infrared[56] spectroscopy. The ratios of mole fractions were employed to determine conformer energy difference, $\Delta H°$, as well as the first measurement of entropy change $\Delta S°$. Equating both thermodynamic constants it was possible to determine difference in Gibbs free energy $\Delta G°$ between *R*3MCP conformers. DFT calculations of *R*3MCP conformers thermodynamic constants in different solvents show good agreement with experimental findings.

# CHAPTER V
# OPTICAL ROTATION OF *R*3MCP CONFORMERS

## Introduction

Optical Rotation[86,87]has been widely used in physical chemistry research mostly for the purpose of characterizing chiral molecules. Optical Rotatory Dispersion[88](ORD), which is defined as a measure of optical rotation as a function of wavelength, was a crucial field of research in the 1950s. However, ORD applications were not considered a very attractive topic until the development of sensitive instrumentation in the ultraviolet-visible region that is responsible for molecular phenomena categorized as Optical Activity in most organic molecules. In principle, the sign and magnitude of optical rotation contains information about absolute stereochemistry of a chiral molecule.[89]

The applications of optical rotation in structural chemistry were limited in the past due to the lack of a reliable theoretical method to interpret the observed rotation in terms of molecular structure. Many empirical methods[90,91] were employed and developed to relate molecular structure and optical rotation. Following the appearance of the seminal papers by Amos[92]and Helgaker et. al.,[93] who implemented the ab initio (Hartree-Fock level of approximation) calculation of the electric dipole-magnetic dipole polarizability tensor in the static limit using CADPAC[94] and DALTON[95] packages, respectively. The first ab initio calculations of optical rotation was pointed out by Polavarapu.[96] Since that time different levels of quantum mechanical theories have been employed to predict optical rotation. Of particular interest, is the Hartree-Fock (HF) calculations reported by Kondru et. al. [97] and

Giorgio et. al.[98] on assignment of molecular absolute configuration through the ab initio calculations of the optical rotation that utilize Hartree-Fock approximation for valence molecular electrons. Under HF treatment, each electron sees all the other electrons as an average distribution; in other words, there is no instantaneous electron-electron interaction included.[99]

Solvent effect on ORD and CD has commonality in terms of the wavelength shifts due to modification in chiral molecules electron arrangement. In particular, ORD and CD are closely related for chiral ketones of carbonyl functional group molecules such as R-(+)-3-methylcyclopentanone. For some carbonyl compounds a reverse in the optical rotation sign has been reported when the ORD spectra were measured in solvents of different polarity.[100,101] The weakly absorbing $n \rightarrow \pi^*$ transition band in the 33300 $cm^{-1}$(300 nm) region of *R*3MCP was studied earlier in chapter IV. ORD measurements of R3MCP in different polar solvents show a variation in ORD curves that can be interpreted as a manifestation of the Cotton effect.[102,103]

ORD measurements of *R*3MCP in 35 different common solvents were performed to give further insight on solvent effects on optical rotation. Hartree-Fock calculations of optical rotation of equatorial and axial conformers were also employed separately. Utilizing determined room temperature conformer population ratios of equatorial to axial (78:22) it was concluded in Chapter IV that using temperature dependent CD, it is possible to construct the predicted ORD curve. ORD calculations will then be compared to observed experimental results.

Optical Rotatory Dispersion in Solvation Theory

A theoretical model of the chiral molecule (solute) ORD in achiral medium (solvent) involves the chiral solute transitional electric $\mu_\alpha$ and magnetic $m_\alpha$ dipole moments. In the absence of a solvent medium, the dipole moments are represented by the polarized light external electric $E_\alpha$ and magnetic $B_\alpha$ fields and their time derivatives as

$$\mu_\alpha = \mu_\alpha^0 + S_{\alpha\beta}E_\beta + \omega^{-1}G_{\alpha\beta}\frac{\partial B_\beta}{\partial t} + \ldots \tag{5.1}$$

$$m_\alpha = m_\alpha^0 - \omega^{-1}G_{\alpha\beta}\frac{\partial E_\beta}{\partial t} + \ldots \tag{5.2}$$

where $S_{\alpha\beta}$ and $G_{\alpha\beta}$ represent,[104,105] respectively, the electric dipole-electric dipole and electric dipole-magnetic dipole polarizability tensors. $\mu_\alpha^0$ and $m_\alpha^0$ represent intrinsic moments in the absence of the external fields, and ω is polarized light angular frequency. Unlike the electric dipole-electric dipole polarizability tensor, electric dipole-magnetic dipole tensor contributes to optical rotation and can be expressed by[12,96]

$$G_{\alpha\beta} = -\frac{4\pi}{h}\sum_{n\neq s}\frac{\omega}{\omega_{ns}^2 - \omega^2}\,\mathrm{Im}\left\{\left\langle \psi_s^0 / \mu_\alpha / \psi_n^0 \right\rangle \cdot \left\langle \psi_n^0 / m_\beta / \psi_s^0 \right\rangle\right\} \tag{5.3}$$

$\psi_s^0$ and $\psi_n^0$ represent the unperturbed ground and excited states, respectively, and $\omega_{ns}$ is the electronic transition angular frequency. A quantity $\beta$ that is related to optical rotation $\alpha$ (in radians.cm$^{-1}$) is defined as

$$\beta = -\frac{\omega^{-1}}{3}\left(G_{xx} + G_{yy} + G_{zz}\right) \tag{5.4}$$

$$\alpha = \frac{4\pi N\beta^2}{3c^2}\left(n^2+2\right) \tag{5.5}$$

where $N$ represents the number of molecules per unit volume, $c$ is solute concentration (in grams of solute in 100 $cm^3$ solution), and $n$ is the refractive index of chiral substance. Substituting (5.4) and (5.5) into (5.3) gives the following expression for specific rotation $[\alpha(\lambda)]$ (in $deg.cm^3.g^{-1}.dm^{-1}$) as a function of polarized light wavelength[106]

$$\left[\alpha(\lambda)\right] = \frac{0.915\times10^{44}}{M}\sum_{n\neq s}\frac{\lambda_{ns}^2}{\lambda^2-\lambda_{ns}^2}\,\mathrm{Im}\left\{\left\langle\psi_s^0/\mu_\alpha/\psi_n^0\right\rangle\cdot\left\langle\psi_n^0/m_\alpha/\psi_s^0\right\rangle\right\} \tag{5.6}$$

The specific rotation above is related to the observed rotation $\alpha(\lambda)$ (in deg.), molar volume $V_m$(in $cm^3.mol^{-1}$), molar mass $M$ (in $g.mol^{-1}$), and $l$ is the path length (in dm) via

$$\left[\alpha(\lambda)\right] = \frac{100\alpha(\lambda)}{cl} = \frac{3600\cdot\phi(\lambda)V_m}{2\pi M} \tag{5.7}$$

where $\phi(\lambda)$ is defined as

$$\phi(\lambda) = \frac{16\pi^3 N_0\beta(\lambda)}{\lambda^2 V_m} \tag{5.8}$$

$N_0$ represents Avogadro's number and the optical rotatory parameter $\beta(\lambda)$ (in $cm^4$). Substituting for rotational strength $R_{sn}$, that is directly related to CD, in equation (5.6) yields

$$\left[\alpha(\lambda)\right] = \frac{0.915\times10^{44}}{M}\sum_{n\neq s}\frac{\lambda_{ns}^2}{\lambda^2-\lambda_{ns}^2}R_{sn} \tag{5.9}$$

Many theories have been incorporated to explain the significant dependence of optical rotation on solvent properties, in the case of flexible molecules, i.e. *R*3MCP,

which exhibit multiple conformations in solution. The solvent effect can often be attributed predominately to changes in conformational populations for various solvents. This would imply that there is a difference in energy for the conformers depending on the solvent. Employing canonical treatment of theory of optical rotatory power, the optical rotation at frequency $\nu$ of an isotropic dilute solution of a chiral molecule is given by

$$\phi(\nu) = \frac{16\pi^3 N \nu^2}{c^2} \gamma_{LF} \beta(\nu) \tag{5.10}$$

where $\beta(\nu)$ is another manifestation of equation (5.4) and is denoted by

$$\beta(\nu) = \frac{1}{3} Tr[G_{\alpha\beta}(\nu)] \tag{5.11}$$

$\gamma_{LF}$ is the "local field correction factor" which is defined as the ratio of the microscopic electric field acting on the chiral molecule to the macroscopic electric field of the light wave of Lorentz,[107-109] and is given by

$$\gamma_{LF} = \frac{\varepsilon_s(\nu) + 2}{3} = \frac{n_s(\nu)^2 + 2}{3} \tag{5.12}$$

where $\varepsilon_s(\nu)$ and $n_s(\nu)$ are the dielectric constant and refractive index of the solvent, respectively. A relatively recent molecular term was proposed by Eliel and Wilen[110] termed "the molecular rotivity" Ω which is denoted by

$$\Omega = \frac{\alpha}{\left(n_s^2 + 2\right)/3} \tag{5.13}$$

Furthermore, solvent effect studies have consistently focused on the variation of Ω with solvent.[109]

Optical Rotation of *R*3MCP Upon Solvation

Optical Rotatory Dispersion (ORD) was recorded using a Perkin-Elmer 241 Polarimeter for neat *R*3MCP and in 35 common solvents, see table 5.1, with different polarity and molecular structure. The operation of this apparatus is restricted to 5 wavelengths. Two of them are generated using a sodium lamp at λ=589,578 nm , the other three wavelengths at λ=546 nm, 436 nm and 365 nm are obtained by operating the the apparatus in the mercury lamp mode. These experimental results were then compared to the calculations performed using the Gaussian03 software package, Optical rotation calculations of Hartree-Fock theory method were employed to understand the effect of each of these conformers on optical rotation. The results show almost equal magnitude but opposite in sign optical rotation between equatorial and axial conformers (figure 5.1). These trends can be explained by considering the different electron arrangement for each *R*3MCP conformer.

When using conformer population ratios obtained from temperature dependent circular dichroism of $n \rightarrow \pi^*$ of 78:22 between equatorial to axial conformers , it was possible to obtain typical specific rotation curve which shows good agreement with experimental data (figures 5.2 and 5.3). The consistency between calculated and experimental results provides strong evidence for the dominance of equatorial and axial *R*3MCP conformers out of the possible five other conformers. Due to the fact that rotatory strength is directly related to CD and ORD, the calculated sign inversion for the two conformers further emphasize the rotatory strength opposite effect in optical rotation that was also concluded by employing CD curves.

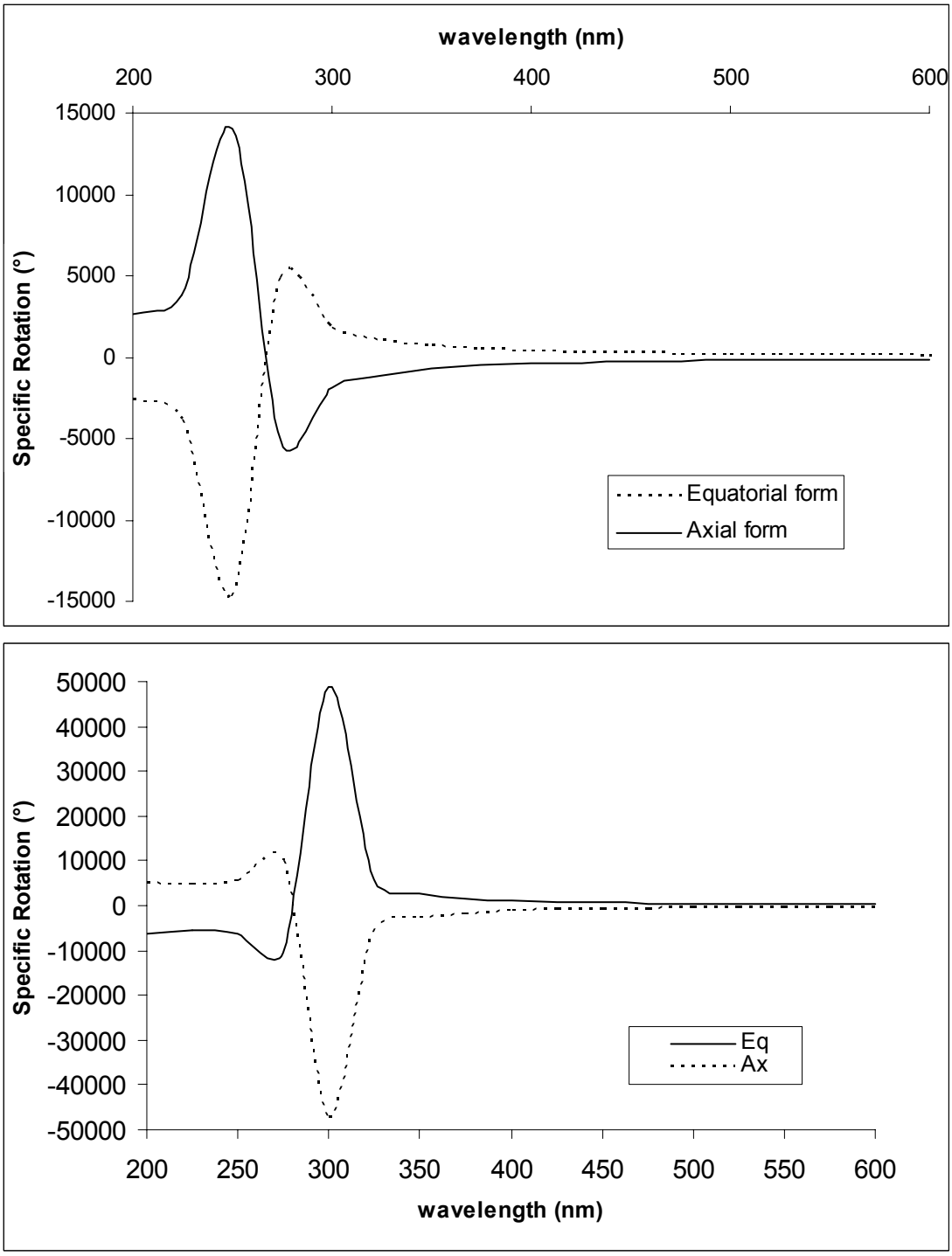


Figure 5.1 Specific rotation calculations versus polarized light wavelength of equatorial and axial conformers of *R*3MCP Using Gaussian03 with basis set 6-31G* both in the neat form (top) and in cyclohexane solution (bottom).

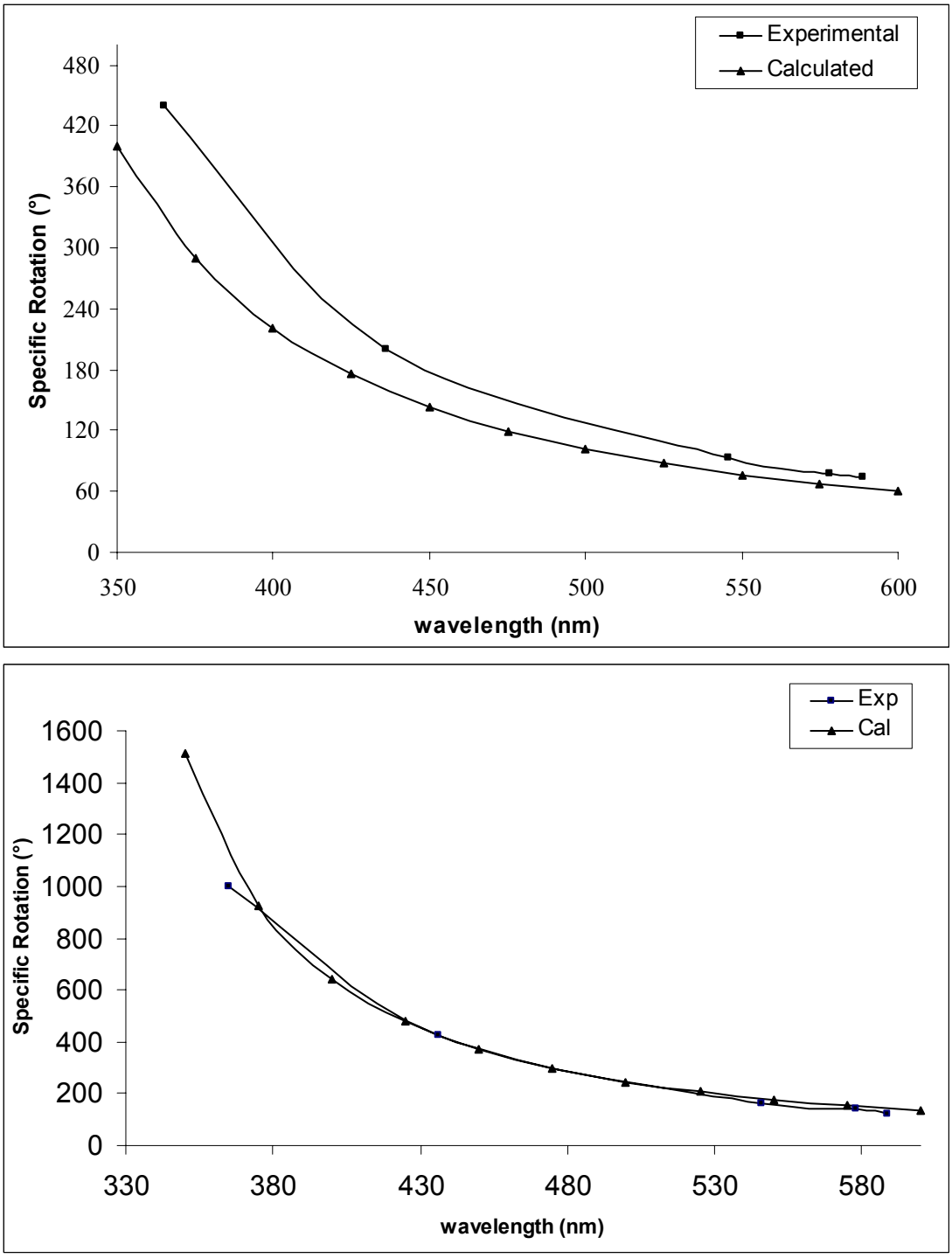


Figure 5.2 Experimental and calculated specific rotation of *R*3MCP in the neat (top) and in cyclohexane solution (bottom), calculations of equatorial: axial conformers population ratio (78:22) which was deduced from Temperature dependent Circular Dichroism.

Table 5.1 Specific rotation of *R*3MCP in 35 common solvents at five different polarized light wavelengths. Whereas, $n_s$ is solvent refractive index.

| Solvent | $n_s$[a,b] | Specific Rotation ( degrees) | | | | |
|---|---|---|---|---|---|---|
| | | 589 (nm) | 578 (nm) | 546 (nm) | 436 (nm) | 365 (nm) |
| cyclohexane | 1.4235 | 122.3 | 142.6 | 163.0 | 427.9 | 998.5 |
| benzene | 1.4979 | 176.6 | 183.4 | 217.4 | 475.5 | 1073.3 |
| toluene | 1.4941 | 200.7 | 216.1 | 231.6 | 524.9 | 1157.9 |
| chlorobenzene | 1.521 | 211.1 | 230.3 | 268.6 | 594.8 | 1343.2 |
| hexafluorobenzene | 1.374 | 101.9 | 122.3 | 163.0 | 326.1 | 815.1 |
| chloroform | 1.442 | 142.6 | 152.8 | 183.4 | 438.1 | 1008.7 |
| carbon tetrachloride | 1.460 | 183.4 | 203.8 | 244.5 | 529.8 | 1283.8 |
| tetrahydropyran | 1.4186 | 163.0 | 173.2 | 193.6 | 397.4 | 896.6 |
| anisole | 1.5143 | 159.0 | 183.5 | 207.9 | 452.6 | 1027.5 |
| benzyl ether | 1.5170 | 163.0 | 183.4 | 224.2 | 468.7 | 1039.3 |
| acetone | 1.3560 | 189.1 | 210.1 | 231.2 | 567.2 | 1365.6 |
| acetonitrile | 1.341 | 200.1 | 216.8 | 250.1 | 533.6 | 1167.3 |
| propionitrile | 1.363 | 127.4 | 143.3 | 175.1 | 382.1 | 875.6 |
| butyronitrile | 1.382 | 132.1 | 154.0 | 176.1 | 418.1 | 990.3 |
| valeronitrile | 1.395 | 107.4 | 122.8 | 153.5 | 368.3 | 890.0 |
| adiponitrile | | 142.6 | 163.0 | 183.4 | 468.7 | 1039.3 |
| crotononitrile | | 142.7 | 163.3 | 203.8 | 448.3 | 1018.9 |
| glutaronitrile | | 142.7 | 163.2 | 203.8 | 448.4 | 957.8 |
| nitroethane | 1.389 | 61.2 | 81.6 | 101.9 | 285.3 | 631.7 |
| trimethylacetonitrile | | 122.5 | 142.8 | 183.4 | 428.0 | 957.9 |
| dimethyl sulfoxide | 1.477 | 102.0 | 122.7 | 163.8 | 407.6 | 937.4 |
| acrylic acid | 1.3843 | 142.7 | 164.1 | 224.2 | 509.5 | 1161.6 |
| formic Acid | 1.3694 | 20.4 | 40.8 | 61.2 | 264.9 | 611.5 |
| acetic acid | 1.3698 | 81.6 | 101.9 | 122.2 | 326.1 | 713.2 |
| trifluoroacetic acid | 1.2850 | 61.2 | 81.6 | 102.4 | 264.9 | 591.0 |
| methanol | 1.3265 | 183.7 | 203.8 | 244.6 | 509.5 | 917.1 |
| ethanol | 1.3594 | 133.8 | 152.9 | 191.2 | 420.6 | 917.6 |
| 2-propanol | 1.3837 | 82.1 | 95.7 | 123.1 | 300.9 | 656.5 |
| isobutyl alcohol | 1.3959 | 122.3 | 142.7 | 163.0 | 407.6 | 937.9 |
| 2-butanol | 1.3953 | 156.5 | 176.1 | 215.2 | 488.9 | 1056.1 |
| t-butanol | 1.3852 | 163.6 | 183.4 | 203.8 | 468.7 | 1039.3 |
| n-amyl alcohol | 1.410 | 142.7 | 166.4 | 204.8 | 409.6 | 857.9 |
| cyclopentanol | 1.4080 | 124.3 | 142.7 | 188.4 | 387.2 | 876.3 |
| phenethyl alcohol | 1.5328 | 125.3 | 147.6 | 189.5 | 448.6 | 978.2 |
| water | 1.3325 | 142.6 | 165.0 | 205.3 | 418.6 | 855.9 |

(a) C. Reichardt, Solvents and solvent Effects In Organic Chemistry, 3rd edition, 2003
(b) Y. Marcus,[83] The Properties of Solvents, (1998).

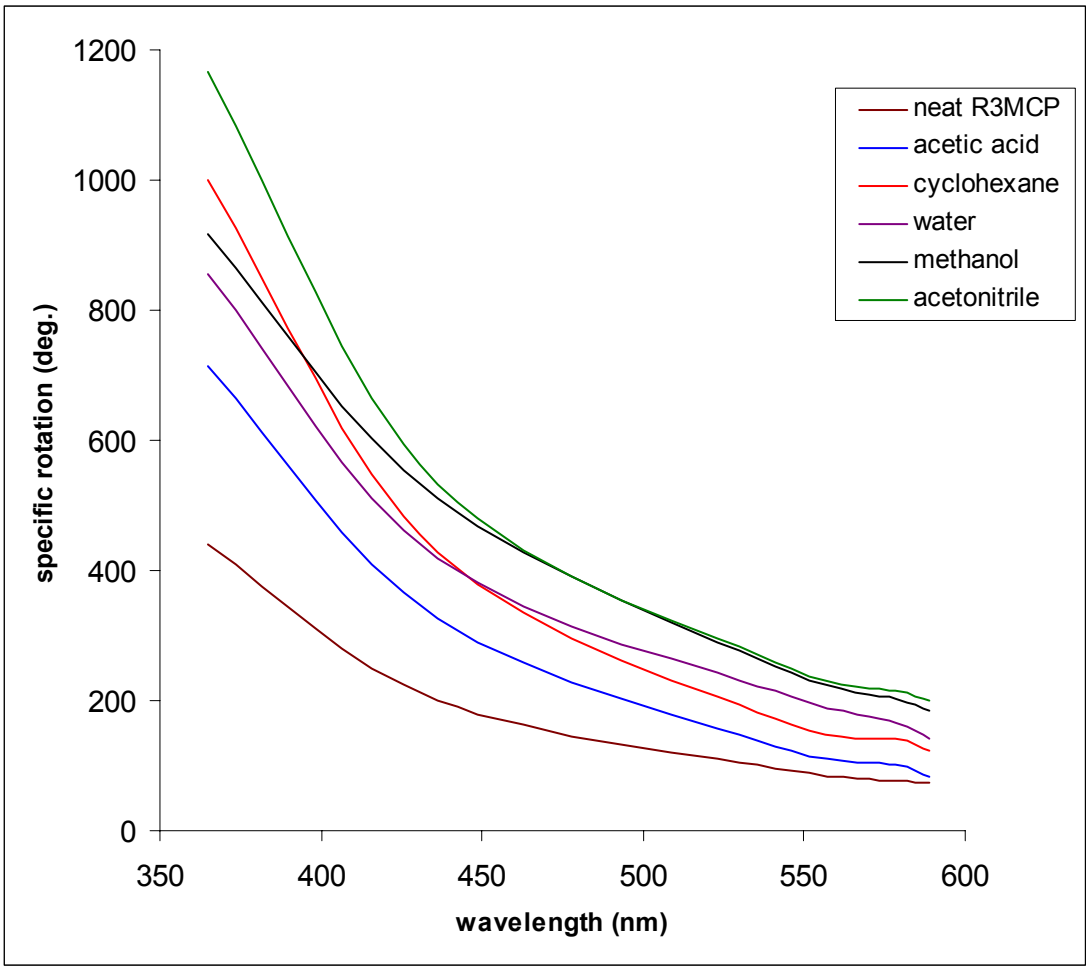


Figure 5.3 specific rotation of *R*3MCP in the neat form and in few common solvents of different molecular groups.

Conclusive Remarks

In summary, *R*-(+)-3-methylcyclopentanone was observed to have a large optical activity as manifested by significant optical rotation at low and high polarized light wavelengths. Unlike most chiral compounds, unsaturated ketones like *R*3MCP are known to exhibit large CD and ORD values near the ultraviolet transition band ($n \rightarrow \pi^*$) that correspond to a symmetry forbidden-transition band. This trend is easily explained due to the fact that both optical activity quantities are directly related by rotational strength which is a measure of the optical activity strength of chiral molecules. Hartree-Fock level calculations using the basis set 6-31G* for *R*3MCP equatorial and axial conformers show equal magnitude and opposite sign optical rotation over a wide wavelength region (200-800 nm) which is attributed to the electron arrangement between the two conformers. The good agreement between HF calculations and experimental results can be explained by HF approximation basis of neglecting electron-electron interaction. In other words, electron-electron interactions have minimal effect on light interaction with matter. A similar trend was also seen in *R*3MCP conformers experimental and predicted CD in previous chapter.

Solvent effect on *R*3MCP optical rotation was studied for 35 common solvents of different physical properties. It was possible to reduce solute concentration effect on ORD by using samples of high dilution (M~ $10^{-2}$ mol/L). Blue shifts in ORD curves were observed in polar solvents due to solute-solvent electrostatic interactions especially hydrogen bonding. Red shifts in the ORD curves were observed in low polarity solvents.

# CHAPTER VI
# TEMPERATURE DEPENDENT RAMAN SPECTROSCOPY OF *R*3MCP

## Introduction to Raman Spectroscopy

Raman spectroscopy is concerned with the phenomenon of a discrete change of frequency when light is scattered by molecules. It was first discovered in 1928 by C.V. Raman and received the Nobel Prize shortly afterwards, and almost simultaneously, by G. Landsberg and L. Mandelstam.[111] The attention paid to this discovery was enormous, probably because of the intense interest in such inelastic phenomena generated by the earlier discovery of the Compton effect. Raman spectroscopy is the inelastic scattering of photons. Unlike other vibrational spectroscopic techniques, i.e. infrared absorption, Raman spectroscopy does not involve absorption or emission from the vibrational energy levels directly, but rather implicates intermediate virtual states. The introduction of laser sources, beginning with the routine availability of 50-100 Mw CW He-Ne lasers in the mid-1960s greatly increased the interest in Raman spectroscopy.[112-114]

When radiation of energy $h\nu_0$ is incident on a molecular sample, the radiation may be absorbed, diffracted, refracted, or reflected. A small fraction of radiation is inelastically scattered, that is, it is reradiated in all directions unchanged in energy, which can be looked at from a quantum mechanical aspect as the excitation of the molecule to a virtual state of energy $h\nu_0$ and the return to the ground state. A fraction of the radiation that is scattered will be inelastically scattered, giving rise to Raman effect. The frequency of scattered light can either be at the original frequency

(refered to as Rayleigh scattering) or at some shifted frequency $v_s = v_0 \pm v_i$ (refered to as Raman scattering). The frequency $v_i$ is an internal frequency corresponding to rotational, vibrational, or electronic transitions. Radiation scattering to the lower frequency side of the exciting line is called Stokes scattering, while the light scattered at higher frequencies than the excitation line is called anti-Stokes scattering. Anti-Stokes scattering results from excited initial state of the molecule so that the scattered light actually gains energy. As a result, the magnitude of the shift between Stokes or the anti-Stokes line and the excited line is called Raman shift, which is denoted by

$$\Delta\nu = |\nu_i - \nu_S| \tag{6.1}$$

Vibrational Raman spectra of *R*3MCP as a fuction of temperature variation are being employed to determine conformer energy differences between equatorial-methyl and axial methyl isomers. Raman spectroscopy performed under liquid nitrogen will also be presented to study Raman vibrational modes at liquid nitrogen temperature (~77 °K). In general, the Raman intensity for vibrational mode[115] *j* can be related to the exciting frequency $\nu_0$ and temperature *T* through[116,117]

$$I\alpha \frac{(\nu_0 - \nu_j)^4}{1 - \exp[-\frac{hc\nu_j}{kT}]} \frac{h}{8\pi^2 c\nu_j} S_j \tag{6.2}$$

Whereas, *h*, *c* and *k* are universal constants and $S_j = 3\beta_j^2$, where $\beta_j^2$ is the depolarized anisotropy tensor.[117] Probing the methyl group C-H stretch region Raman vibrations intensity it is possible to identify vibrational modes that correspond to both *R*3MCP conformers.

Theoretical Basis of Raman Spectroscopy

A theoretical approach to the Raman effect is possible by employing classical and quantum mechanical models. The classical approach to a description of the Raman effect considers the scattering molecule as a collection of atoms undergoing simple harmonic vibrations without consideration of the quantization of the vibrational energy. When an electric field (radiation) is applied to a molecule, according to coulomb law, both nuclei and electrons will respond to the external electric field by moving in opposite directions, thus inducing a dipole moment in the molecule, and as long as the electric field is not strong enough to cause ionization, the induced dipole moment is linearly proportional to the applied electric field as

$$\mu_{Ind} = \alpha E \tag{6.3}$$

Where $\alpha$ is the polarizability constant and is an intrinsic characteristic of the molecule, and is attributed to the ease with which the electron cloud of the molecule can be distorted.[118]The electric field $E$ associated with an incident beam of frequency $v_0$ can be written in time-dependent form as

$$E = E_0 \cos(2\pi v_0 t) \tag{6.4}$$

$E_0$ is the amplitude of the oscillating field. In a real physical 3 dimensional world, the polarizability is a tensor quantity and as such has components in each of the $x$, $y$, $z$ directions of a Cartesian coordinate system. Thus equation (6.3) can be written in matrix notation as

$$\begin{pmatrix} \mu_x \\ \mu_y \\ \mu_z \end{pmatrix} = \begin{pmatrix} \alpha_{xx} & \alpha_{xy} & \alpha_{xz} \\ \alpha_{yx} & \alpha_{yy} & \alpha_{yz} \\ \alpha_{zx} & \alpha_{zy} & \alpha_{zz} \end{pmatrix} \begin{pmatrix} E_x \\ E_y \\ E_z \end{pmatrix} \tag{6.5}$$

If molecular polarizability changes during the vibration, its value for small vibrational amplitude is given by,

$$\alpha = \alpha^0 + \left(\frac{\partial \alpha}{\partial q_v}\right)_0 q_v \tag{6.6}$$

where $q_v$ is the coordinate along the axis of vibration at a time $t$, and is given by

$$q_v = q_0 \cos(2\pi \nu_v t) \tag{6.7}$$

Substituting (6.7) into (6.6) yields

$$\alpha = \alpha^0 + \left(\frac{\partial \alpha}{\partial q_v}\right)_0 q_0 \cos(2\pi \nu_v t) \tag{6.8}$$

Plugging (6.8) and (6.4) into (6.3) with suitable trigonometric manipulation gives

$$\mu_i = \alpha^0 E^0 \cos(2\pi \nu_v t) + \left(\frac{\partial \alpha}{\partial q_v}\right)_0 \frac{E^0 q_0}{2}$$

$$\times \left\{\cos[2\pi(\nu_0 + \nu_v)t] + \cos[2\pi(\nu_0 - \nu_v)t]\right\} \tag{6.9}$$

The first term in equation (6.9) describes Rayleigh scattering, whereas, the remaining terms describe Stokes and anti-Stokes Raman scatter. Equation (6.9) suggests that for Raman scattering to occur, the polarizability of the molecule must change during a vibration if the vibration is to be Raman active. This condition is expressed mathematically as

$$\left(\frac{\partial \alpha}{\partial q_v}\right)_0 \neq 0 \tag{6.10}$$

The quantum theory approach to Raman scattering takes into consideration the fact that the vibrational energy of a molecule is quantized and expressed as

$$E_s = h\nu(s + \frac{1}{2}) \tag{6.11}$$

where $v$ is the frequency of vibration and $s$ is the vibrational quantum number. The quantum mechanical treatment considers the perturbation of the wave-functions of the scattering molecule by the electric field of incident light frequency $v_0$ , for the induced electric moment of matrix element $P_{nm}$ associated between the initial state $n$ and the final state $m$ which is defined as

$$P_{nm} = \int \psi_m^* P \psi_n d\tau \tag{6.12}$$

where $P_{nm}$ is the induced dipole moment operator, $\psi_m$ and $\psi_n$ are the time-independent wave functions of the states. The quantum-mechanical result for $P_{nm}$ is of the form

$$P_{nm} = \frac{1}{h} \sum_r \left( \frac{M_{nr} M_{rm}}{\nu_{rn} - \nu_0} + \frac{M_{nr} M_{rm}}{\nu_{rm} + \nu_0} \right) E \tag{6.13}$$

where $h$ is the Planck's constant, $r$ denotes any level of the complete set belonging to the unperturbed molecule, $\nu_{rn}$ and $\nu_{rm}$ are the frequencies corresponding to the difference between the states denoted by the subscripts,[119] and $M_{nr}$ and $M_{rm}$ are the corresponding transition moment. Thus the intensity of scattering between states $n$, $m$

$$I_{nm} = C(\nu_0 + \nu_{nm})^4 P_{nm}^2 \tag{6.14}$$

In this equation $C$ is a universal constant equal to $64\pi^2/(3c^2)$, $c$ is velocity of light. To obtain total intensity of $N_n$ in initial state, multiplication by factor $N_n$ is crucial.[119]

Raman Under Liquid Nitrogen of *R*3MCP

All Raman spectra were recorded using a Dilor XY 800 Raman spectrometer at the University of Tennessee, Department of chemistry, which is equipped with a microscope for micro-Raman studies; the modular spectrometer is equipped with three 1200 g/mm gratings. Two in a foremonochromator and one in spectrograph. The gratings are of the holographic type and are blazed at 8000 A°. Laser excitation was obtained using a 100 mW Lexer Laser, Inc. 3500 Argon Ion Laser (5145 A°), Raman Under liquid nitrogen (RUN) was first recorded to obtain comprehensive information about Raman vibrations at low temperature where the population of the equatorial conformer is predicted to be dominant ( figure 6.1).

Polavarapu et. al.[117]assigned Raman lines of *R*3MCP for most of the vibrational modes. The lines at 459.67 $cm^{-1}$ and 487.69 $cm^{-1}$ are due to the out- of -plane and-in- plane C=O bending modes, respectively. Strong Raman lines observed at 813.14 $cm^{-1}$and 986.71 $cm^{-1}$ are due to cyclopentanone ring bond stretching and angle bending, Carbonyl stretching band[120] found in all ketones was observed at 1727.58 $cm^{-1}$. The RUN experiment sample was introduced by placing a few drops of neat *R*3MCP sample in a curved nest on the surface of a good heat conducting stainless steel piece which is made by two dewars, the outer liquid nitrogen dewar is made of modified Styrofoam packing material used to protect bottles containing liquids while the inner Styrofoam container is a common coffee cup with small notch is cut at the top to allow liquid nitrogen flow, the liquid nitrogen was poured gradually into the space

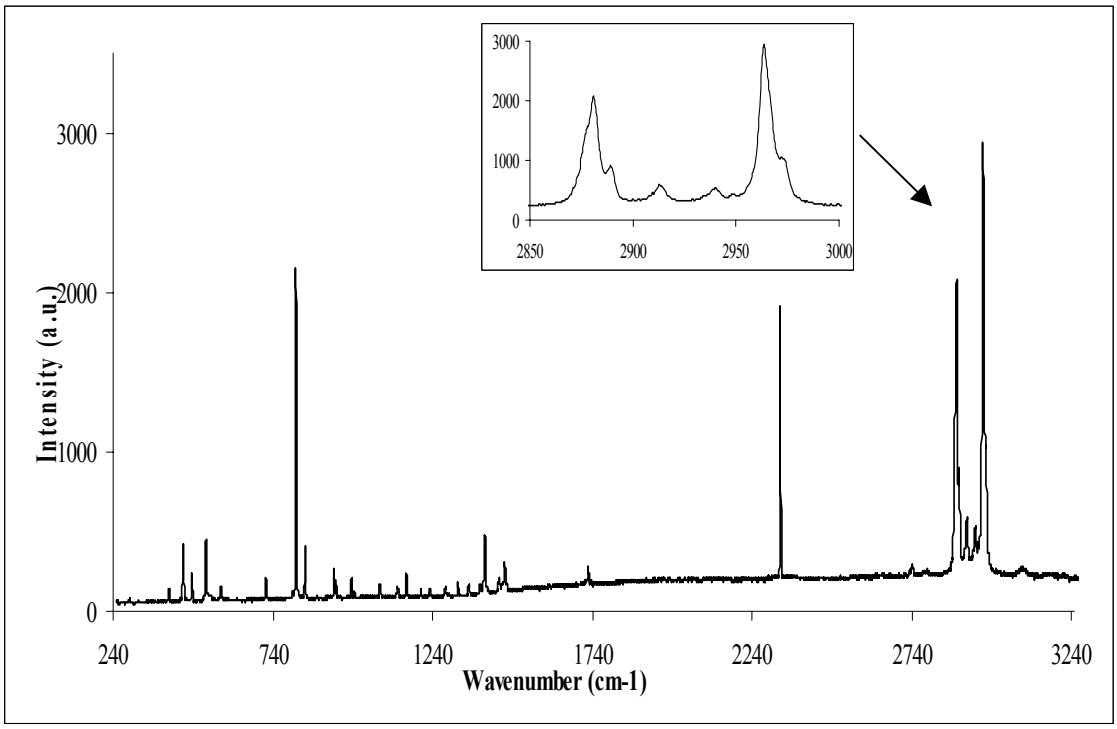


Figure 6.1 Raman under liquid nitrogen (RUN) (T = 77 °K)spectrum of neat *R*3MCP, the small figure within represents the magnified C-H stretch region(2850-3000 $cm^{-1}$).

between the two Styrofoam cups to achieve slow freezing in order to eliminate sudden crystallization effects, such as amorphous solids[121]that can affect higher energy vibrational transitions as well as the lattice modes of vibrations that may overlap with Raman modes. The sample "nest" was maintained to be completely under the liquid $N_2$ as much as possible while maintaining a shallow liquid nitrogen level to minimize the loss of Argon laser intensity while incident on and scattered from the crystalline *R*3MCP surface. Slow freezing as opposed to nozzle-jet expansions allows for relaxation into the lowest energy conformer.

Liquid nitrogen effects on R3MCP spectra exhibits two main Raman lines, the significant liquid nitrogen Raman line is at 2328.23 $cm^{-1}$ which is due to $^{14}N_2$ in addition to a weak Raman line at 2287.21 $cm^{-1}$ which corresponds to least abundant $^{14}N^{15}N$ isotope. The distinct precise and accurate location of the liquid nitrogen Raman lines serves as a calibration reference for Raman spectra under liquid nitrogen.[122]

Another aspect of RUN is the a few wavenumbers bathochromic (red) shift in Raman lines frequencies from liquid phase varying temperature data, as will be shown in the next section. In which observation of the C-H stretch region ranging from ~ 2 $cm^{-1}$ for major Raman lines at , 2905.03 $cm^{-1}$, 2927.13 $cm^{-1}$, 2961.82 $cm^{-1}$ to ~ 9 $cm^{-1}$ at 2872.3 $cm^{-1}$ at Room temperature. Another RUN effect was the improved resolution and high signal to noise ratio[123] due to the cooling direct effect on reducing number of possible rovibrational states.

Temperature Varying Raman *R*3MCP Spectra

Recording Raman spectra for the C-H region as a function of temperature is employed as a conformational analysis method by observing the sample temperature effect on Raman intensity lines, figure 6.2. The experimental setup was modified by placing neat R3MCP sample in a standard NMR tube which was heated by tungsten wire wrapped uniformly on the outer surface of the NMR tube and attached to the outlets of an AC varying voltage power supply to raise the sample temperature above room temperature, whereas, a dry ice nest and cooling plate were used to obtain low temperatures, a Cd-Ni thermocouple was immersed in sample to probe and observe temperature instantly. Data were recorded rapidly to reduce sample temperature fluctuations. It was observed that the intensity and area under the curve for the Raman lines at 2905.03 $cm^{-1}$ and 2927.13 $cm^{-1}$ increase as sample temperature increase, whereas, Raman lines at 2872.3 $cm^{-1}$ and 2961.82 $cm^{-1}$ show opposite correlation with temperature, this observation is directly related to the axial-methyl and equatorial-methyl conformers contribution of *R*3MCP where the first two lines are assigned to the axial while the other two are due to the Raman vibraional mode of the equatorial, RUN spectra further emphasized peak assignments since at 77 ºK axial peaks heights were substantially smaller relative to the equatorial Raman lines.

Employing peak fit software for baseline corrections and peak deconvolution it was possible to obtain the area under each Raman peak by plotting the natural logarithm, see figure 6.3, of the ratios of area under the curve for axial-methyl to equatorial methyl at 2927.13 $cm^{-1}$and 2961.82 $cm^{-1}$,

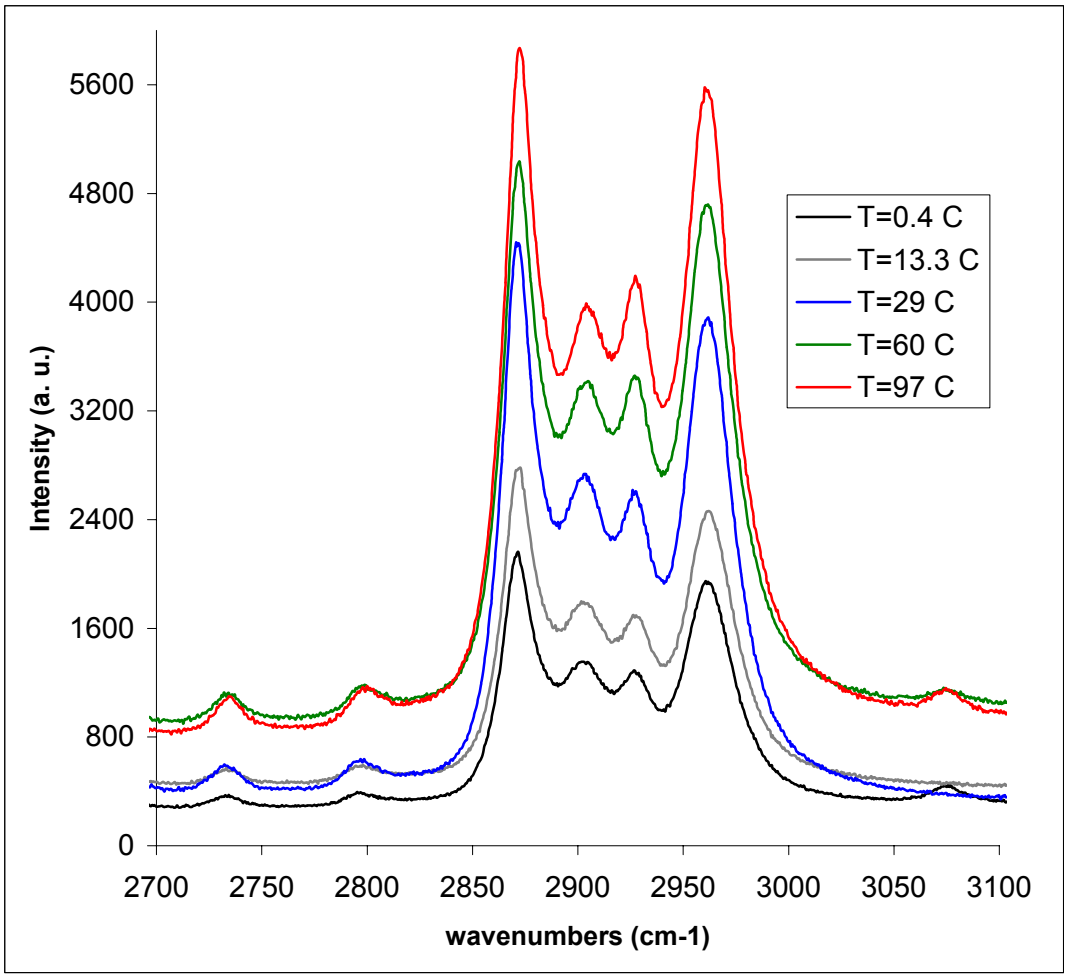


Figure 6.2 Varying temperature Raman spectra for the C-H stretch region (2850-3000 $cm^{-1}$) of the *R*3MCP.

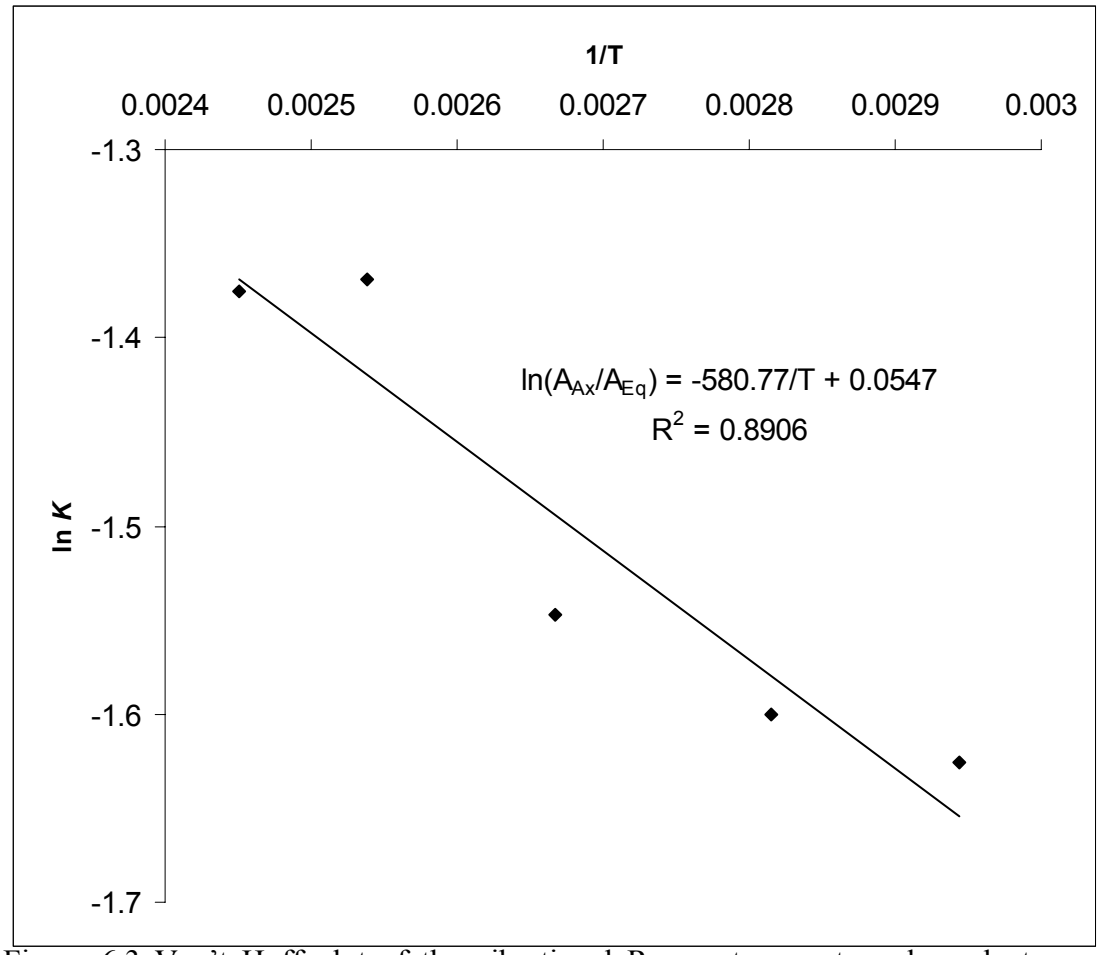


Figure 6.3 Van't Hoff plot of the vibrational Raman temperature dependent area under the peak spectra corresponding to the axial and equatorial conformers at 2927.13 $cm^{-1}$ and 2961.82 $cm^{-1}$, respectively.

respectively, versus reciprocal temperature, it is possible to construct Van't Hoff plot. The Van't Hoff plot slope is shown in figure 6.3 which provides a $\Delta H° = 4.83$ kJ/mol, RUN data were not included in Van't Hoff plot to avoid lattice vibrations effects that could negatively affect conformational analysis study.

Conclusion

In summary, temperature dependent Raman spectroscopy was employed to investigate the *R*3MCP conformations. Raman under liquid nitrogen spectrum of neat *R*3MCP was presented first as a preliminary tool to observe Raman spectroscopy at liquid nitrogen temperature, where in addition to the improved resolution provided by RUN. The cross section of the assigned Raman vibrational modes due to the equatorial conformer, at 2872.3 $cm^{-1}$ and 2961.82 $cm^{-1}$, was observed to be relatively larger than those assigned to axial modes at 2905.03 $cm^{-1}$ and 2927.13 $cm^{-1}$. Furthermore, the same trend was observed for different sample temperatures over a wide temperature range (~ 100 °*C*) of the vibrational Raman spectra for the C-H stretch region (2850 – 3000 $cm^{-1}$) which was employed to determine axial and equatorial conformers energy difference ($\Delta H° = 4.83$ kJ/mol) by utilizing the Van't Hoff plot.[124]

Density Function Theory calculations were performed for *R*3MCP conformers. The poor matching between experimental and predicted findings was attributed to the difficulty in predicting Raman intensities, since Raman calculations involve the derivatives of polarizabilities ($3^{rd}$ order derivatives of energy).

# CHAPTER VII
# INFRARED AND VIBRATIONAL CIRCULAR DICHROISM OF CARVONE AND LIMONENE

## IR Absorption and VCD Theory and Principles

Infrared absorption spectroscopy (IR) is widely recognized as a principal tool for the study of molecular vibrations. In addition, within the past few years Vibrational Circular Dichroism (VCD), which is defined as the differential absorption of the left and right circularly polarized infrared radiation, has been conclusively demonstrated as a reliable method, when combined with theory, to provide absolute conformation determination for chiral molecules. VCD and IR are related in the same way that CD is related to UV/VIS absorption. The key impetus for exploring the vibrational region of the spectrum is the discrete and predictable features which are characteristic of localized regions of the molecule. In other words, the chromophores active in the molecule for VCD measurements are representative of the bonding giving rise to the stretching and bond deformation excitations. Furthermore, these excitations are part of the ground electronic state of the molecule, therefore stereochemical insights gained from analysis of the spectra are not complicated by geometrical changes involved in excitation to states composed of antibonding orbitals, as is typical for electronic CD.[125]

Holzwarth et. al.[126,127]experimentally observed the first VCD spectrum in the mid 1970s using single crystals of $NiSO_4.6H_2O$. This work also reported VCD for the C-H stretching band in trifluoro-1-phenylethanol. These studies sparked interest in experimental VCD studies of a wide variety of liquid chiral molecules.[128-130]The instrumentation developed over the past three decades makes the measurement of VCD

reasonably routine over much of the IR region. At the present time there are no major difficulties of recording VCD measurements from the near IR 3000 $cm^{-1}$ (e.g. C-H, N-H, and O-H stretching regions) through the mid IR down to ~ 700 $cm^{-1}$ for most samples.[125]

On the theoretical front, the theory of IR absorption and VCD is well-established and has developed within the framework of several classical assumptions.[131-137]IR intensities can be expressed via the dipole strength *D*. For a transition of the molecule between the ν = 0 and the ν = 1 levels of the *a*th vibrational mode in the ground electronic state g, the dipole strength can be denoted by

$$D^{a}_{g1,g0} = \left| \left\langle \psi^{a}_{g1} / \mu_{\beta} / \psi^{a}_{g0} \right\rangle \right|^{2} \tag{7.1}$$

The dipole strength is the absolute square of the electric-dipole transition moment, while the subscript $\beta$ referes to a molecule-based Cartesian coordinate system. The $\beta$ component of the electric-dipole moment operator in the position form is given by

$$\mu_{\beta} = \mu^{E}_{\beta} + \mu^{N}_{\beta} = -\sum_{j} e r_{j\beta} + \sum_{J} Z_{J} e R_{J\beta} \tag{7.2}$$

where the sum occurs over the products of the charges and positions of all of the electrons and nuclei of the molecule. Equation (7.1) can also be represented in the dipole velocity formalism, which gives[136]

$$D^{a}_{g1,g0} = \omega_{a}^{-2} \left| \left\langle \psi^{a}_{g1} / \dot{\mu}_{\beta} / \psi^{a}_{g0} \right\rangle \right|^{2} \tag{7.3}$$

$\omega_a$ is the angular frequency of normal mode *a*. The electric-dipole velocity can be written as

$$\overset{g}{\mu}_\beta = \overset{gE}{\mu}_\beta + \overset{gN}{\mu}_\beta = -\sum_j e\overset{g}{r}_{j\beta} + \sum_J Z_J e \overset{g}{R}_{J\beta}$$

$$= -\sum_j \frac{e}{m} P_{j\beta} + \sum_J \frac{Z_J e}{M_J} P_{J\beta} \tag{7.4}$$

The velocity dipole operator is obtained from the product of the charge and the velocity of the electrons, and the nuclei in the molecule. The velocity can also be obtained from the ratio of the momentum to the mass of each particle. The intensity of the VCD band is defined through the rotational strength[137]

$$R^a_{g1,g0} = \mathrm{Im}[\langle \psi^a_{g0} / \mu_\beta / \psi^a_{g1} \rangle \langle \psi^a_{g1} / m_\beta / \psi^a_{g0} \rangle] \tag{7.5}$$

The magnetic-dipole moment operator can be expressed in the notation of eqs (7.2) and (7.4) as

$$m_\beta = m^E_\beta + m^N_\beta = -\sum_j \frac{e}{2mc} \varepsilon_{\beta\gamma\delta} r_{j\gamma} p_{j\delta} + \sum_J \frac{Z_J e}{2M_J c} \varepsilon_{\beta\gamma\delta} R_{J\gamma} P_{J\delta} \tag{7.6}$$

and $\varepsilon_{\beta\gamma\delta}$ is the alternating tensor that is +1 for even permutations of *xyz* and -1 for odd permutations. The rotational strength is a scalar quantity that can assume positive and negative, as well as 0 values.

The intensities of vibrational bands of chiral molecules that exist in two or more conformations can be represented in matrix notation as

$$\begin{pmatrix} I_1 \\ I_2 \\ I_3 \\ - \\ - \\ I_m \end{pmatrix} = \begin{pmatrix} P_{1,1} & P_{1,2} & P_{1,3} & - & P_{1,N} \\ P_{2,1} & P_{2,2} & P_{2,3} & - & P_{2,N} \\ P_{3,1} & P_{3,2} & P_{3,3} & - & P_{3,N} \\ - & - & - & - & - \\ - & - & - & - & - \\ P_{m,1} & P_{m,2} & P_{m,3} & - & P_{m,N} \end{pmatrix} \begin{pmatrix} X_1 \\ X_2 \\ - \\ - \\ X_N \end{pmatrix} \tag{7.7a}$$

The experimental vibrational intensities are represented by column vector, $\{I\}$, and the contribution of each conformer is represented by rectangular matrix, $\{P\}$. The last column vector, $\{X\}$, denotes the mole fraction of each possible conformer of a conformational isomer. The previous matrix can be simplified in summation notation as

$$I_i = \sum_{j=1}^{N} P_{ij} X_j \qquad \text{for } i = 1,2,\ldots, m \qquad (7.7b)$$

It is commonly observed that the number of vibrational bands ($m$), is far greater than the number of conformations ($N$). Furthermore, the sum of the fractional populations of conformers is 1. In modern day VCD spectrometers, dipole strengths ($D_i$) and rotational strengths ($R_i$) are expressed as

$$D_i = \frac{0.92 \times 10^{-38}}{\nu_0} \int \varepsilon(\nu) d\nu \qquad (7.8)$$

$$R_i = \frac{0.23 \times 10^{-38}}{\nu_0} \int \varepsilon(\nu) d\nu \qquad (7.9)$$

Where $\varepsilon(\nu)$ is the molar absorptivity (in L.mol$^{-1}$.cm$^{-1}$) at frequency ν (cm$^{-1}$), and $\nu_0$ is frequency of the band center.

Vibrational spectroscopy has been widely used for conformational analysis[138] of most organic molecules. Temperature dependent IR techniques are based on the principle to identify vibrational bands characteristic of conformers, consequently, the ratio of those bands as a function of temperature can be used to determine the energy difference between conformers.[139]

IR and VCD of Carvone and Limonene Conformers

All IR and VCD measurements were recorded on a commercial Fourier transform VCD spectrometer *Chiralir* with dual photo-elastic modulators PEM (set at 412 nm and 1400 $cm^{-1}$. The sample was contained in a variable path length cell of (5-25 $\mu$m) with $BaF_2$ windows that is convenient for FTIR spectroscopy. The spectra were recorded with 1-hr data collection time at 4 $cm^{-1}$ resolution for 100 scans. Two different samples in the liquid phase were under study separately; carvone and limonene enantiomers. Diagnostic measurements were first performed to select proper solvation parameters, and consequently, a decision was made to use the samples in the neat form without any solvents based on the infinitesimal noise observed in the IR spectra. Background measurements were first recorded and then subtracted from the sample spectra in order to further minimize signal noise.

All ring conformations are classifiable as axial and equatorial with their rotamers being similarly Eq (T), Ax (T) and Eq (C), Ax (C),[140] where T and C stand for Trans and Cis, respectively. Likewise, carvone is known to have four possible conformers (figure 7.1); whereas, limonene exists in three conformers (Ax (C) is not possible), see figure 7.2. VCD spectra of carvone and limonene enantiomers (*R*, *S*) show absolute equal magnitude but opposite sign (figure 7.3) as expected. IR and VCD Density Functional Theory (DFT) calculations of the optimized geometry were carried out with Gauusian03.[141] A moderately powerful set of equations using the basis set aug-cc-pVDZ were employed for all IR and VCD calculations for all of the possible conformers of carvone and limonene (figures 7.4-7.9).

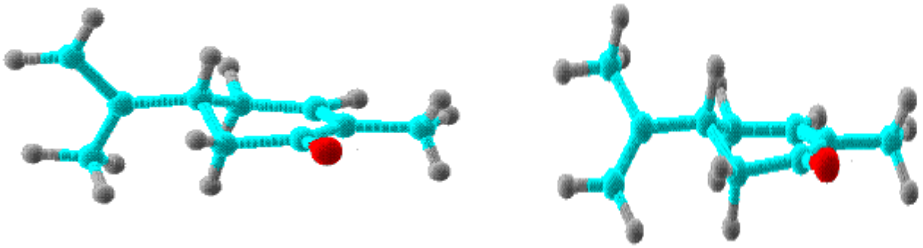

Equatorial (C) Equatorial (T)

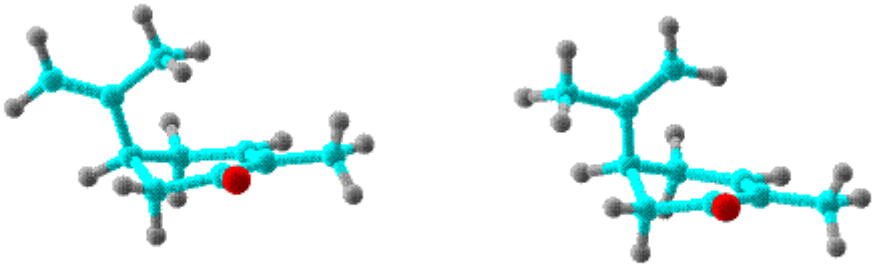

Axial (C) Axial (T)

Figure 7.1 *R*-(-)-carvone optimized minimum energy conformers, Equatorial and Axial, and the rotamers T and C.

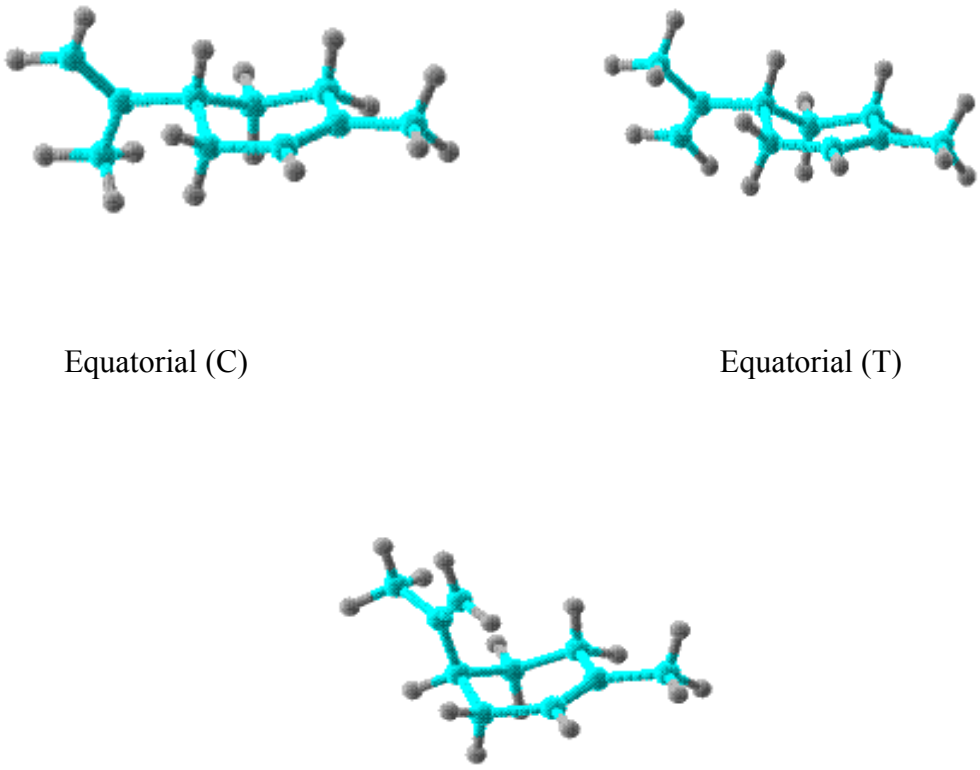

Equatorial (C)

Equatorial (T)

Axial (T)

Figure 7.2 *R*-(+)-limonene optimized minimum energy conformers, Equatorial and Axial, and the rotamers T and C.

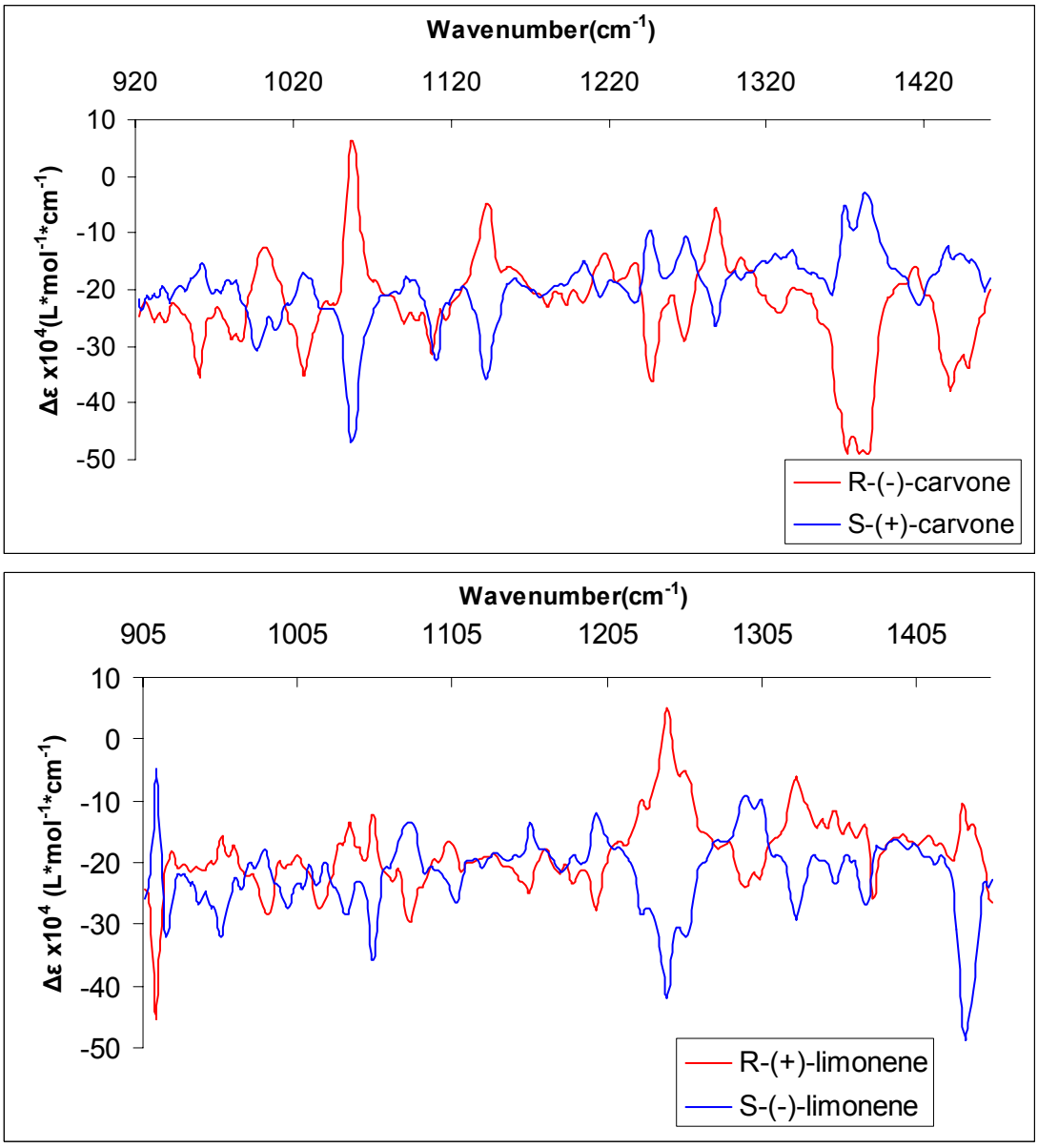


Figure 7.3 Experimental VCD spectra of *R*, *S* enantiomers of Carvone (top) and Limonene (Bottom).

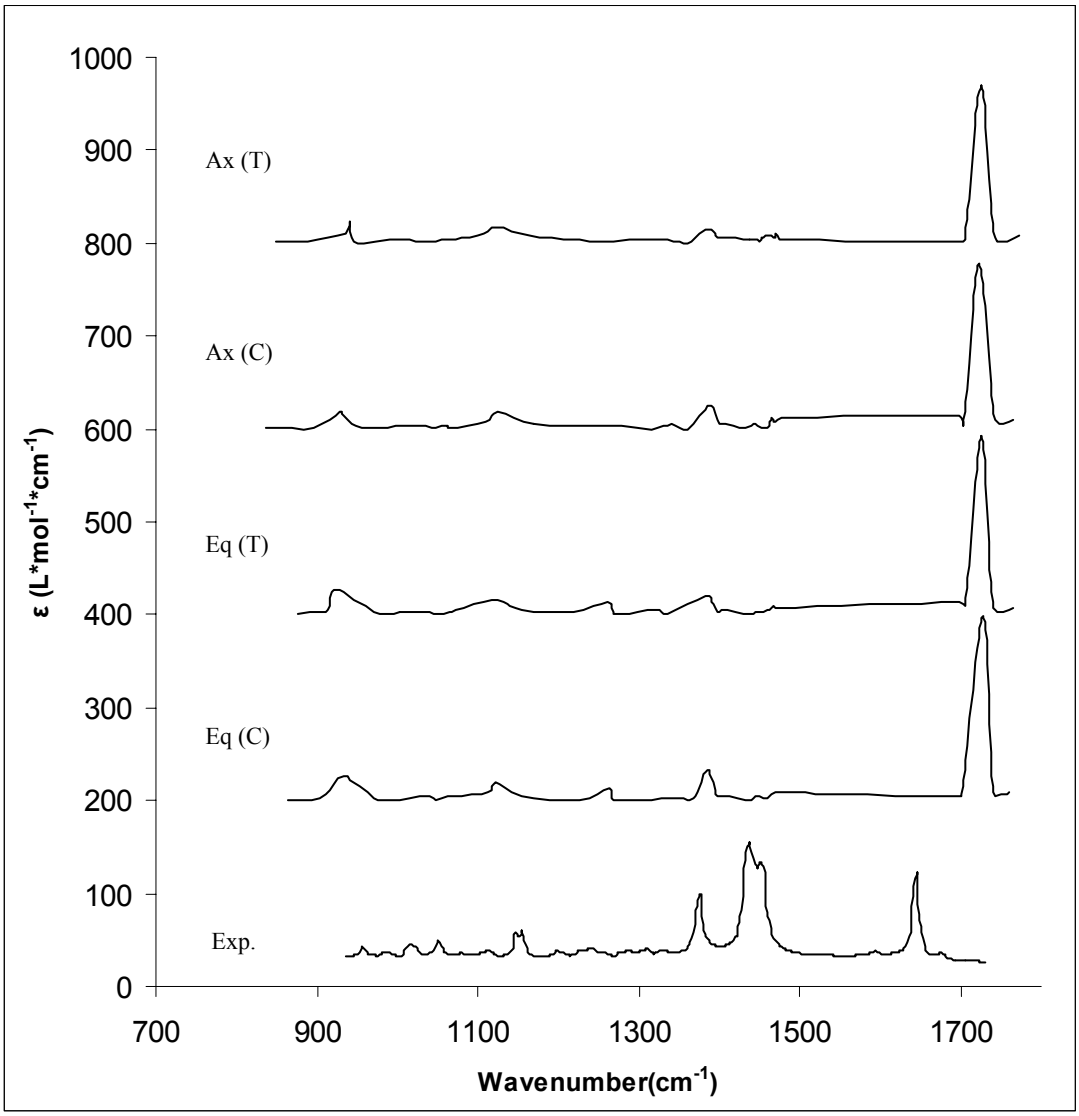


Figure 7.4 correlations between experimental and calculated IR spectra obtained at B3LYP/aug-cc-pVDZ level for *R*-(-)-carvone possible conformers, Eq (C), Eq (T), and Ax (T).

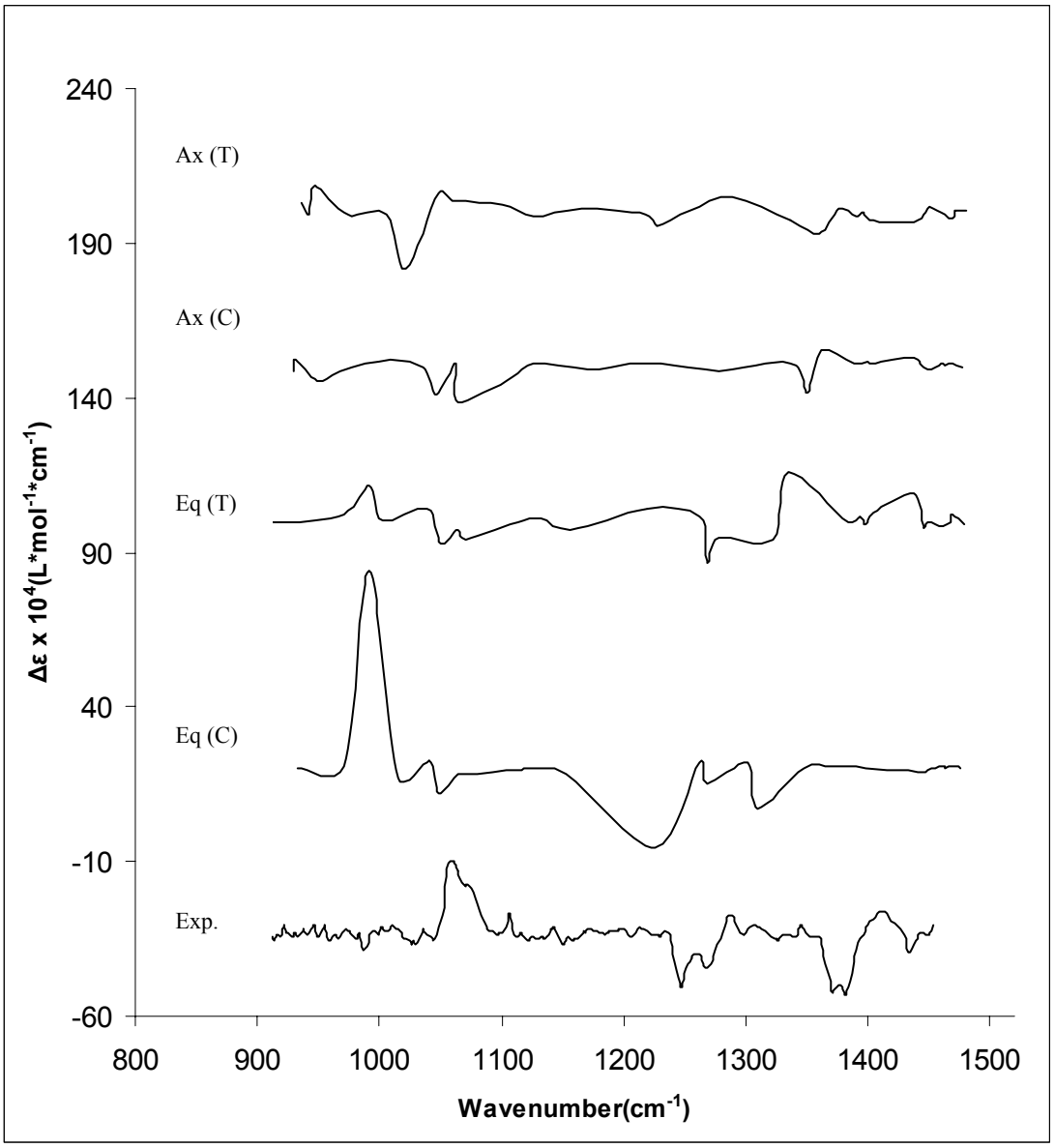


Figure 7.5 Correlations between experimental and calculated VCD spectra obtained at B3LYP/aug-cc-pVDZ level for *R*-(-)-carvone possible conformers, Eq (C), Eq (T), Ax (C) and Ax (T).

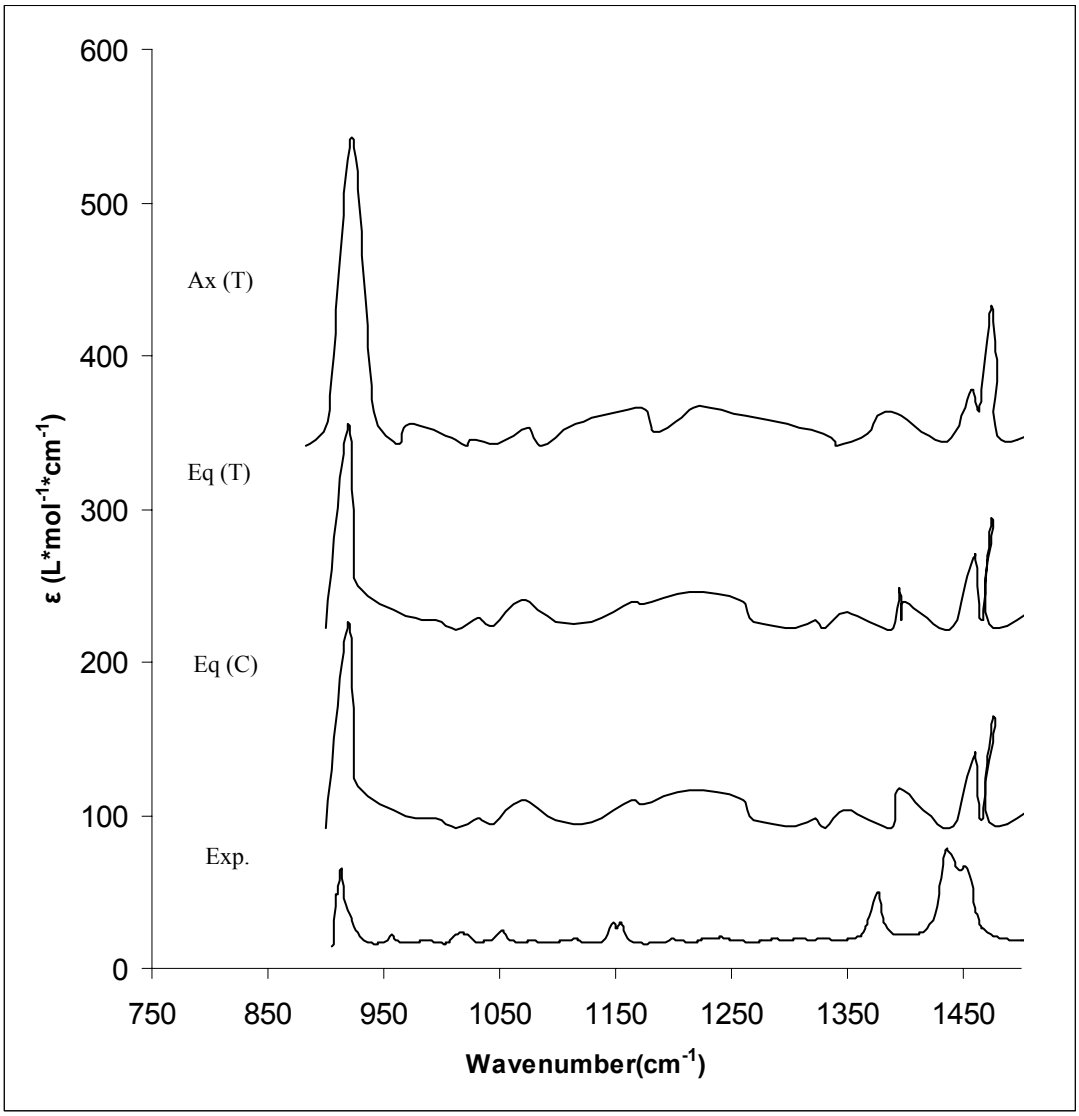


Figure 7.6 Correlations between experimental and calculated IR spectra obtained at B3LYP/aug-cc-pVDZ level for *R*-(+)-limonene possible conformers, Eq (C), Eq (T), and Ax (T).

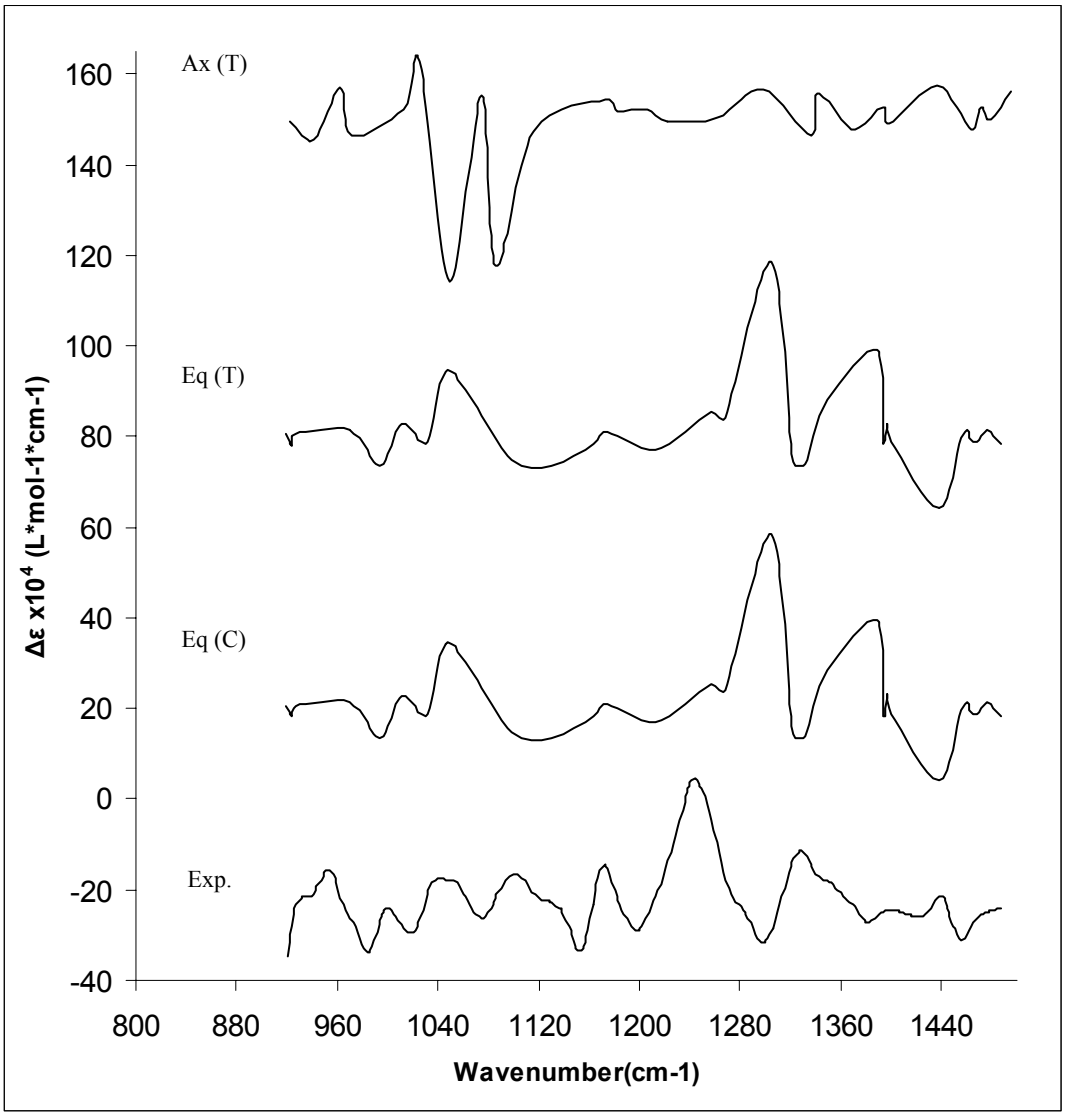


Figure 7.7 Correlations between experimental and calculated VCD spectra obtained at B3LYP/aug-cc-pVDZ level for *R*-(+)-limonene possible conformers, Eq (C), Eq (T), and Ax (T).

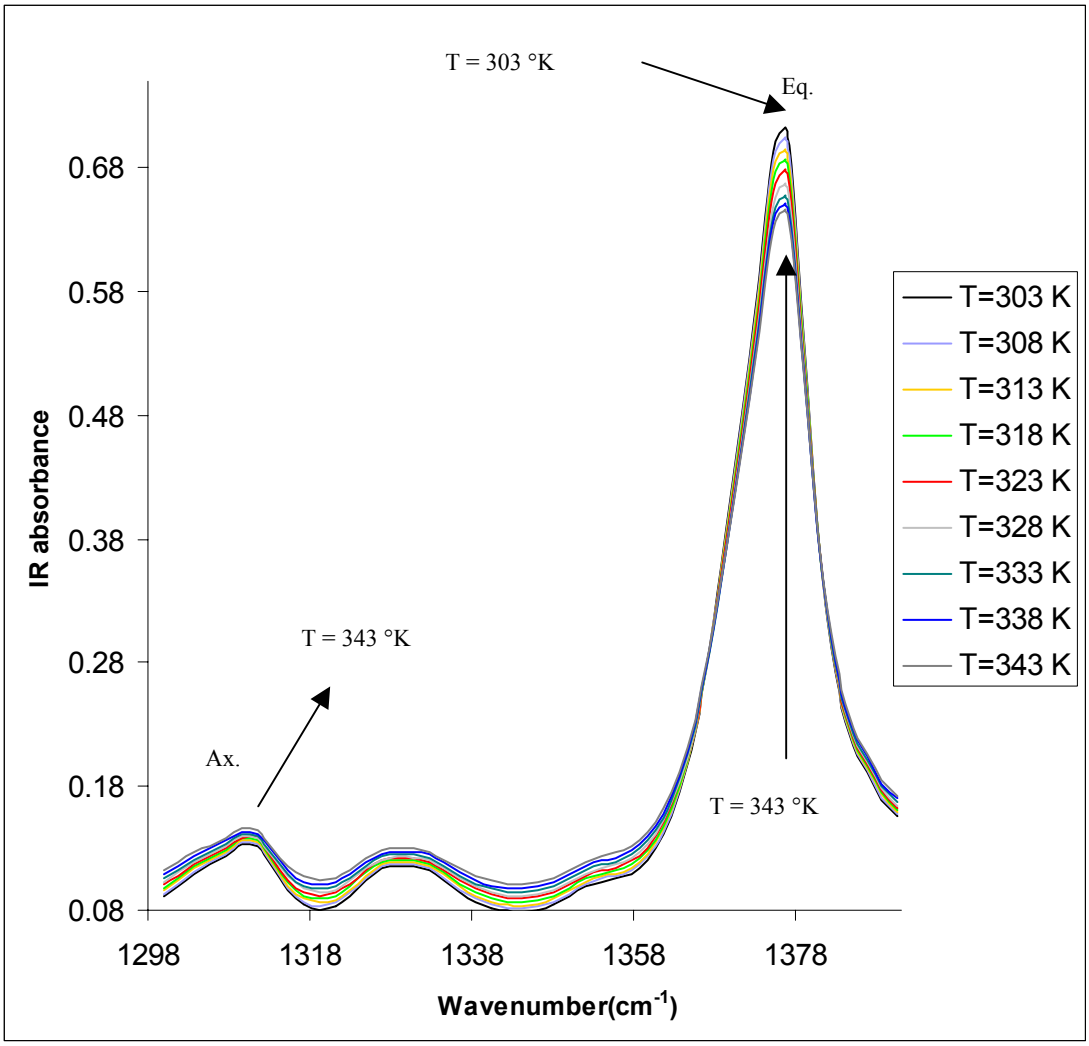


Figure 7.8 Temperature dependent IR spectra between 303 and 343 °K at 5 degrees interval of liquid *R*-(+)-limonene. The absorption bands at 1309.5 $cm^{-1}$ and 1377 $cm^{-1}$are assigned to the axial and equatorial conformations, respectively.

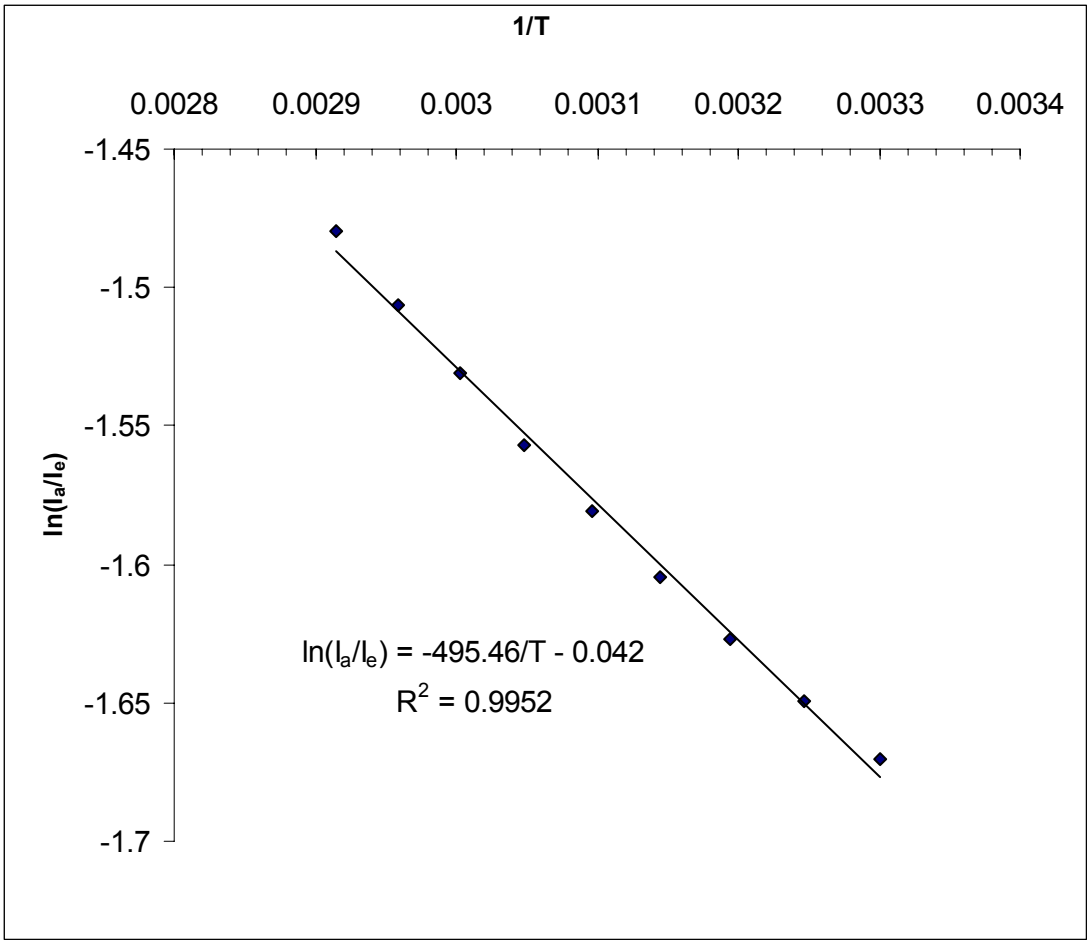


Figure 7.9 Van't Hoff plot obtained from the ratio of axial (at 1309.5 $cm^{-1}$) to the equatorial ( at 1377 $cm^{-1}$) IR intensities as a function of temperature for *R*-(+)-limonene. $\Delta H°$ derived from the slope is 4.12 kJ/mol.

Summary & Discussions

This chapter provides the first experimental and theoretical study of the VCD of the carvone and limonene molecules. VCD has the advantage, over all other chirality probing methods, of being capable of determining absolute conformation of chiral molecules in conjunction with ab initio calculations. In this work Density Function Theory (DFT) calculations of each possible conformer, is employed to identify the most abundant conformers in the chiral sample. These studies are very similar to that of He et. al.[139] who have recently studied the absolute configuration of R-(+)-3-methylcyclopenatnone using IR absorption and VCD.

Limonene and carvone samples were employed to generalize the He[139] findings for the possibility of more than two conformers. In figure 7.3, it was observed that the VCD spectra of limonene and carvone enantiomers exhibit a similar trend to that observed for electronic CD, i.e. VCD is equal in magnitude and opposite in sign for the two enantiomers as expected. This provides some confidence in the experimental methods employed. Fortunately, the signal to noise ratio was sufficient to observe fine structure in the VCD spectra over (905-1453 $cm^{-1}$). It was not necessary to use carvone solutions. IR spectra of neat *R*-(-)-carvone, in figure 7.4, show good agreement between experimental and calculated spectra of all four conformers except for the strong peak at ~ 1450 $cm^{-1}$. This peak corresponds to the expected strong IR bending vibration of $CH_2$. The C=O vibration is represented by a very strong IR peak at ~ 1680 $cm^{-1}$, and the bending mode of $CH_3$ is seen as a significant peak at ~ 1380 $cm^{-1}$.[142] VCD spectra of *R*-(-)-carvone, figure 7.5, show good

agreement between experiment and calculations for the Eq (C) conformer. Reasonable agreement is also seen with Eq (T). VCD calculations of the Ax (C) and Ax (T) conformers show poor agreement with experimental spectra which can be attributed to the fact that Eq (C) is lowest in energy and most populated conformer in carvone sample.

A similar trend was observed for the IR spectra of *R*-(+)-limonene (Figure 7.6) where spectra calculated for the Eq (C), Eq (T) and Ax (T) conformers spectra were found to be consistent with the observed experimental spectrum. Calculated VCD spectra for the equatorial conformer show good agreement with observed spectra unlike that for the axial conformer. The axial conformer has a small contribution due to its low population at room temperature.

Temperature dependent IR spectra were recorded for *R*-(+)-limonene in order to determine the energy difference between the equatorial and axial conformers. By observing the temperature dependence, it was possible to assign the weak IR peaks at ~ 1309.5 $cm^{-1}$ and 1377 $cm^{-1}$ to the axial and equatorial conformers, respectively. A value for the conformers energy difference was concluded from the slope of Van't Hoff plot of the natural logarithm for the ratio between peak intensity versus reciprocal of sample temperature. The result obtained ($\Delta H$ = 4.12 kJ/mol) was consistent with the predicted value using B3LYP DFT calculations with basis sets 6-31G* and aug-cc-pVDZ. Both calculations yield $\Delta H$ = 4.85 kJ/mol. Although temperature dependent studies were also recorded for VCD, it was not possible to utilize this data due to the extremely low signal relative to IR absorption.

# CHAPTER VIII
# CONCLUSIONS

This Dissertation presents results from a variety of chiroptical spectroscopic techniques along with theoretical calculations to investigate linear and nonlinear chiroptical effects for three natural products (3MCP, carvone and limonene). Optical Activity can be classified in terms of the molecular transition scale into electronic; which include ORD and CD, and vibrational that consists of Raman scattering and VCD of IR absorption. Raman optical activity, ROA, is also possible but not studied in this thesis.

The development of high-power, tunable lasers has opened a new field of nonlinear chiroptical spectroscopy. Although nonlinear optics is a well established field, nonlinear chiroptical spectroscopy is in its infancy. In Chapter III, we introduced a new technique, Resonantly Enhanced Multiphoton Ionization Circular Dichroism (REMPICD), as an application of nonlinear interaction of light with chiral matter by generating (2+1) multiphoton electronic transition of racemic and chiral 3MCP using high power pulsed laser light. The dissymmetric factor g of one photon CD was enhanced by a factor of three using REMPICD which was attributed to the alignment of the resonantly enhanced intermediates. Future research will focus on probing other chiral molecules as well as by employing multicolored laser light at each real and virtual transition including the continuum.

Solvent effects on ORD and CD of *R*3MCP in 35 common solvents was thoroughly investigated. The criteria of solvent selection were based on covering the spectrum of different mechanisms of solute-solvent interaction. Vibronic effects

demonstrated as CD fine structure, are particularly important in the CD spectrum because the transition which give large dissymmetry factors (i.e. carbonyl $n \rightarrow \pi^*$) are often fully magnetic dipole allowed and electric dipole forbidden so that light absorption is usually made partially allowed by symmetry breaking vibronic transitions.

Conformational analysis of enantiomers of all three named molecules was studied using different tools, such as temperature dependent CD, ORD, Raman scattering, IR and VCD. Due to the fact that the ratio of molecular conformations are temperature sensitive, it was possible to determine conformer population and energy differences between equatorial and axial conformers for *R*3MCP using TDCD. Measured values are compared with results from temperature dependent vibrational Raman spectroscopy. Furthermore, Raman Under liquid nitrogen was a useful technique to obtain Raman vibrations with high resolution, and was used to confirm the assignment of temperature dependence of the Raman Analysis.

IR and VCD of multi-conformer molecules (limonene and carvone) were presented along with theoretical calculations. A conclusion was reached that the equatorial conformer is the lowest in energy and the most populated of all other conformers, so that it forms most features of IR and VCD spectra.

The advancement of chirality science has been motivated by the quest to find the origin of life. Nowadays, understanding chiral matter and optical activity is of tremendous importance and applications, from study of galaxies to the DNA structure and living cells.

# LIST OF REFERENCES

[1] R. S. Cahn, C. K. Ingold, and V. Prelog, Angew. Chem., 78, 413-447, (1966).

[2] R. N. Compton, and R. Pagni, Advances in Atomic, Molecular, and Opical Physics, vol., 220-260, (2002).

[3] David C. Walker, Origins Of Optical Activity In Nature, Elsevier Scientific Publishing Company, Amesterdam-Oxford- New York,(1979).

[4] W. A. Bonner, Exobiology, North Holland, Amsterdam, pp.117-181, (1972).

[5] B. Norden, J. Mol. Evol., 11, 313, (1978).

[6] Optimal Design of the Archimedes screw by Charles Rorres, pp. 72-80, Journal of Hydraulic engineering/ Jan. 2000.

[7] Stephen F. Mason, Molecular Optical Activity and chiral discriminations, Cambridge University Press 1982.

[8] L. Velluz, M. Legrand, and M. Grosjean, Optical circular Dichroism, principles measurements and applications, Academic Press Inc., New York, ( 1965).

[9] H. C. Berg, R. A. Anderson, Nature, 245, 5425, 380-2, (1973).

[10] H. C. Berg, Nature, 249, 425, 77-9, (1974).

[11] A. Moscowitz, Adv. Chem. Phys., 4, 67, (1962).

[12] L. D. Barron, Molecular Light Scattering and Optical Activity, Cambridge University Press, (1982).

[13] H. A. Kramers, Atti. Congr. Intern. dei Fisici, como, 2, 545, (1927)

[14] R. de L. Kronig, J. Opt. Soc. Am., 12, 547, (1926).

[15] J. H. Van Vleck, M.I.T. Radiation Laboratory Rept. No. 735, May 28, (1945).

[16] J. R. MacDonald, M. K. Brachman, Rev. Modern Phys., 28, 393, (1956).

[17] Kuhn, Zeits. F. Physik Chemie B20, 325 (1933).

[18] Condon, Altar and Eyring , J. Chem. Phys. 5, 753 (1937).

[19] Kuhn, Trans. Faraday Soc., p.299 (1930).

[20] E. U. Condon, Rev. Mod. Phys., 9,432-457. (1937).

[21] L. Rosenfeld, Z. Physik, 52, 161, (1928).

[22] A. Roger, and B. Norden, Circular Dichroism and linear Dichroism, Oxford University Press, (1997).

[23] W. Moffitt, R. B. Woodward, A. Moscowitz, A. W. Klyne, and C. Djerassi, J. Am. Chem. Soc., 83, 4013-4018, (1961).

[24] A. Moscowitz, Adv. Chem. Phys., 4, 67-112, (1962).

[25] W. Moffitt, and A. Moscowitz, J. Chem. Phys., 30, 648-660, (1959).

[26] D. A. Lightner, J. E. Gurst, Organic Conformational Analysis and Stereochemistry from Circular Dichroism Spectroscopy, John Wiley& Sons, (2000).

[27] W. Curtis Johnson Jr., Rev. Sci. Ins., 42,9, Sept., (1971).

[28] A. Gold., B. Bebb, Phys. Rev. Let., vol. 14,3,18 Jan., (1965).

[29] C. S. Chang , Stehle P., Phys. Rev. Let., vol., 30,26 , 25 Jan., (1973).

[30] C. Tai, and F. W. Dalby , Can. J. Phys., 56, 183, (1978).

[31] R. N. Compton , J. C. Miller, A. E. Carter, and P. Kruit , Chem. Phys. Lett., 71,87, (1980).

[32] J. C. Miller, and R. N. Compton, J. Chem. Phys., 75,22, (1981).

[33] J. R. Appling, M.G. White, R. L. Dubs, S.N. Dixit, V. Mckoy.. *J. Chem. Phys*., **87**,12, 6927-6933, (1987).

[34] C. Westphal, J. Bansmann, m. Getzlaff, and G. Schönhense. *Phys. Rev. Lett*., **63**, 2, 151-154, (1989).

[35] L.E. Cuellar, C.S. Feigerle, H.S. Carman, Jr. and R.N. Compton. *Phys. Rev.,* 43, 11, 6437,(1991): C.S. Feigerle, L.E. Cuellar, N.A. Cherepkov, and L.V. Chernysheva. *Phys. Rev*., **53**, 6,4183, (1996).

[38] A. Vrancic, K. Rupnik, and Mcglynn, Rev. Sci. Instrum. 69(1), Jan., (1998).

[39] S. Piccirillo, C. Bosman, D. Toja, and W. Ange, Chem. Int. Ed. Engl.,36, 16, (1997).

[40] A. Latini , D. Toja, and Giardini-guidoni, Chirality, 11, 376-380, (1999).

[41] K. Lebarbu, A. Zehnacker, and F. Lahmani, Chirality, 13,715-721, (2001).

[42] W. J. Meath, E. A. Power, J. Phys. B: At. Mol. Phys., 17, 763-781, (1984a).

[43] W. J. Meath, E. A. Power, J. Phys. B: At. Mol. Phys., 20, 1945-1964, (1987).

[44] E. A. Power, T. Thirunamachandran, J. Chem. Phys., 60, 3695-3701, (1974).

[45] I. Tinoco, J. Chem. Phys., 62, 1006-1609, (1975).

[46] E. A. Power, J. Chem. Phys., 63, 1348-1350, (1975).

[47] D. L. Andrews, and T. Thirunamachandran, J. Chem. Phys., 60, 5026-5033, (1977).

[48] W. L. Fite, Research Note #1, Extranuclear Laboratories, Inc., (1971).

[49] J. E. Mathis, PhD Dissertation, The University of Tennessee, (1995).

[50] T. J. Cornish, T. Baer, J. Am. Chem. Soc., 110,3099-3106, (1988).

[51] N. I. Hammer, PhD Dissertation, The university of Tennessee, (2003).

[52] N. I. Hammer, F. Gao, R. M. Pagni, and R. N. Compton, J. Chem. Phys., 117, 9; 4299-4305, (2002).

[53] R. Li, R. Sullivan, W. Al-basheer, R. M. Pagni, and R. N. Compton, J. Chem. Phys., 125, 144304, (2006).

[54] Z. Dzakula, M. L. DeRider, J. L. Markley, J. Am. Chem. Soc.118 ,50, 12796, (1996).

[55] F. V. Jr. Brutcher, T. Roberts, S. J. Barr, N. Pearson, J. Am. Chem. Soc., 81,4915, (1959).

[56] J. He, Ana G. Petrovic, and P. L. Polavarapu, J. Phys. Chem. B (2004), 108, 20451-20457.

[57] R. Boese, H. Oberhammer, P. Pulay, A. Waterfeld, J. Phys. Chem.,97, 38, 9625, (1993)

[58] K. Milsow, E. Bunnenberg, R. Records, K. Wellman and C. Djerassi, J. Am. Chem. Soc.,84,1342 (1962).

[59] K. Wellman, E. Bunnenberg and C. Djerassi, J. Am. Chem. Soc., 85, 1870, (1963).

[60] A. Moscowitz, K. Wellman and C. Djerassi, J. Am. Chem. Soc., 85, 3515, (1963).

[61] A. Moscowitz , K. Wellman and C. Djerassi, Proc. N. A. S., 50, 799, (1963).

[62] K. Wellman, R. Records, E. Bunnenberg and C. Djerassi, J. Am. Chem. Soc., 86, 492, (1963).

[63] K. Wellman, and C. Djerassi, J. Am. Chem. Soc., 86,60, (1964).

[64] K. Wellman, P. H. A. Laur, W. S. Briggs, A. Moscowitz and C. Djerassi, J. Am. Chem. Soc., 87,66, (1965).

[65] K. Wellman, W. S. Briggs and C. Djerassi, J. Am. Chem. Soc.,86, 73, (1964).

[66] D. N. Kirk, W. Kyle, and S. R. Wallis, J. Chem. Soc. C 350, (1970).

[67] D. A. Lightner, T. D Bouman, W. M. D. Wijekoon, A. E. Hansen, J. Am. Chem. Soc., 108, 4484, (1986).

[68] Y-S. Li, J. Mol. Spectr., 104, 302-307, (1985).

[69] D. Kim, T. Baer, Chemical physics, 256, 251-258, (2000).

[70] F. C. Grozema, and Piet Th. Van Duijnen, J. Phys. Chem. A , 102, 7984-7989, (1998).

[71] C. Reichchardt, Solvents and Solvent Effects in Organic Chemistry, 3rd edition, (2003), WILEY-VCH Verlag GmbH & Co KgaA , Weinheim.

[72] Esther Vaz, Isabelle Fernandez, Luis Munoz and Juan Lior, J. Org. Chem., 71,2558-2564, (2006).

[73] R. E. Ballard, S. F. Mason and G. W. Vane, Discussions Of The Faraday Society, 35,43-47, (1963).

[74] W. A. Fordyce, J. G. Brummer, G. A. Crosby, J. Am. Chem. Soc., 103, 24, 7061-7064, (1981).

[75] P. R. Taylor, J. Am. Chem. Soc., 104, 19, 5248-5249, (1982).

[76] E. P. Leal, L. E. Machado, L. Mu-Tao, J. phys. B: Atom. Mol. Phys., 17, 7, L569-L575, (1984).

[77] J. Lee, G. W. Robinson, J. Phys. Chem., 89, 10, 1872-1875, (1985).

[78] T. Andruniow, M. Pawlikowski, M. Sterzel, Vib. Spec., 21, 1-2, 45-50, (1999).

[79] M. Makowski, M. Pawlikowski, Chem. Phys. Lett., 393, 4-6, 305-308, (2004).

[80] M. J. Kamlet, R. W. Taft, J. Am. Chem. Soc., 98, 377, (1976).

[81] M. J. Kamlet, R. W. Taft, J. Am. Chem. Soc., 99, 6027, (1977).

[82] V. Gutmann, The Donor-Accepetor Approach to Molecular Interaction, Plenum Press, New York, (1978).

[83] Y. Marcus, the Properties of Solvents,(1998).

[84] W. A. Al-basheer, R. M. Pagni, R. N. Compton, in press.

[85] W. A. Al-basheer, R. Sullivan, R. M. Pagni, R. Li, R. N. Compton, 230th American Chemical Society National Meeting, Washington, DC, United states, AN 2005:741209,Aug. 82th- Sep. 1, (2005).

[86] H. Eyring, J. Walter, G. Kimball, Quantum Chemistry, John Wiley & Sons, New York, (1944).

[87] T. Lowry, Optical Rotatory Power, Dover publications Inc., New York, (1964).

[88] C. Djerassi, Optical Rotatory Disperion, McGraw Hill, New York, (1960).

[89] P. L. Polavarapu, and D. K. Chakraborty, J. Am. Chem. Soc., 120, 6160-6164, (1998).

[90] J. Applequist, J. Chem. Phys., 58, 4251-4259, (1973).

[91] J. H. Brewster, J. Am. Chem. Soc., 81, 5475-5483, (1959).

[92] R. D. Amos, Chem. Phys. Lett., 87,23, (1982).

[93] T. Helgaker, K. Ruud, K. L. Bak, P. Jorgensen, J. Olsen, Faraday Discuss., 99, 165, (1994).

[94] R. D. Amos, J. E. Rice, The Cambridge Analytical Derivative Package, Cambridge University, Cambridge, U. K., (1997).

[95] T. Helgaker et. al., Dalton release 1.2, (2001).

[96] P. L. Polavarapu, Mol. Phys., 91, 551-554, (1997).

[97] R. K. Kondru, P. Wipf, D. N. Beratan, J. Am. Chem. Soc., 120, 2204, (1998).

[98] E. Giorgio, C. Minichino, R. G. Viglione, R. Zanasi, C. Rosini, J. Org. Chem., 68, 5186-5192, (2003).

[99] J. B. Foresman, and A. Frisch, Exploring Chemistry with Electronic Structure Method, 2nd edition, Gaussian, Inc., Pittsburg, PA, (1996).

[100] S. Ohta et. al., Chem. Lett., 1331, (1985).

[101] S. Ohta et. al., Bull. Chem. Soc. Jpn., 59, 1181, (1986).

[102] E. Charney, The Molecular Basis of Optical Activity: ORD and CD, Wiley, New York, (1979).

[103] F. Ciardelli, and P. Salvadori, Fundamental Aspects and Recent Developments in ORD and CD, Heyden and Son, London, (1973).

[104] A. D. Buckingham, Adv. Chem. Phys., 12, 107, (1967).

[105] A. D. Buckingham, and G. C. Longuet-Higgins, Mol. Phys., 14, 63, (1968).

[106] P. L. Polavarapu, Chirality, 18, 348-356, (2006).

[107] H. A. Lorentz, The Theory of Electrons; Leipzig, Germany, reprinted by Dover: New York, (1951).

[108] B. Mennucci, J. Tomasi, R. Cammi, J. R. Cheeseman, M. J. Frisch, F. J. Devlin, S. Gabriel, and P. J. Stephens, J. Phys. Chem. A, 106, 6102-6113, (2002).

[109] Y. Kumata, J. Furukawa, T. Fueno, Bull. Chem. Soc. Jpn., 43, 12, 3920, (1970).

[110] E. L. Eliel, S. H. Wilen, Stereochemistry of Organic Compounds; Chapter 13 Wiley: New York, (1994).

[111] G. Landsberg, and L. Mandelstam, Naturwissenschaften, 16, 557 and 772, (1928).

[112] G. Eckhardt, R. W. Hellwarth, F. J. McClung, S. E. Schwarz, and D. Weiner, Phys. Rev. Lett., 9, 455, (1962).

[113] B. P. Stoicheff, Phys. Rev. Lett., 7, 186, (1963).

[114] R. Chiao, and B. P. Stoicheff, Phys. Rev. Lett., 12, 290, (1964).

[115] A. Weber and co-authors, Raman Spectroscopy of gases and liquids, Heidelberg, Germany, ( 1979).

[116] P. L. Polavarapu, J. Phys. Chem., 94, 8106-8112, (1990).

[117] P. L. Polavarapu, P. K. Bose, L. Hecht, and L. D. Barron, J. Phys. Chem., 97, 11211-11215, (1993).

[118] H. J. Bowley, D. J. Gardiner, D. L. Gerrard, P. R. Graves, J. D. Louden, G. Turrell, Practical Raman Spectroscopy, Springer-Verlag, Berlin, Germany, (1989).

[119] H. A. Szymanski, Raman Spectroscopy: Theory and Practice, Chapter 1, by L. A. Woodward, Plenum Press, New York, (1967).

[120] S. K. Freeman, Applications of laser Raman spectroscopy, John Wiley & sons, (1974).

[121] J. S. Hager, J. Zahardis, R. Pagni, R. N. Compton, and Jun Li, J. Chem. Phys.,

120, 6, (2004).

[122] J. S. Hager, R. N. Compton, C. S. Feigerle, R. J. Hinde, and M. J. Sepaniak, Raman spectroscopy Under Liquid Nitrogen.

[123] R. J. Hinde, M. J. Sepaniak, R. N. Compton, J. Nordling, N. Lavrik, Chem. Phys. Lett., 339, 167-173, (2001).

[124] W. A. Al-basheer, R. M. Pagni, R. N. Compton, 231st American Chemical Society National Meeting, Atlanta, GA, United states, AN 2006:249782, Mar. 26th-30th, (2006).

[125] G. D. Fasman, Circular Dichroism and the Conformational Analysis of Biomolecules, Plenum press, New York, (1996).

[126] E. C. Hsu, and G. Holzwarth, J. Chem. Phys., 59, 4678, (1973).

[127] G. Holzwarth, E. C. Hsu, H. S. Mosher, T. R. Faulkner, and A. Moscowitz, J. Am. Chem. Soc., 96, 251, (1974).

[128] L. A. Nafie, J. C. Cheng, and P. J. Stephens, J. Am. Chem. Soc., 97, 3842, (1975).

[129] L. A. Nafie, T. A. Keiderling, and P. J. Stephens, J. Am. Chem. Soc., 98, 2715, (1976).

[130] T. A. Keiderling, and P. J. Stephens, Chem. Phys. Lett., 41, 46, (1976).

[131] L. A. Nafie, A. J. Chem. Phys., 79, 4950, (1983).

[132] L. A. Nafie, T. B. Freedman, J. Chem. Phys., 78, 7108, (1983).

[133] P. J. Stephens, J. Phys. Chem., 89, 748, (1985).

[134] A. D. Buckingham, P. W. Fowler, P. A. Galwas, Chem. Phys., 112, (1987).

[135] L. A. Nafie, A. J. Chem. Phys., 96, 5687, (1992).

[136] L. A. Nafie, Annu. Rev. Phys. Chem., 48, 357, (1997).

[137] L. A. Nafie, J. Phys. Chem. A, 108, 7222-7231, (2004).

[138] D. Nasipuri, Stereochemistry of Organic Compounds, Wiley & Sons, New York, (1991).

[139] J. He, A. G. Petrovic, P. L. Polavarapu, J. Phys. Chem. B, 108, 20451-20457, (2004).

[140] R. D. Singh, T. A. Keiderling, J. Am. Chem. Soc., 103, 2387-2394, (1981).

[141] M. J. Frisch et al., Gaussian 03, Revision B.03, Gaussian Inc. Pittsburgh, PA, (2003).

[142] J. G. Grasselli, M. K. Snavely, and B. J. Bulkin, Chemical Applications of Raman Specroscopy, A Wiley-Interscience Publication, New York, (1981).

# APPENDIX

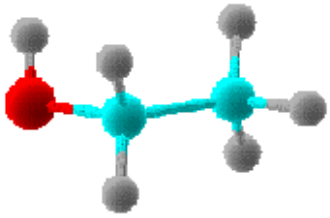

ethanol ($C_2H_6O$)

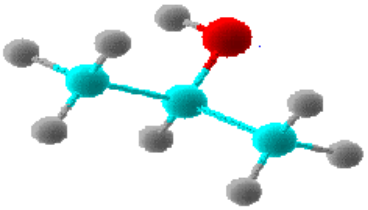

2-propanol ($C_3H_8O$)

2-butanol ($C_4H_{10}O$)

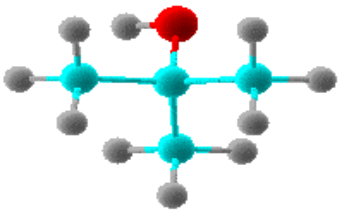

t-butanol ($C_4H_{10}O$)

isobutyl alcohol ($C_4H_{10}O$)

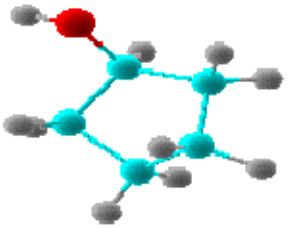

cyclopentanol ($C_5H_{10}O$)

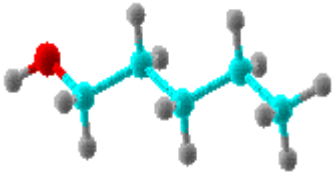

n-amyl alcohol ($C_5H_{12}O$)

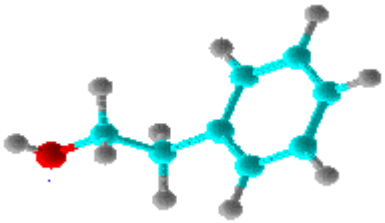

phenethyl alcohol ($C_8H_{10}O$)

Figure A.1 List of most alcohols molecular structure used as solvents.

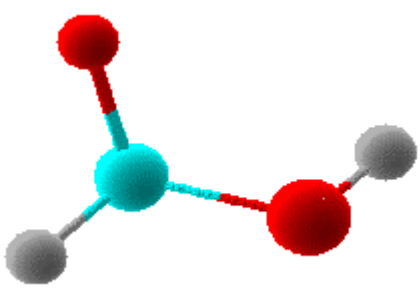

formic acid ($CH_2O_2$)

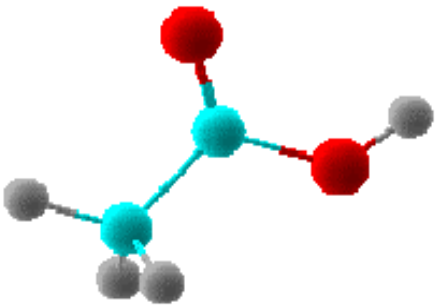

acetic acid ($C_2H_4O_2$)

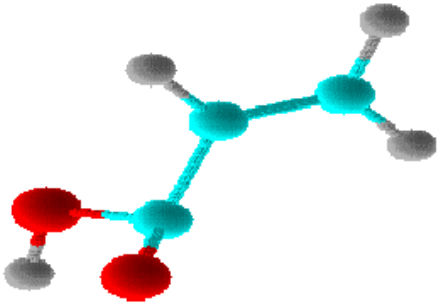

acrylic acid ($C_3H_4O_2$)

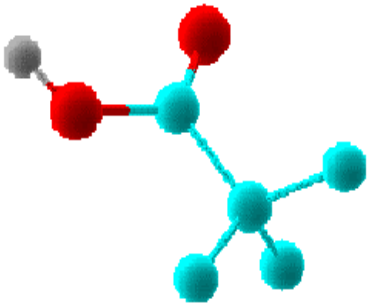

trifluoroacetic acid ($C_2HF_3O_2$)

Figure A.2 List of acids molecular structure used as solvents.

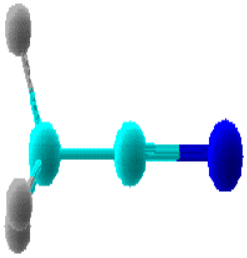

acetonitrile ($C_2H_3N$)

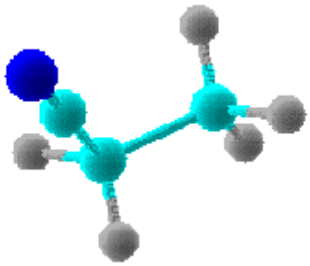

propionitrile ($C_3H_5N$)

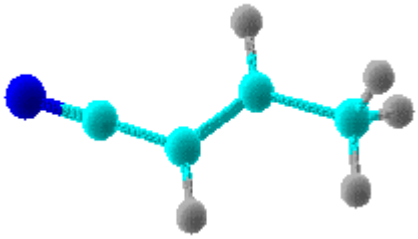

crotononitrile ($C_4H_5N$)

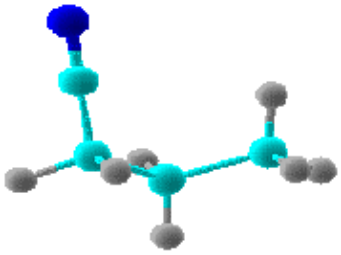

butyronitrile ($C_4H_7N$)

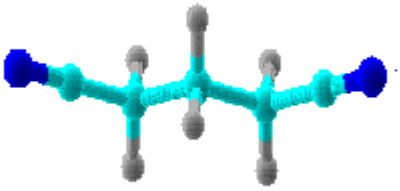

glutaronitrile ($C_5H_6N_2$)

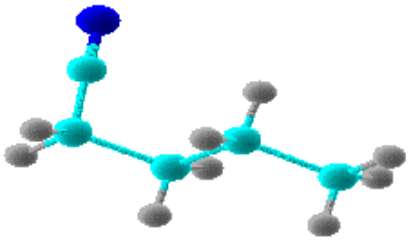

valeronitrile ($C_5H_9N$)

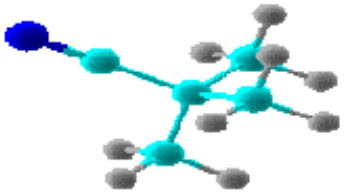

trimethylacetonitrile ($C_5H_9N$)

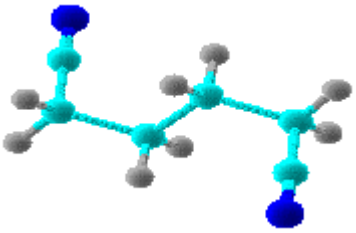

adiponitrile ($C_6H_8N_2$)

Figure A.3 List of nitriles molecular structure employed.

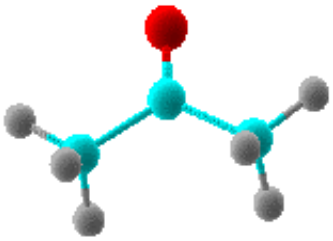

acetone ($C_3H_6O$)

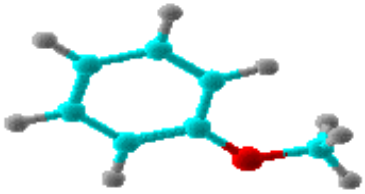

anisole ($C_7H_8O$)

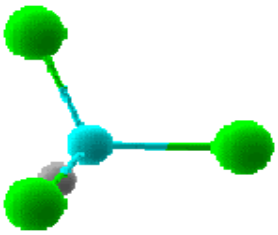

chloroform ($CCl_3H$)

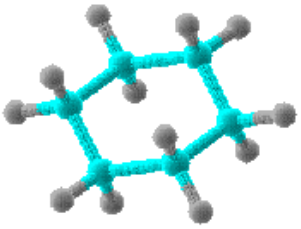

cyclohexane ($C_6H_{12}$)

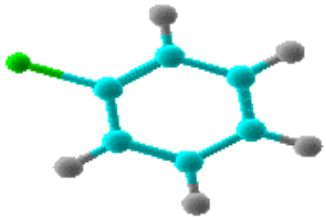

chlorobenzene ($C_6H_5Cl$)

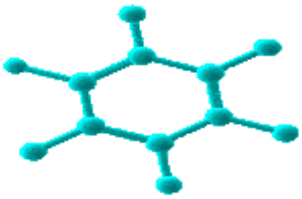

hexafloroubenzene ($C_6F_6$)

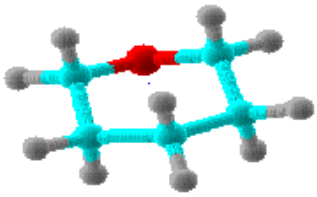

tetrahydropyran ($C_5H_{10}O$)

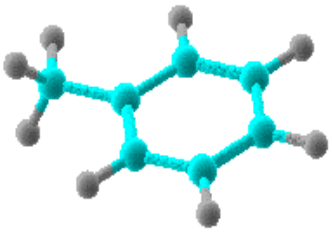

toluene ($C_7H_8$)

Figure A.4 List of miscellaneous solvents applied in Dissertation.

Table A.1 IR frequency and absorption calculations for *R*-(+)-limonene conformers of B3LYP and basis set aug-cc-pVDZ

| *Frequency Eq (C) ($cm^{-1}$)* | *IR Eq (C) (a. u.)* | *Frequency Eq (T) ($cm^{-1}$)* | *IR Eq (T) (a. u.)* | *Frequency Ax (T) ($cm^{-1}$)* | *IR Ax (T) (a. u.)* |
|---|---|---|---|---|---|
| 919.4856 | 26.915 | 919.4942 | 26.961 | 901.5464 | 3.3551 |
| 924.1467 | 11.6875 | 924.1264 | 11.6088 | 921.9522 | 40.3708 |
| 927.3168 | 5.8438 | 927.3348 | 5.8807 | 941.4462 | 4.6251 |
| 969.2883 | 1.8933 | 969.2798 | 1.8906 | 962.3756 | 0.5488 |
| 994.0248 | 1.5617 | 993.9675 | 1.5735 | 971.9213 | 3.13 |
| 1011.7761 | 0.277 | 1011.7964 | 0.2777 | 1012.5158 | 1.0831 |
| 1031.0688 | 1.6294 | 1031.0429 | 1.6313 | 1020.2642 | 0.2231 |
| 1037.4458 | 1.0933 | 1037.4322 | 1.0878 | 1025.4654 | 1.014 |
| 1045.5371 | 0.7779 | 1045.5569 | 0.7548 | 1048.8065 | 0.4199 |
| 1068.7998 | 4.0076 | 1068.7911 | 4.0221 | 1074.426 | 2.4641 |
| 1097.7115 | 1.2194 | 1097.7075 | 1.218 | 1086.065 | 0.2377 |
| 1129.8585 | 1.11 | 1129.7893 | 1.1123 | 1115.5837 | 3.1041 |
| 1163.1254 | 3.873 | 1163.1241 | 3.8762 | 1172.9826 | 5.2093 |
| 1174.5058 | 3.532 | 1174.5041 | 3.5377 | 1182.843 | 2.1449 |
| 1213.297 | 5.1409 | 1213.2692 | 5.1316 | 1206.0663 | 3.8401 |
| 1256.48 | 4.1776 | 1256.4546 | 4.1625 | 1222.5551 | 5.463 |
| 1269.0341 | 1.3522 | 1269.0286 | 1.3569 | 1261.3887 | 4.0407 |
| 1304.7467 | 0.4361 | 1304.7873 | 0.4353 | 1299.1246 | 3.0339 |
| 1322.2925 | 1.5865 | 1322.3091 | 1.5893 | 1335.8717 | 1.224 |

Table A.1 Continued

| *Frequency Eq (C) ($cm^{-1}$)* | *IR Eq (C) (a. u.)* | *Frequency Eq (T) ($cm^{-1}$)* | *IR Eq (T) (a. u.)* | *Frequency Ax (T) ($cm^{-1}$)* | *IR Ax (T) (a. u.)* |
|---|---|---|---|---|---|
| 1330.9849 | 0.4265 | 1330.9942 | 0.4228 | 1340.9983 | 0.2778 |
| 1349.2294 | 2.6479 | 1349.1977 | 2.6522 | 1367.4484 | 1.7231 |
| 1388.3153 | 0.251 | 1388.3243 | 0.2518 | 1375.2783 | 4.2585 |
| 1394.0018 | 5.6005 | 1393.9706 | 5.5706 | 1393.3229 | 4.4266 |
| 1437.5695 | 0.1791 | 1397.0948 | 1.4429 | 1435.7438 | 0.8155 |
| 1455.4087 | 7.9612 | 1399.3119 | 3.8976 | 1456.1925 | 7.4537 |
| 1460.0013 | 9.9221 | 1437.5283 | 0.1727 | 1463.106 | 4.8804 |
| 1463.2705 | 1.6457 | 1455.4134 | 7.9606 | 1473.529 | 18.1864 |
| 1468.087 | 1.5521 | 1459.9171 | 9.9211 | 1480.1169 | 11.4593 |
| 1471.5019 | 8.7526 | 1463.2603 | 1.6495 | 1495.7434 | 0.9111 |
| 1476.7281 | 14.6771 | 1468.0244 | 1.4641 | 1699.7012 | 22.3392 |
| 1487.6449 | 0.7952 | 1471.4713 | 8.8468 | 1734.8341 | 2.3013 |
| 1703.6686 | 29.115 | 1476.7198 | 14.6599 | | |
| 1734.4833 | 1.3017 | 1487.6009 | 0.8043 | | |

Table A.2 VCD calculations for *R*-(+)-limonene Eq (C) conformer using B3LYP with basis set aug-cc-pVDZ

| *Frequency* ($cm^{-1}$) | *Rotational Strength* (R) ($10^{-44} esu^2 cm^2$) | *Dipole strength* (D) ($10^{-40} esu^2 cm^2$) | *VCD* (a. u.) |
|---|---|---|---|
| 919.4856 | 12.7854 | 116.777 | 0.437942403 |
| 924.1467 | -23.0274 | 50.4533 | -1.825640741 |
| 927.3168 | 4.6773 | 25.1406 | 0.744182716 |
| 969.2883 | 2.8251 | 7.7922 | 1.45021945 |
| 994.0248 | -10.407 | 6.2678 | -6.641564823 |
| 1011.7761 | 0.74 | 1.0923 | 2.709878239 |
| 1031.0688 | -1.8853 | 6.3044 | -1.196180445 |
| 1045.5371 | 10.4415 | 2.9683 | 14.07068019 |
| 1068.7998 | 28.999 | 14.9587 | 7.754417162 |
| 1097.7115 | -5.5361 | 4.4317 | -4.996818377 |
| 1129.8585 | -6.1983 | 3.9191 | -6.326248373 |
| 1163.1254 | -5.3154 | 13.2841 | -1.600529957 |
| 1174.5058 | 3.1764 | 11.9969 | 1.059073594 |
| 1213.297 | -13.0728 | 16.9037 | -3.093476576 |
| 1256.48 | 17.9804 | 13.2641 | 5.422275164 |
| 1269.0341 | 4.4185 | 4.251 | 4.157609974 |
| 1304.7467 | 12.8882 | 1.3334 | 38.66266687 |
| 1322.2925 | -7.0063 | 4.7866 | -5.854928342 |
| 1330.9849 | -1.9767 | 1.2782 | -6.185886403 |

Table A.2 Continued

| *Frequency* ($cm^{-1}$) | *Rotational Strength* (R) ($10^{-44} esu^2 cm^2$) | *Dipole strength* (D) ($10^{-40} esu^2 cm^2$) | *VCD* *(a. u.)* |
|---|---|---|---|
| 1349.2294 | 16.2221 | 7.8293 | 8.287892915 |
| 1388.3153 | 3.5404 | 0.7213 | 19.63343962 |
| 1394.0018 | -5.2704 | 16.0278 | -1.315314641 |
| 1397.0788 | 3.0835 | 4.0969 | 3.010568967 |
| 1399.2985 | -3.7 | 11.0349 | -1.341199286 |
| 1437.5693 | -1.958 | 0.497 | -15.75855131 |
| 1455.4087 | -2.1572 | 21.8224 | -0.395410221 |
| 1460.0013 | 11.0058 | 27.1118 | 1.623765298 |
| 1463.2705 | -0.7495 | 4.4867 | -0.668197116 |
| 1468.087 | -1.2222 | 4.2176 | -1.15914264 |
| 1476.7281 | 12.832 | 39.6503 | 1.294517318 |
| 1487.6449 | -0.939 | 2.1324 | -1.761395611 |

Table A.3 VCD calculations for *R*-(+)-limonene Eq (T) conformer using B3LYP with basis set aug-cc-pVDZ

| *Frequency* ($cm^{-1}$) | *Rotational Strength* (R) ($10^{-44} esu^2 cm^2$) | *Dipole strength* (D) ($10^{-40} esu^2 cm^2$) | *VCD* (a. u.) |
|---|---|---|---|
| 919.4942 | 12.7504 | 116.9753 | 0.436003 |
| 924.1264 | -23.0082 | 50.1147 | -1.83644 |
| 927.3348 | 4.5608 | 25.299 | 0.721104 |
| 969.2798 | 2.7981 | 7.7815 | 1.438335 |
| 993.9675 | -10.4851 | 6.3153 | -6.64108 |
| 1011.7964 | 0.8196 | 1.095 | 2.993973 |
| 1031.0429 | -1.7687 | 6.3119 | -1.12087 |
| 1045.5569 | 10.232 | 2.8798 | 14.2121 |
| 1068.7911 | 29.0361 | 15.0129 | 7.736307 |
| 1097.7075 | -5.4962 | 4.4267 | -4.96641 |
| 1129.7893 | -6.2047 | 3.9276 | -6.31908 |
| 1163.1241 | -5.3531 | 13.295 | -1.61056 |
| 1174.5041 | 3.1931 | 12.0163 | 1.062923 |
| 1213.2692 | -13.0469 | 16.8736 | -3.09286 |
| 1256.4546 | 17.9411 | 13.2166 | 5.429868 |
| 1269.0286 | 4.4465 | 4.2656 | 4.169636 |
| 1304.7873 | 12.8743 | 1.331 | 38.69061 |
| 1322.3091 | -6.9356 | 4.7949 | -5.78581 |
| 1330.9942 | -1.9513 | 1.2671 | -6.15989 |

Table A.3 Continued

| *Frequency* ($cm^{-1}$) | *Rotational Strength* (R) ($10^{-44} esu^2 cm^2$) | *Dipole strength* (D) ($10^{-40} esu^2 cm^2$) | *VCD* (a. u.) |
|---|---|---|---|
| 1349.1977 | 16.2087 | 7.8421 | 8.26753 |
| 1388.3243 | 3.4839 | 0.7235 | 19.26137 |
| 1393.9706 | -5.198 | 15.9423 | -1.3042 |
| 1397.0948 | 3.0003 | 4.1202 | 2.912771 |
| 1399.3119 | -3.7109 | 11.112 | -1.33582 |
| 1437.5283 | -1.906 | 0.4792 | -15.9098 |
| 1455.4134 | -2.1545 | 21.8205 | -0.39495 |
| 1459.9171 | 10.8639 | 27.1105 | 1.602907 |
| 1463.2603 | -0.7705 | 4.4973 | -0.6853 |
| 1468.0244 | -1.2831 | 3.9786 | -1.29 |
| 1476.7198 | 12.8538 | 39.6042 | 1.298226 |
| 1487.6009 | -0.9301 | 2.157 | -1.7248 |

Table A.4 VCD calculations for *R*-(+)-limonene Ax (T) conformer using B3LYP with basis set aug-cc-pVDZ

| *Frequency* ($cm^{-1}$) | *Rotational Strength* (R) ($10^{-44} esu^2 cm^2$) | *Dipole strength* (D) ($10^{-40} esu^2 cm^2$) | *VCD* (a. u.) |
|---|---|---|---|
| 921.9522 | -20.6426 | 174.6894 | -0.472669778 |
| 941.4462 | -22.6778 | 19.5991 | -4.628334975 |
| 962.3756 | 3.9144 | 2.2749 | 6.882764078 |
| 971.9213 | -11.0009 | 12.8474 | -3.425097685 |
| 1012.5158 | 2.2629 | 4.2674 | 2.121104185 |
| 1025.4654 | 12.7445 | 3.9448 | 12.92283512 |
| 1048.8065 | -14.2134 | 1.5973 | -35.59356414 |
| 1074.426 | 11.9175 | 9.1492 | 5.21029161 |
| 1086.065 | -7.0801 | 0.8731 | -32.4366052 |
| 1115.5837 | -7.9679 | 11.1003 | -2.871237714 |
| 1172.9826 | 20.0354 | 17.7173 | 4.523352881 |
| 1182.843 | 3.3266 | 7.2341 | 1.839399511 |
| 1206.0663 | 6.7415 | 12.7021 | 2.122956047 |
| 1222.5551 | -2.6969 | 17.8267 | -0.605137238 |
| 1261.3887 | 1.8764 | 12.7797 | 0.587306431 |
| 1299.1246 | 15.2886 | 9.3165 | 6.564095959 |
| 1335.8717 | -3.3611 | 3.6553 | -3.678056521 |
| 1340.9983 | 1.1556 | 0.8265 | 5.592740472 |
| 1367.4484 | -2.5177 | 5.0271 | -2.003302103 |

Table A.4 Continued

| *Frequency* ($cm^{-1}$) | *Rotational Strength* (R) ($10^{-44} esu^2 cm^2$) | *Dipole strength* (D) ($10^{-40} esu^2 cm^2$) | *VCD* (a. u.) |
|---|---|---|---|
| 1375.2783 | -5.5277 | 12.3551 | -1.789609149 |
| 1393.3229 | 8.1177 | 12.6742 | 2.561960518 |
| 1399.0791 | -2.7125 | 11.0981 | -0.977644822 |
| 1435.7438 | 4.3145 | 2.2659 | 7.616399665 |
| 1463.106 | -7.6009 | 13.3071 | -2.284765276 |
| 1470.7128 | 12.7057 | 19.7568 | 2.572420635 |
| 1480.1169 | 0.658 | 30.8866 | 0.085214948 |
| 1495.7434 | 3.6211 | 2.43 | 5.960658436 |

Table A.5 DFT calculations of IR absorption for *R*-(-)-carvone conformers.

| *Freq. Eq (C)* ($cm^{-1}$) | *IR Eq (C)* (*a. u.*) | *Freq. Eq (T)* ($cm^{-1}$) | *IR Eq (T)* (*a. u.*) | *Freq. Ax (C)* ($cm^{-1}$) | *IR Ax (C)* (*a. u.*) | *Freq. Ax (T)* ($cm^{-1}$) | *IR Ax (T)* (*a. u.*) |
|---|---|---|---|---|---|---|---|
| 862.750 | 0.6249 | 875.965 | 0.2897 | 835.828 | 2.777 | 849.387 | 2.2397 |
| 892.847 | 1.2093 | 903.527 | 3.8793 | 895.707 | 1.0678 | 888.287 | 2.6155 |
| 910.741 | 9.0667 | 912.758 | 7.7548 | 929.398 | 25.018 | 936.564 | 14.397 |
| 932.798 | 37.875 | 924.355 | 37.2635 | 930.781 | 22.519 | 941.693 | 33.114 |
| 971.285 | 3.0222 | 971.085 | 4.2458 | 949.533 | 3.9114 | 946.724 | 0.9755 |
| 990.795 | 0.0904 | 991.286 | 1.0363 | 968.212 | 2.3906 | 974.163 | 2.5523 |
| 1014.50 | 2.3543 | 1002.56 | 5.2585 | 1008.09 | 5.1271 | 1006.14 | 4.8867 |
| 1040.49 | 7.3393 | 1039.30 | 3.5446 | 1035.89 | 5.2144 | 1021.93 | 1.5324 |
| 1048.35 | 1.1609 | 1050.59 | 1.233 | 1046.51 | 2.4044 | 1048.23 | 2.3946 |
| 1063.50 | 6.8663 | 1064.67 | 4.1038 | 1062.93 | 5.1292 | 1059.89 | 4.1254 |
| 1072.52 | 8.2818 | 1071.26 | 6.3197 | 1064.40 | 0.9243 | 1064.87 | 4.2314 |
| 1112.60 | 13.1987 | 1118.08 | 22.9323 | 1108.57 | 11.333 | 1100.80 | 11.755 |
| 1123.29 | 26.9556 | 1131.64 | 18.8259 | 1125.38 | 25.274 | 1125.39 | 22.882 |
| 1153.45 | 6.8169 | 1155.40 | 6.1417 | 1170.50 | 9.0102 | 1165.38 | 11.558 |
| 1226.30 | 0.2876 | 1219.64 | 3.0767 | 1205.68 | 5.153 | 1217.38 | 5.1407 |
| 1262.68 | 20.3562 | 1261.75 | 19.3026 | 1230.09 | 5.2585 | 1227.61 | 6.4483 |
| 1269.16 | 1.318 | 1268.32 | 2.5505 | 1278.51 | 6.4102 | 1253.74 | 3.9622 |
| 1301.10 | 1.0075 | 1277.42 | 1.506 | 1316.07 | 0.2778 | 1289.02 | 5.0417 |

Table A.5 Continued

| *Freq. Eq (C) ($cm^{-1}$)* | *IR Eq (C) (a. u.)* | *Freq. Eq (T) ($cm^{-1}$)* | *IR Eq (T) (a. u.)* | *Freq. Ax (C) ($cm^{-1}$)* | *IR Ax (C) (a. u.)* | *Freq. Ax (T) ($cm^{-1}$)* | *IR Ax (T) (a. u.)* |
|---|---|---|---|---|---|---|---|
| 1309.14 | 2.1288 | 1321.53 | 6.1664 | 1341.37 | 8.4765 | 1336.14 | 4.3047 |
| 1347.41 | 4.1809 | 1335.46 | 0.4362 | 1351.36 | 0.9552 | 1360.77 | 0.8305 |
| 1369.02 | 4.7627 | 1383.87 | 28.134 | 1362.23 | 2.9555 | 1375.87 | 16.053 |
| 1384.19 | 46.4889 | 1393.41 | 16.1598 | 1388.46 | 36.099 | 1390.56 | 22.289 |
| 1397.10 | 7.9606 | 1397.97 | 3.3186 | 1400.01 | 7.1062 | 1397.21 | 7.325 |
| 1404.21 | 6.1487 | 1403.79 | 6.4468 | 1402.96 | 7.3879 | 1402.02 | 7.8757 |
| 1439.43 | 0.4419 | 1437.26 | 0.4267 | 1432.17 | 0.6451 | 1438.39 | 5.3961 |
| 1445.82 | 5.3511 | 1445.37 | 3.9734 | 1443.34 | 9.1222 | 1447.74 | 7.0812 |
| 1449.32 | 5.7039 | 1448.56 | 5.6351 | 1448.59 | 5.4459 | 1450.37 | 2.679 |
| 1460.69 | 4.128 | 1462.17 | 7.0189 | 1460.02 | 3.0774 | 1456.52 | 13.234 |
| 1463.67 | 8.6501 | 1467.22 | 13.2641 | 1463.69 | 16.090 | 1469.07 | 7.2377 |
| 1470.19 | 12.739 | 1469.26 | 10.7532 | 1469.94 | 11.838 | 1470.61 | 16.030 |
| 1475.79 | 13.639 | 1478.06 | 11.4825 | 1476.83 | 17.857 | 1480.52 | 6.5402 |
| 1695.86 | 8.2529 | 1695.91 | 20.6213 | 1699.16 | 19.225 | 1700.35 | 3.2719 |
| 1703.2 | 21.1178 | 1704.94 | 17.8181 | 1702.21 | 4.086 | 1704.73 | 13.408 |
| 1727.32 | 285.139 | 1726.34 | 276.476 | 1722.88 | 254.93 | 1725.00 | 241.86 |
| 1740.52 | 11.8512 | 1740 | 10.3231 | 1741.75 | 13.210 | 1743.56 | 9.2315 |
| 1760.13 | 11.86 | 1764.21 | 9.8654 | 1766.32 | 12.789 | 1773.26 | 10.234 |

Table A.6 DFT calculations for *R*-(-)-carvone VCD Eq (C) conformer.

| *Frequency* ($cm^{-1}$) | *Rotational Strength* (R) ($10^{-44} esu^2 cm^2$) | *Dipole strength* (D) ($10^{-40} esu^2 cm^2$) | *VCD* (*a. u.*) |
|---|---|---|---|
| 932.7981 | -4.3886 | 161.9839 | -0.10837 |
| 971.2855 | 3.4103 | 12.4133 | 1.098918 |
| 990.7957 | 5.8254 | 0.3638 | 64.05058 |
| 1014.5063 | -7.495 | 9.2579 | -3.23832 |
| 1040.4899 | 19.7447 | 28.14 | 2.806638 |
| 1048.3497 | -8.9427 | 4.4177 | -8.09715 |
| 1063.5086 | -12.8301 | 25.7566 | -1.99251 |
| 1072.5239 | -15.2656 | 30.8054 | -1.9822 |
| 1112.6012 | -2.5201 | 47.3258 | -0.213 |
| 1123.2951 | 8.8076 | 95.733 | 0.368007 |
| 1153.4511 | -9.3775 | 23.5775 | -1.59092 |
| 1226.3078 | -5.9663 | 0.9355 | -25.5106 |
| 1262.6823 | 33.5318 | 64.3146 | 2.085486 |
| 1269.161 | -5.1206 | 4.1429 | -4.94398 |
| 1301.1036 | 1.666 | 3.0892 | 2.157193 |
| 1309.1477 | -20.767 | 6.487 | -12.8053 |
| 1347.4149 | -0.1938 | 12.3788 | -0.06262 |
| 1369.0217 | 0.6483 | 4.7627 | 0.544481 |

Table A.6 Continued

| *Frequency* ($cm^{-1}$) | *Rotational Strength* (R) ($10^{-44} esu^2 cm^2$) | *Dipole strength* (D) ($10^{-40} esu^2 cm^2$) | *VCD* (a. u.) |
|---|---|---|---|
| 1384.1948 | 35.1876 | 133.986 | 1.050486 |
| 1445.827 | -4.3907 | 14.7651 | -1.18948 |
| 1449.3292 | -2.3123 | 15.7005 | -0.5891 |
| 1460.6989 | 1.6099 | 11.2744 | 0.57117 |
| 1463.6706 | 0.7191 | 23.5767 | 0.122002 |
| 1470.1915 | 9.4012 | 34.5676 | 1.087863 |
| 1475.7981 | 1.0195 | 36.8692 | 0.110607 |

Table A.7 VCD calculations for *R*-(-)-carvone Eq (T) conformer.

| *Frequency* ($cm^{-1}$) | *Rotational Strength* (R) ($10^{-44} esu^2 cm^2$) | *Dipole strength* (D) ($10^{-40} esu^2 cm^2$) | *VCD* (a. u.) |
|---|---|---|---|
| 912.7584 | -0.8781 | 33.8941 | -0.10363 |
| 924.3552 | -2.1702 | 160.8246 | -0.05398 |
| 971.0858 | 8.6196 | 17.4425 | 1.976689 |
| 991.2867 | 11.9456 | 4.1706 | 11.45696 |
| 1002.564 | 1.5792 | 20.9245 | 0.301885 |
| 1039.308 | 14.7434 | 13.6061 | 4.33435 |
| 1050.595 | -8.0861 | 4.6819 | -6.90839 |
| 1064.67 | -10.3275 | 15.3773 | -2.68643 |
| 1071.261 | -34.3925 | 23.5347 | -5.84541 |
| 1118.086 | 4.7589 | 81.824 | 0.232641 |
| 1131.646 | 13.4354 | 66.3671 | 0.809763 |
| 1155.408 | -16.1589 | 21.2059 | -3.048 |
| 1219.648 | 9.9489 | 10.0638 | 3.954331 |
| 1261.751 | 23.1139 | 61.0308 | 1.514901 |
| 1268.326 | -27.1484 | 8.0223 | -13.5365 |
| 1277.42 | -6.388 | 4.7032 | -5.4329 |
| 1321.54 | -27.4286 | 18.6148 | -5.89393 |
| 1335.468 | 5.2842 | 1.3029 | 16.22289 |
| 1383.875 | -1.2749 | 81.1039 | -0.06288 |

Table A.7 Continued

| *Frequency* ($cm^{-1}$) | *Rotational Strength* (R) ($10^{-44} esu^2 cm^2$) | *Dipole strength* (D) ($10^{-40} esu^2 cm^2$) | *VCD* (a. u.) |
|---|---|---|---|
| 1393.413 | 17.3924 | 46.2663 | 1.503678 |
| 1397.973 | -2.4525 | 9.4704 | -1.03586 |
| 1403.793 | 12.4643 | 18.321 | 2.721314 |
| 1437.269 | 2.6953 | 1.1845 | 9.1019 |
| 1445.378 | -5.2496 | 10.967 | -1.91469 |
| 1448.564 | -1.2452 | 15.5194 | -0.32094 |
| 1462.176 | -6.169 | 19.1503 | -1.28854 |
| 1467.227 | -2.8174 | 36.0653 | -0.31248 |
| 1469.263 | 15.7876 | 29.1975 | 2.16287 |
| 1478.067 | -9.5147 | 30.9919 | -1.22802 |

Table A.8 VCD calculations for *R*-(-)-carvone Ax (C) conformer.

| *Frequency* ($cm^{-1}$) | *Rotational Strength* (R) ($10^{-44} esu^2 cm^2$) | *Dipole strength* (D) ($10^{-40} esu^2 cm^2$) | *VCD* (a. u.) |
|---|---|---|---|
| 929.3984 | -46.1681 | 107.3913 | -1.719621608 |
| 930.7815 | 55.1398 | 96.5216 | 2.285076087 |
| 949.5331 | -19.11 | 16.4336 | -4.651445818 |
| 968.2128 | -3.6733 | 9.8501 | -1.491680288 |
| 1008.094 | 12.0947 | 20.29 | 2.384366683 |
| 1035.895 | -1.114 | 20.0813 | -0.221897985 |
| 1046.5194 | -20.5003 | 9.1657 | -8.946528907 |
| 1062.9384 | 6.324 | 19.2506 | 1.314036965 |
| 1064.4006 | -10.0317 | 3.4644 | -11.58261171 |
| 1108.5781 | -31.8231 | 40.7868 | -3.120921475 |
| 1125.3835 | 18.0618 | 89.5975 | 0.806352856 |
| 1170.5006 | -6.4066 | 30.7093 | -0.834483365 |
| 1205.6844 | 5.2676 | 17.0503 | 1.235778843 |
| 1230.091 | 5.4867 | 17.0543 | 1.286877796 |

Table A.8 Continued

| *Frequency* ($cm^{-1}$) | *Rotational Strength* (R) ($10^{-44} esu^2 cm^2$) | *Dipole strength* (D) ($10^{-40} esu^2 cm^2$) | *VCD* (a. u.) |
|---|---|---|---|
| 1278.5194 | -7.3367 | 20.0018 | -1.467207951 |
| 1316.0729 | 0.2411 | 0.8421 | 1.145232158 |
| 1341.3776 | 1.4085 | 25.2101 | 0.223481858 |
| 1351.3662 | -6.078 | 2.82 | -8.621276596 |
| 1362.2313 | 12.0018 | 8.6555 | 5.546438681 |
| 1388.4674 | 35.4539 | 103.7232 | 1.367250528 |
| 1400.0146 | 8.5273 | 20.2493 | 1.684463167 |
| 1402.9642 | 5.1135 | 21.008 | 0.973629094 |
| 1438.171 | 1.2553 | 1.7893 | 2.806237076 |
| 1443.3396 | 2.1672 | 25.2139 | 0.343810359 |
| 1448.5924 | -3.549 | 14.9979 | -0.946532515 |
| 1460.0212 | 1.8901 | 8.4089 | 0.899095006 |
| 1463.6945 | 2.5867 | 43.8565 | 0.235923979 |
| 1469.9417 | 10.5475 | 32.1284 | 1.313168412 |
| 1476.8372 | -5.6603 | 48.2382 | -0.469362455 |

Table A.9 VCD calculations for *R*-(-)-carvone Ax (T) conformer.

| *Frequency* ($cm^{-1}$) | *Rotational Strength* (R) ($10^{-44} esu^2 cm^2$) | *Dipole strength* (D) ($10^{-40} esu^2 cm^2$) | *VCD* (a. u.) |
|---|---|---|---|
| 936.5648 | 49.4196 | 61.3257 | 3.223418567 |
| 941.693 | -19.5286 | 140.2982 | -0.556774071 |
| 946.7247 | 8.7275 | 4.1105 | 8.492884077 |
| 974.163 | -1.3705 | 10.4523 | -0.524477866 |
| 1006.1415 | -2.8462 | 19.376 | -0.587572254 |
| 1021.9371 | -26.8231 | 5.9819 | -17.93617413 |
| 1048.2346 | 14.2431 | 9.1133 | 6.251566392 |
| 1059.8949 | 13.931 | 15.5278 | 3.588660338 |
| 1064.87 | 15.6625 | 15.8523 | 3.952107896 |
| 1100.8002 | 26.1428 | 42.6028 | 2.454561672 |
| 1125.3986 | -24.8039 | 81.1151 | -1.223145875 |
| 1165.3843 | 9.1468 | 39.5686 | 0.924652376 |
| 1217.3867 | -2.575 | 16.8461 | -0.611417479 |
| 1227.6175 | -24.8524 | 20.9551 | -4.743933458 |
| 1253.7442 | 1.8963 | 12.6078 | 0.601627564 |
| 1289.0218 | 19.735 | 15.6037 | 5.059056506 |
| 1336.1465 | -8.9785 | 12.8528 | -2.794254948 |
| 1360.7799 | -4.1526 | 2.4347 | -6.822360044 |
| 1375.8718 | 10.0048 | 46.5463 | 0.859771883 |
| 1390.5652 | -22.0539 | 63.946 | -1.379532731 |
| 1397.2142 | -0.1488 | 20.9148 | -0.028458317 |
| 1402.0276 | -13.4106 | 22.4098 | -2.393702755 |

Table A.9 Continued

| *Frequency* ($cm^{-1}$) | *Rotational Strength* (R) ($10^{-44} esu^2 cm^2$) | *Dipole strength* (D) ($10^{-40} esu^2 cm^2$) | *VCD* (a. u.) |
|---|---|---|---|
| 1438.3997 | -11.2336 | 14.966 | -3.00243218 |
| 1447.7446 | 0.637 | 19.513 | 0.130579614 |
| 1450.372 | 3.2806 | 7.3688 | 1.780805559 |
| 1456.5221 | 6.5375 | 36.2478 | 0.721423093 |
| 1469.0715 | -10.0016 | 19.6547 | -2.035462256 |
| 1470.6199 | 4.8009 | 43.4876 | 0.441587947 |
| 1480.5221 | 1.0145 | 17.6233 | 0.230263345 |

# VITA

Watheq Ahmad Al-Basheer was born in Amman, The Hashemite Kingdom of Jordan on May 16, 1977. He attended public schools in Amman city where he graduated from Obida High School at the top of his class. He enrolled at the University of Jordan, Amman, in August 1995 and received a Bachelor degree in physics in June 1999. He entered the graduate physics program at the University of Jordan and received a Masters degree in Physics in October 2001. After working as a lecturer at the Hashemite University in Jordan, he received The Hashemite University Board Fellowship to pursue a PhD degree at the University of Tennessee, Knoxville, where he joint the physics department in August 2002 and worked under the direction of Dr. Robert N. Compton in the area of Chemical and molecular Physics. The doctoral degree was received in December 2006.